

ANALYSIS OF EFFECTS OF TEMPERATURE VARIATION ON DEEP  
DRAWING PROCESS USING DIFFERENT CONSTITUTIVE LAWS

A THESIS SUBMITTED TO  
THE GRADUATE SCHOOL OF NATURAL AND APPLIED SCIENCES  
OF  
MIDDLE EAST TECHNICAL UNIVERSITY

BY

RASİH HAKAN DEMİRKOL

IN PARTIAL FULFILLMENT OF THE REQUIREMENTS  
FOR  
THE DEGREE OF MASTER OF SCIENCE  
IN  
MECHANICAL ENGINEERING

DECEMBER 2019



Approval of the thesis:

**ANALYSIS OF EFFECTS OF TEMPERATURE VARIATION ON DEEP  
DRAWING PROCESS USING DIFFERENT CONSTITUTIVE LAWS**

submitted by **RASİH HAKAN DEMİRKOL** in partial fulfillment of  
the requirements for the degree of **Master of Science in Mechanical  
Engineering Department, Middle East Technical University** by,

Prof. Dr. Halil Kalıpçılar  
Dean, Graduate School of **Natural and Applied Sciences**

\_\_\_\_\_

Prof. Dr. M. A. Sahir Arıkan  
Head of Department, **Mechanical Engineering**

\_\_\_\_\_

Prof. Dr. Haluk Darendeliler  
Supervisor, **Mechanical Engineering, METU**

\_\_\_\_\_

**Examining Committee Members:**

Prof. Dr. Süha Oral  
Mechanical Engineering, METU

\_\_\_\_\_

Prof. Dr. Haluk Darendeliler  
Mechanical Engineering, METU

\_\_\_\_\_

Prof. Dr. Suat Kadioğlu  
Mechanical Engineering, METU

\_\_\_\_\_

Assist. Prof. Dr. Orkun Özşahin  
Mechanical Engineering, METU

\_\_\_\_\_

Prof. Dr. Can Çoğun  
Mechatronics Engineering, Çankaya University

\_\_\_\_\_

Date: 03.12.2019

**I hereby declare that all information in this document has been obtained and presented in accordance with academic rules and ethical conduct. I also declare that, as required by these rules and conduct, I have fully cited and referenced all material and results that are not original to this work.**

Name, Surname: Rasih Hakan Demirkol

Signature :

## **ABSTRACT**

### **ANALYSIS OF EFFECTS OF TEMPERATURE VARIATION ON DEEP DRAWING PROCESS USING DIFFERENT CONSTITUTIVE LAWS**

Demirkol, Rasih Hakan  
M.S., Department of Mechanical Engineering  
Supervisor: Prof. Dr. Haluk Darendeliler

December 2019, 122 pages

In this study, the influences of temperature variation in deep drawing process are investigated by changing the temperatures of the whole blank, a part of the blank, the punch and die. Different yield criteria and hardening rules are considered to form the constitutive relations. The numerical results are obtained by using a commercial finite element software. Whereas Von-Mises and Hill48 yield criteria are available in the finite element code, a subroutine is developed for embedding the Yld2003 yield criteria. Simulation results for isotropic, kinematic and combined hardening rules formulated with Von-Mises yield criterion are also acquired. Circular and square and complex shaped parts made of AA5754 and SS304 materials are used in the numerical analyses. The local heating simulations are conducted for a circular part through the heating of punch, die and, flange and inner regions of the blank for different combinations. For each case, the drawability of the part is obtained by using the Johnson-Cook failure criteria. Hot Forming and in-die Quenching (HFQ) analyses are carried out and the results are evaluated by using the mentioned constitutive equations for a complex shaped part made of AA5754. The complex shaped part also

utilized in conducting local heating simulations. The results obtained for different constitutive equations by the finite element analyses are compared with each other and experimental results according to thickness strain distribution, punch force variation and rim shape of the deformed blank.

Keywords: Deep Drawing Process, Hot Forming and in-die Quenching, Sheet Metal, Local Heating, Yield Criteria

## ÖZ

### **SICAKLIK DEĞİŞİMİNİN DERİN ÇEKME İŞLEMİ ÜZERİNDEKİ ETKİLERİNİN FARKLI BÜNYE DENKLEMLERİ KULLANILARAK ANALİZ EDİLMESİ**

Demirkol, Rasih Hakan  
Yüksek Lisans, Makina Mühendisliği Bölümü  
Tez Yöneticisi: Prof. Dr. Haluk Darendeliler

Aralık 2019 , 122 sayfa

Bu çalışmada, sıcaklık değişiminin derin çekme işlemi üzerindeki etkileri sac taslağın tamamının, sac taslağın bazı bölgelerinin, zımbanın ve kalıbın sıcaklıkları değiştirilerek incelenmiştir. Bünye denklemleri farklı akma kriterleri ve pekleşme kuralları kullanılarak oluşturulmuştur. Sayısal sonuçlar, ticari bir sonlu elemanlar programı kullanılarak elde edilmiştir. Sonlu elemanlar programında Von-Mises ve Hill48 akma kriterleri hazır olarak bulunurken, YLD2003 akma kriteri için bir alt program hazırlanmıştır. Ayrıca von-Mises akma kriteri, izotropik, kinematik and kombine pekleşme kurallarıyla beraber kullanılarak simülasyon sonuçları da elde edilmiştir. Yuvarlak, kare ve kompleks şekilli AA5754 ve SS304 sac metaller sayısal analizler için kullanılmıştır. Zımbaya, kalıba ve sac metalin kenar ve iç bölgelerine farklı sıcaklık değerleri tanımlanarak, yuvarlak sac metalin bölgesel ısıtma benzetimleri farklı kombinasyonlarda yapılmıştır. Her farklı durum için, Johnson-Cook kırılma kriteri kullanılarak sac metalin çekilebilme miktarları karşılaştırılmıştır. AA5754 kompleks şekilli sac metal için sıcak şekillendirme ve

soğutma işlemi (HFQ) bahsedilen bünye denklemleriyle analiz edilip, sonuçlar değerlendirilmiştir. Kompleks şekil için bölgesel ısıtma benzetimi de yapılmıştır. Farklı bünye denklemleri kullanılarak sonlu elemanlar analizlerinden elde edilen kalınlık gerinim dağılımları, zımba kuvvet değişimleri ve kenar profil sonuçları birbirleri ile ve deneysel bulgularla karşılaştırılmıştır.

Anahtar Kelimeler: Derin Çekme İşlemi, Sıcak Şekillendirme ve Soğutma İşlemi, Sac Metal, Bölgesel Isıtma, Akma Kriteri

To my mother

## **ACKNOWLEDGMENTS**

I would like to thank my supervisor Prof. Dr. Haluk Darendeliler, for his patience and appreciate his treasured advices.

I want to thank Esra Şahin for her patience and endless supports.

## TABLE OF CONTENTS

ABSTRACT . . . . .	v
ÖZ . . . . .	vii
ACKNOWLEDGMENTS . . . . .	x
TABLE OF CONTENTS . . . . .	xi
LIST OF TABLES . . . . .	xv
LIST OF FIGURES . . . . .	xvi
CHAPTERS	
1 INTRODUCTION . . . . .	1
1.1 Motivation . . . . .	1
1.2 Background . . . . .	2
1.2.1 Hot Forming and in-die Quenching Process . . . . .	3
1.3 Objective and Scope of the Thesis . . . . .	3
1.4 Outline of the Thesis . . . . .	4
2 LITERATURE SURVEY . . . . .	7
3 CONSTITUTIVE MODELS AND FORMULATION OF THERMAL PROBLEMS . . . . .	13
3.1 Von Mises Yield Criteria with Isotropic Hardening Rule . . . . .	14
3.2 Von Mises Yield Criteria with Kinematic Hardening Rule . . . . .	16

3.3	Von Mises Yield Criteria with Combined Hardening Rule . . . . .	17
3.4	Hill48 Yield Criterion with Isotropic Hardening Rule . . . . .	18
3.5	Johnson Cook Model with von Mises Yield Criteria and Isotropic Hardening Rule . . . . .	19
3.6	YLD2003-8P Yield Criteria . . . . .	20
3.7	Formulation of Thermal Problems . . . . .	24
4	FINITE ELEMENT ANALYSIS . . . . .	25
4.1	Finite Element Method . . . . .	25
4.2	Finite Element Analysis . . . . .	25
4.3	Finite Element Models . . . . .	26
4.3.1	Cylindrical Deep Drawing . . . . .	26
4.3.2	Hemispherical Deep Drawing . . . . .	28
4.3.3	Square Deep Drawing . . . . .	30
4.3.4	Local Heating of Cylindrical Cup Drawing . . . . .	31
4.3.5	Local Heating of Complex Shape in Deep Drawing Process and HFQ . . . . .	33
5	MATERIAL DATA . . . . .	37
5.1	AA5754 and Tool Materials . . . . .	37
5.1.1	Properties and Parameters of AA5754 for Cylindrical, Hemispherical and Square Deep Drawing . . . . .	37
5.1.2	Properties and Parameters of AA5754 and Tool Material for Circular Blank of Local Heating Process . . . . .	38
5.1.3	Properties and Parameters of AA5754 and Tool Material for HFQ Process . . . . .	39
5.2	SS304 Material . . . . .	40

6	RESULTS AND DISCUSSION . . . . .	41
6.1	Results of Cylindrical Deep Drawing for AA5754 . . . . .	41
6.1.1	Thickness Strain Distributions on Cylindrical Cup Deep Drawing for AA5754 . . . . .	42
6.1.2	Variation of Punch Force with Punch Displacement on Cylindrical Cup Deep Drawing for AA5754 . . . . .	50
6.1.3	Rim Shape of Cylindrical Cup Deep Drawing for AA5754 . . . . .	56
6.2	Results of Cylindrical Deep Drawing for SS304 . . . . .	59
6.2.1	Thickness Strain Distribution on Cylindrical Cup Deep Drawing for SS304 . . . . .	59
6.2.2	Variation of Punch Force with Punch Displacement on Cylindrical Cup Deep Drawing for SS304 . . . . .	59
6.2.3	Rim Shapes of Cylindrical Cup Deep Drawing for SS304 . . . . .	61
6.3	Results of Hemispherical Deep Drawing for SS304 . . . . .	61
6.3.1	Thickness Strain Distribution on Hemispherical Cup Deep Drawing for SS304 . . . . .	62
6.3.2	Variation of Punch Force with Punch Displacement on Hemispherical Cup Deep Drawing for SS304 . . . . .	67
6.3.3	Rim Shapes of Hemispherical Cup Deep Drawing for SS304 . . . . .	71
6.4	Results of Hemispherical Deep Drawing for AA5754 . . . . .	74
6.4.1	Thickness Strain Distribution on Hemispherical Cup Deep Drawing for AA5754 . . . . .	74
6.4.2	Variation of Punch Force with Punch Displacement on Hemispherical Cup Deep Drawing for AA5754 . . . . .	75
6.4.3	Rim Shapes of Hemispherical Cup Deep Drawing for AA5754 . . . . .	76
6.5	Results of Square Deep Drawing for SS304 . . . . .	77
6.5.1	Thickness Strain Distribution on Square Cup Deep Drawing for SS304 . . . . .	77

6.5.2	Variation of Punch Force with Punch Displacement on Square Cup Deep Drawing for SS304 . . . . .	84
6.5.3	Rim Shapes of Square Cup Deep Drawing for SS304 . . . . .	87
6.6	Results of Square Deep Drawing for AA5754 . . . . .	90
6.6.1	Thickness Strain Distribution on Square Cup Deep Drawing for AA5754 . . . . .	90
6.6.2	Variation of Punch Force with Punch Displacement on Square Cup Deep Drawing for AA5754 . . . . .	91
6.6.3	Rim Shapes of Square Cup Deep Drawing for AA5754 . . . . .	92
6.7	Results of Local Heating of Cylindrical Deep Drawing . . . . .	93
6.7.1	Thickness Strain Distribution, Temperature Distribution and Rim Shapes of Local Heating Circular Blank for AA5754 . . . . .	94
6.7.2	Failure of the Deep Drawing of the Local Heating Circular Blank for AA5754 . . . . .	98
6.8	HFQ Process and Local Heating of Complex Formed Blank . . . . .	99
6.8.1	Results of Complex Formed Blank for HFQ Process . . . . .	100
6.8.2	Results of Local Heating of Complex Formed Shape . . . . .	108
7	CONCLUSIONS . . . . .	115
	REFERENCES . . . . .	117
APPENDIX		
A	THICKNESS STRAIN DISTRIBUTION AT DIFFERENT DIRECTIONS OF THE BLANK . . . . .	121

## LIST OF TABLES

### TABLES

Table 4.1	Dimensions of the tools of the cylindrical cup deep drawing [1] . . . .	26
Table 4.2	Dimensions of the tools of the hemispherical cup deep drawing [2] .	28
Table 4.3	Dimensions of the tools of the square cup deep drawing [2] . . . . .	30
Table 5.1	Mechanical properties and density of AA5754 [1] . . . . .	37
Table 5.2	Johnson Cook Parameters of AA5754 [3] . . . . .	37
Table 5.3	Lankford Parameters of AA5754 [4] . . . . .	38
Table 5.4	Thermal and mechanical properties of blank and tool material [1] and [5] . . . . .	39
Table 5.5	Material and thermal properties of blank and tools [6]. . . . .	39
Table 5.6	Mechanical Parameters of SS304 [2] . . . . .	40
Table 5.7	Lankford Parameters of SS304 [2] . . . . .	40
Table 6.1	Temperature of the tools and regions of the blank in local heating processes . . . . .	93
Table 6.2	Depth of cup at different local heating cases . . . . .	99
Table 6.3	Temperature of the tools and regions of the blank in local heating processes for complex shape . . . . .	108

## LIST OF FIGURES

### FIGURES

Figure 4.1	FE modeling of cylindrical deep drawing . . . . .	27
Figure 4.2	FE modeling of cylindrical deep drawing without blank holder .	27
Figure 4.3	Mesh Modeling of quarter circular blank (Cylindrical) . . . . .	28
Figure 4.4	FE modeling of hemispherical deep drawing . . . . .	29
Figure 4.5	FE modeling of hemispherical deep drawing without blank holder . . . . .	29
Figure 4.6	Mesh modeling of quart. of circular blank (Hemispherical) . . .	29
Figure 4.7	FE modeling of square deep drawing . . . . .	30
Figure 4.8	Mesh modeling of quarter of square blank . . . . .	31
Figure 4.9	FE modeling of cylindrical deep drawing . . . . .	32
Figure 4.10	Mesh modeling of cylindrical deep drawing . . . . .	32
Figure 4.11	(a) Initial section of the blank and tools, (b) 1st stage of the process in where BHF is applied top BH, and (c) 2nd stage of the process in where sheet metal contacts with bottom die and BHF is also applied by gas springs. [6] . . . . .	33
Figure 4.12	Assembly modeling of deep drawing of complex shape. . . . .	34
Figure 4.13	Modeling of rectangular blank. . . . .	34
Figure 4.14	Modeling of top punch. . . . .	35

Figure 4.15	Modeling of top blank holder. . . . .	35
Figure 4.16	Modeling of bottom punch. . . . .	35
Figure 4.17	Modeling of bottom die. . . . .	36
Figure 4.18	Modeling of bottom blank holder. . . . .	36
Figure 5.1	True stress-strain curve of AA5754-O at room temperature, 175°C and 250°C [1]. . . . .	38
Figure 6.1	Thickness strain distributions for different models and experiment at room temperature (AA5754-O, cylindrical, 80 mm punch travel) . . . . .	43
Figure 6.2	Thickness strain distributions for different models and experiment at 175°C (AA5754-O, cylindrical, 80 mm punch travel) . . .	43
Figure 6.3	Thickness strain distributions for different models and experiment at 250°C (AA5754-O, cylindrical, 80 mm punch travel) . .	44
Figure 6.4	Effect of temperature on thickness strain distributions for experiments with different temperatures. [1] (AA5754-O, cylindrical, 80 mm punch travel). . . . .	45
Figure 6.5	Effect of temperature on thickness strain distributions on von Mises-Isotropic (AA5754-O, cylindrical, 80 mm punch travel) . . . . .	46
Figure 6.6	Effect of temperature on thickness strain distributions on von Mises-Kinematic (AA5754-O, cylindrical, 80 mm punch travel) . . . .	47
Figure 6.7	Effect of temperature on thickness strain distributions on von Mises-Combined (AA5754-O, cylindrical, 80 mm punch travel) . . . .	47
Figure 6.8	Effect of temperature on thickness strain distributions on Hill48 criteria (AA5754-O, cylindrical, 80 mm punch travel) . . . . .	48

Figure 6.9	Effect of temperature on thickness strain distributions on YLD2003-8P Yield Criteria (AA5754-O, cylindrical, 80 mm punch travel) . . . . .	49
Figure 6.10	Punch force vs cylindrical punch displacement at room temperature for different models (AA5754-O) . . . . .	51
Figure 6.11	Punch force vs cylindrical punch displacement at 175°C for different models (AA5754-O) . . . . .	51
Figure 6.12	Punch force vs cylindrical punch displacement at 250°C for different models (AA5754-O) . . . . .	52
Figure 6.13	Punch force vs cylindrical punch displacement at different temperatures for von Mises-Isotropic (AA5754-O) . . . . .	53
Figure 6.14	Punch force vs cylindrical punch displacement at different temperatures for von Mises-Kinematic (AA5754-O) . . . . .	53
Figure 6.15	Punch force vs cylindrical punch displacement at different temperatures for von Mises-Combined (AA5754-O) . . . . .	54
Figure 6.16	Punch force vs cylindrical punch displacement at different temperatures for Hill48 Criterion (AA5754-O) . . . . .	54
Figure 6.17	Punch force vs cylindrical punch displacement at different temperatures for Johnson Cook Model (AA5754-O) . . . . .	55
Figure 6.18	Punch force vs cylindrical punch displacement at different temperatures for YLD2003-8P Yield Criterion (AA5754-O) . . . . .	55
Figure 6.19	Rim shapes of the undeformed blank and deep drawn cylindrical cup at different temperatures. (AA5754-O, VonMises-Isotropic) . . . .	56
Figure 6.20	Rim shapes of the undeformed blank and deep drawn cylindrical cup at different temperatures. (AA5754-O, VonMises-Kinematic) . . . .	57
Figure 6.21	Rim shapes of the undeformed blank and deep drawn cylindrical cup at different temperatures. (AA5754-O, VonMises-Combined) . . . .	57

Figure 6.22	Rim shapes of the undeformed blank and deep drawn cylindrical cup at different temperatures. (AA5754-O, Hill48) . . . . .	58
Figure 6.23	Rim shapes of the undeformed blank and deep drawn cylindrical cup at different temperatures. (AA5754-O, YLD2003) . . . . .	58
Figure 6.24	Effect of temperature on thickness strain distributions for YLD2003-8P Yield Criteria (SS304, cylindrical, 80 mm punch travel) .	60
Figure 6.25	Punch force vs cylindrical punch displacement at different temperatures for YLD2003-8P Yield Criteria (SS304) . . . . .	60
Figure 6.26	Rim shapes of the undeformed blank and deep drawn cylindrical cup at different temperatures. (SS304, YLD2003) . . . . .	61
Figure 6.27	Thickness strain distributions for different models and experiment at room temperature (SS304, hemispherical, 45 mm punch travel) . . . . .	62
Figure 6.28	Thickness strain distributions for different models at 300°C (SS304, hemispherical, 45 mm punch travel) . . . . .	63
Figure 6.29	Thickness strain distributions for different models at 600°C (SS304, hemispherical, 45 mm punch travel) . . . . .	64
Figure 6.30	Effect of temperature on thickness strain distributions for von Mises-Isotropic (SS304, hemispherical, 45 mm punch travel) . . . . .	64
Figure 6.31	Effect of temperature on thickness strain distributions for von Mises-Kinematic (SS304, hemispherical, 45 mm punch travel) . . . . .	65
Figure 6.32	Effect of temperature on thickness strain distributions for von Mises-Combined (SS304, hemispherical, 45 mm punch travel) . . . . .	66
Figure 6.33	Effect of temperature on thickness strain distributions for Hill48 (SS304, hemispherical, 45 mm punch travel) . . . . .	66
Figure 6.34	Effect of temperature on thickness strain distributions for YLD2003 (SS304, hemispherical, 45 mm punch travel) . . . . .	67

Figure 6.35	Punch force vs hemispherical punch displacement at room temperature for different models (SS304) . . . . .	68
Figure 6.36	Punch force vs hemispherical punch displacement at 300°C for different models (SS304) . . . . .	68
Figure 6.37	Punch force vs hemispherical punch displacement at 600°C for different models (SS304) . . . . .	69
Figure 6.38	Punch force vs hemispherical punch displacement at different temperatures for von Mises-Isotropic (SS304) . . . . .	70
Figure 6.39	Punch force vs hemispherical punch displacement at different temperatures for von Mises-Combined (SS304) . . . . .	70
Figure 6.40	Punch force vs hemispherical punch displacement at different temperatures for von Mises-Kinematic (SS304) . . . . .	70
Figure 6.41	Punch force vs hemispherical punch displacement at different temperatures for Hill48 (SS304) . . . . .	71
Figure 6.42	Punch force vs hemispherical punch displacement at different temperatures for YLD2003 (SS304) . . . . .	71
Figure 6.43	Rim shapes of the undeformed blank and deep drawn hemispherical cup at different temperatures. (SS304, VonMises-Isotropic) . . . . .	72
Figure 6.44	Rim shapes of the undeformed blank and deep drawn hemispherical cup at different temperatures. (SS304, VonMises-Kinematic) . . . . .	72
Figure 6.45	Rim shapes of the undeformed blank and deep drawn hemispherical cup at different temperatures. (SS304, VonMises-Combined) . . . . .	73
Figure 6.46	Rim shapes of the undeformed blank and deep drawn hemispherical cup at different temperatures. (SS304, Hill48) . . . . .	73

Figure 6.47	Rim shapes of the undeformed blank and deep drawn hemispherical cup at different temperatures. (SS304, YLD2003) . . . .	74
Figure 6.48	Effect of temperature on thickness strain distributions for YLD2003 (AA5754, hemispherical, 25 mm punch travel) . . . . .	75
Figure 6.49	Punch force vs hemispherical punch displacement at different temperatures for YLD2003 (AA5754) . . . . .	76
Figure 6.50	Rim shapes of the undeformed blank and deep drawn hemispherical cup at different temperatures. (AA5754, YLD2003) . . .	77
Figure 6.51	Thickness strain distributions for different models and experiment at room temperature (SS304, square, 25 mm punch travel) .	78
Figure 6.52	Thickness strain distributions for different yield criteria at 300°C (SS304, square, 25 mm punch travel) . . . . .	79
Figure 6.53	Thickness strain distributions for different yield criteria at 600°C (SS304, square, 25 mm punch travel) . . . . .	80
Figure 6.54	Effect of temperature on thickness strain distributions for von Mises-Isotropic (SS304, square, 25 mm punch travel) . . . . .	81
Figure 6.55	Effect of temperature on thickness strain distributions for von Mises-Kinematic (SS304, square, 25 mm punch travel) . . . . .	81
Figure 6.56	Effect of temperature on thickness strain distributions for von Mises-Combined (SS304, square, 25 mm punch travel) . . . . .	82
Figure 6.57	Effect of temperature on thickness strain distributions for Hill48 (SS304, square, 25 mm punch travel) . . . . .	83
Figure 6.58	Effect of temperature on thickness strain distributions for YLD2003-8P Yield Criteria (SS304, square, 25 mm punch travel) . . .	83
Figure 6.59	Punch force vs square punch displacement at room temperature for different models (SS304) . . . . .	84

Figure 6.60	Punch force vs square punch displacement at 300°C for different models (SS304) . . . . .	84
Figure 6.61	Punch force vs square punch displacement at 600°C for different models (SS304) . . . . .	85
Figure 6.62	Punch force vs square punch displacement at different temperatures for von Mises-Isotropic (SS304) . . . . .	85
Figure 6.63	Punch force vs square punch displacement at different temperatures for von Mises-Combined (SS304) . . . . .	86
Figure 6.64	Punch force vs square punch displacement at different temperatures for von Mises-Kinematic (SS304) . . . . .	86
Figure 6.65	Punch force vs square punch displacement at different temperatures for Hill48 (SS304) . . . . .	87
Figure 6.66	Punch force vs square punch displacement at different temperatures for YLD2003-8P (SS304) . . . . .	87
Figure 6.67	Rim shapes of the undeformed blank and deep drawn square cup at different temperatures. (SS304, VonMises-Isotropic) . . . . .	88
Figure 6.68	Rim shapes of the undeformed blank and deep drawn square cup at different temperatures. (SS304, VonMises-Kinematic) . . . . .	88
Figure 6.69	Rim shapes of the undeformed blank and deep drawn square cup at different temperatures. (SS304, VonMises-Combined) . . . . .	89
Figure 6.70	Rim shapes of the undeformed blank and deep drawn square cup at different temperatures. (SS304, Hill48) . . . . .	89
Figure 6.71	Rim shapes of the undeformed blank and deep drawn square cup at different temperatures. (SS304, YLD2003) . . . . .	90
Figure 6.72	Effect of temperature on thickness strain distributions for YLD2003 (AA5754, square, 25 mm punch travel) . . . . .	91

Figure 6.73	Punch force vs square punch displacement at different temperatures for YLD2003-8P (AA5754) . . . . .	92
Figure 6.74	Rim shapes of the undeformed blank and deep drawn square cup at different temperatures. (AA5754, YLD2003) . . . . .	92
Figure 6.75	Partition of the blank for local heating process. . . . .	93
Figure 6.76	Thickness strain on deformed shape in Case-1 (AA5754-O) . . . .	94
Figure 6.77	Temperature distribution on deformed shape in Case-1 (AA5754-O) . . . . .	95
Figure 6.78	Thickness strain on deformed shape in Case-2 (AA5754-O) . . . .	95
Figure 6.79	Temperature distribution on deformed shape in Case-2 (AA5754-O) . . . . .	95
Figure 6.80	Thickness strain on deformed shape in Case-4 (AA5754-O) . . . .	96
Figure 6.81	Temperature distribution on deformed shape in Case-4 (AA5754-O) . . . . .	96
Figure 6.82	Temperature distribution vs distance from center of the blank for Cases 1, 2 and 4 (AA5754-O) . . . . .	97
Figure 6.83	Thickness strain distribution vs distance from center of the blank for Cases 1, 2 and 4 (AA5754-O) . . . . .	97
Figure 6.84	Rim shapes of undeformed blank and heated locally deep drawn cylindrical cup for Cases 1, 2 and 4 (AA5754-O) . . . . .	98
Figure 6.85	Beginning of failure for cylindrical deep drawing (AA5754-O) . . .	98
Figure 6.86	(a) Formed whole sheet metal shape and trimmed part of the sheet metal and (b) section formed, highlighted by rectangle in (a). [6] .	100
Figure 6.87	Plastic thickness strain distributions for different yield criteria at 200°C (HFQ process for complex shape) . . . . .	101

Figure 6.88	Stress distribution on deformed shape at 200°C . . . . .	101
Figure 6.89	Plastic thickness strain distribution on deformed shape at 200°C .	102
Figure 6.90	Plastic thickness strain distributions for different yield criteria at 350°C (HFQ process for complex shape) . . . . .	102
Figure 6.91	Stress distribution on deformed shape at 350°C . . . . .	103
Figure 6.92	Plastic thickness strain distribution on deformed shape at 350°C .	103
Figure 6.93	Plastic thickness strain distributions for different yield criteria at 480°C (HFQ process for complex shape) . . . . .	104
Figure 6.94	Stress distribution on deformed shape at 480°C . . . . .	104
Figure 6.95	Plastic thickness strain distribution on deformed shape at 480°C .	104
Figure 6.96	Effect of temperature on thickness strain distributions for vonMises-Isotropic (HFQ process for complex shape) . . . . .	105
Figure 6.97	Effect of temperature on thickness strain distributions for vonMises - Kinematic (HFQ process for complex shape) . . . . .	105
Figure 6.98	Effect of temperature on thickness strain distributions for vonMises - Combined (HFQ process for complex shape) . . . . .	106
Figure 6.99	Effect of temperature on thickness strain distributions for Hill48 (HFQ process for complex shape) . . . . .	106
Figure 6.100	Effect of temperature on thickness strain distributions for YLD2003 (HFQ process for complex shape) . . . . .	107
Figure 6.101	Rim shapes of undeformed blank and complex formed blank with HFQ process (AA5754-O) . . . . .	107
Figure 6.102	Partition of rectangular blank. . . . .	108
Figure 6.103	Temperature distribution with blank distance along x-axis for Cases 1, 2, 3, 4 and 5 ( for complex shape-AA5754-O) . . . . .	109

Figure 6.104	Thickness strain with distance along x-axis of local heating of complex shape for Cases 1, 2, 3, 4 and 5 (AA5754-O) . . . . .	110
Figure 6.105	Stress distribution on deformed shape for Case-1 . . . . .	110
Figure 6.106	Temperature distribution on deformed shape for Case-1 . . . . .	111
Figure 6.107	Stress distribution on deformed shape for Case-2 . . . . .	111
Figure 6.108	Temperature distribution on deformed shape for Case-2 . . . . .	111
Figure 6.109	Stress distribution on deformed shape for Case-3 . . . . .	112
Figure 6.110	Temperature distribution on deformed shape for Case-3 . . . . .	112
Figure 6.111	Stress distribution on deformed shape for Case-4 . . . . .	113
Figure 6.112	Temperature distribution on deformed shape for Case-4 . . . . .	113
Figure 6.113	Stress distribution on deformed shape for Case-5 . . . . .	113
Figure 6.114	Temperature distribution on deformed shape for Case-5 . . . . .	114
Figure A.1	Thickness strain distributions of circular blank on different directions at room temperature for Hill48 (80 mm punch travel, cylindrical) . . . . .	121
Figure A.2	Thickness strain distributions of circular blank on different directions at 175°C for Hill48 (80 mm punch travel, cylindrical) . . . . .	122



# CHAPTER 1

## INTRODUCTION

### 1.1 Motivation

The manufacturing of a lot of parts, which can be from sheet metal, can be seen in many areas of industries. Different types of sheet metal forming processes are used to manufacture any designed parts from simple inexpensive tools to large parts such as aerospace structures. In most cases, some industries like automobile industry has an important role in the development and finding availability of new materials and proper processes because of a lot of metal parts used. Using aluminum alloys and steels with higher strengths allowing compact design because of a thickness reduction and lower weight begins to find its way into the automobile industry.

By means of industrial revolutions, engineers and scientists start to search to enhance the forming processes and increase quality of the production. By doing this, they have tried to find easy ways of forming of materials.

Subjects of formability and the ductility, which determine when material fails, are two important points for forming processes. Both formability and ductility of materials depend on many material parameters explained by mechanical and material engineers. To overcome the formability issue of mostly used metals warm sheet metal forming, in which process is applied at proper elevated temperatures to get production of good quality can be used. By using sheet metals at elevated temperature, it can be observed how the structural and molecular forms of the sheet metals change. At very high temperature, metals seem like fluid materials and they can be easily formed.

## 1.2 Background

Sheet metal forming process is the important manufacturing process to give a material having simple geometry to desired shape with defined dimensions. Although sheet metal forming processes are used widely in different manufacturing industries, development of the sheet metal forming suffers from expensive tools and work pieces and, because this process mostly depends on experiments. Since this process is affected by different parameters such as design-dimension of the die and tools, material properties, complexity of blank and interactions between blank and sheet metal forming tools, more iteration of experiments of this process can be needed. Moreover, there are different types of sheet metal forming processes such as deep drawing, blanking, piercing, notching, ironing, bending and hydroforming. In deep drawing process, a sheet metal called blank is installed on a die. The blank is held in position by the blank holder and it exerts a force on blank. Moreover, blank is pressed against the die cavity using punch. In this thesis, deep drawing process is focused.

During the deep drawing process, some undesired defects can be observed if proper parameters are not used. These defects can occur because of several factors such as blank holder force, geometry of the part, dimensions of the punch and die, die punch clearance, lubrication, the friction between blank and the other elements, material characteristics and contact conditions. When heating is concerned, temperature values of the blank and heating techniques are other parameters that affect the deformation during forming process.

To give nearly accurate desired shape to the material having simple geometry, proper forming parameters should be used. Temperature of the sheet metal is an important parameter because temperature affects directly ductility of the material as well molecular-atomic structure. Up to recrystallization temperature of the material, there cannot be any change in the atomic-molecular structure.

From other aspect of using deep drawing process, FE simulation takes important role because if FEA (finite element analysis) is used effectively, there will be little need to use experiments and scrap will be reduced significantly.

### **1.2.1 Hot Forming and in-die Quenching Process**

In heat forming and in-die quenching (HFQ) process is such a technology, the sheet metal heated up to solution heat treatment (SHT) temperature. The solubility of the used solid increases at SHT temperature, moreover; the alloying elements dissolve into the aluminum matrix. The yield stress of the used sheet material decreases because dislocation movement takes place more easily. Hence, used material becomes more ductile and any complex shape can be easily formed. Then, the sheet metal is formed at a high speed. After that quenching process takes place for that reason formed part is cooled to room temperature. The quenching process enable to increase the yield stress and strength of the formed part and obtain supersaturated solid solution.

### **1.3 Objective and Scope of the Thesis**

The objective of the thesis is to investigate the effects of the temperature variation on deformed sheet material in deep drawing process by using different yield criteria and hardening models. By comparing simulation results at different temperatures with experimental results, it is be decided which yield criterion gives closer results to experimental ones. Von-Mises, Hill48 and Yld2003 yield criteria are used in this study. Simulation of cylindrical, hemispherical and square cup drawing processes are modeled for homogeneous heating of sheet metal. Both AA5754-O and SS304 materials properties are used for these three types of deep drawing processes. Sheet material with 1.2 mm thickness is modelled for cylindrical cup drawing and sheet material with 1 mm thickness is modelled for hemispherical and square cup drawing.

Numerical analyses of AA5754-O and SS304 sheet materials for cylindrical cup drawing are carried out at room temperature, 175°C and 250°C and analyses of SS304 sheet material are carried out for cylindrical, hemispherical and square parts at room temperature, 300°C and 600°C. Moreover, analyses of AA5754 sheet material are carried out for hemispherical and square parts at room temperature, 300°C and 520°C. Temperature value of 600°C cannot be used for AA5754-O sheet materials because melting point of the AA5754 materials is 600°C and ductility of aluminum is

higher than stainless steel. Thickness strain and punch force variations with punch displacements are compared for all analyses cases. Rim shapes of the deformed blanks are also shown.

In this thesis, local heating process of the sheet material is also investigated. Circular and complex shaped parts are used for local heating process. Mechanical and thermal properties of AA5754-O sheet material and tools of drawing process are used for all cases. By allowing the heat transfer between blank and tools in analyses, the temperature and thickness strain variations with local heating of sheet metal are observed. Local region of sheet metal aims to get more uniform thickness strain variations.

The Johnson-Cook failure criterion is used to investigate the drawability of the locally heated circular blanks in cylindrical deep drawing process. For these cases, the blank holder forces are increased to cause failure of the sheet materials.

For the complex shaped part made of AA5754-O, HFQ process is investigated. Homogeneous heating of the blank used in the complex shaped part analyses is carried out at 200°C, 350°C and 480°C and effects of temperature on thickness strain distribution are investigated. Quenching process is not analyzed since quenching process only changes the strength of the materials, without any forming simulations.

#### **1.4 Outline of the Thesis**

This study includes six chapters. In chapter 1, a brief introduction is given about the subject of the thesis. Information about deep drawing, heat forming and in-die quenching (HFQ) processes are presented and, objective and scope of the thesis are mentioned. In Chapter 2, information about the literature survey related to effects of elevated temperatures on deep drawing processes in which local and homogeneous heating of blank is taken into consideration, HFQ process, different heating techniques and implementation of yield criteria and hardening rules to FE (finite element) software for cup deep drawing processes and the comparison of the simulation results with the experiment results, will be given. After that constitutive models and formulas of yield criteria and hardening rules will be given in chapter

3. After that, detailed information about finite element method will be given. Finite element models of three different types of deep drawing processes, which are cylindrical, hemispherical and square deep drawings, will be presented. Modelling and tooling of local heating of circular and complex shaped blanks will be shown in Chapter 4. HFQ process on the same complex shape will be also expressed in Chapter 4. Material properties of AA5754, SS304 and tool materials are presented in Chapter 5. Obtained results from numerical finite element analyses and experimental results taking from before studies will be shown in graphics; moreover, rim shapes of deformed sheet materials also will be available in chapter 6. In chapter 7, conclusions of the results are presented. Finally, the Appendix contains the thickness strain distributions at different directions of circular blank for Hill48 yield criterion.



## CHAPTER 2

### LITERATURE SURVEY

This section of the thesis is reserved on the research works related to the effects of elevated temperature on deep drawing process, heating techniques of sheet materials, HFQ process, hardening rules, yield criteria, finite element analysis, constitutive models used in deep drawing and comparison of the results of simulation and experiments.

Abedrabbo et al. [7] have developed a temperature dependent, anisotropic yield criterion to show formability of two different aluminum alloys (5182 and 5754) used in automobile industry by the finite element analysis. The anisotropy coefficients of the YLD2000-2d model [8] for different temperatures from 25°C to 260°C have been determined experimentally. At this temperature range, the FEA of the sheet metal forming process was carried out by a coupled thermo mechanical model; moreover, this temperature dependent and anisotropic model is implemented LS-DYNA as UMAT. Authors have used two different failure criteria which are strain and stress-based FLD. After optimization procedure, the best evaluation is obtained for the temperature values of the punch, blank, upper and lower dies as 25.85°C, 53.85°C and 63.85°C respectively. Moreover, simulation results have confirmed the experimental results.

In the study of Basril et al. [9], the effect of heating temperature and heating methods towards the formability of square metal cup deep drawing process has been investigated experimentally. In deep drawing process, room temperature may cause poor formability and failure because of high strength of materials at room temperature. Different sizes of square blanks, which are aluminum, mild steel and stainless steel (SS), were deep drawn at four different temperatures. Three different

heating techniques were used; heating die only, heating punch only and heating both die and punch. In this study, by comparing thickness distribution and using an optimization technique, combination of using SS with size 45 mm and die heating at 150°C gave the optimal result to get uniform thickness distribution of square blank.

Warm deep drawing of magnesium alloy sheet has attracted in recent years. Chang et al. [10] have investigated limiting drawing ratio (LDR) of AZ31 magnesium alloy sheet by performing experiment and simulations by the finite element method. Since the magnesium alloy is very sensitive to forming temperature, forming processes were performed at different temperatures. The AZ31 magnesium alloy sheet fractures at earlier temperatures values lower than 150°C and cracks occurred at the round corner of die during the experiments. Authors have seen that this sheet has shown good formability at temperatures in the range of 200°C and 300°C and LDR can reach 3.0 and cracks occurred at the round corner of the punch. However, at forming temperature of 150°C, LDR can reach 2.0. the authors obtained a good agreement between the results of simulation and experiments in this study. The other study using same material about effects of temperature and punch and die corner radii on the formability of square cup deep drawing has been investigated by Chen et al. [11]. In this study, tensile tests at various temperatures in the range room temperature to 400°C were performed. Forming limit tests were performed at 100, 200 and 300°C and by looking FLD, when the forming limit curve is higher, the formability of specimen becomes better. For warm square deep drawing process, FE simulations and experiment results were compared and a good agreement between them was obtained. Both experimental and finite element simulation results indicated that the optimum forming temperature is about 200°C for the square cup deep drawing in which maximum depth drawn was obtained. Similar research has been done by Zhang et al. [12] for warm deep drawing magnesium alloy at elevated temperatures. They have declared that magnesium alloy sheet is used in different industrial area such as automobile and electric industry, and these sheet metals are generally formed at temperatures between 200°C to 400 °C since this material has low formability at room temperature. In the study, effects of blank holder force and temperature has been investigated and internal heating method has been used. Blank is heated by using electric heater inside the die. It has been concluded that proper forming temperature

range is between 105°C and 170 °C. Limit drawing ratio has exceeded 2.0 at 140 °C and the limit drawing ratio has reached 2.6 at 170 °C

Ethiraj et al. [13] developed a new technique to calculate thickness variation in warm deep drawn circular cup. Used blank was made of AISI 304 stainless steel which was drawn at different elevated temperatures below the recrystallization temperature. To get stress-strain curve at different temperature, Hollomon equation is used. For four different temperatures, the new technique gives good results when compared with experimental result. In Kotkunde et al.'s study, 5 different anisotropic yield criteria are implemented for FE simulation of warm deep drawing [14]. Deep drawing process is carried out at 400°C for Ti6Al4V alloy sheet metal. Yield criteria and experimental results are compared in terms of different points, one of which is thickness variation. Results of Cazacu Barlat yield criteria gives good correlation with experimental result with respect to thickness variation. In the other study about failure and formability of Ti6Al4V alloy sheet that has been done by Kotkunde et al. [15]. The experiments has been carried out at temperature range between room temperature and 400°C. Below 150°C it was observed that formability of this material is very poor. Failure of drawn cup has been seen nearly at the same regions, that are neck and upper wall, for both FE simulation and experiment. They have been observed that maximum LDR 1.8 is obtained at 400°C and more uniform thickness variation is obtained at about 200°C. Furthermore, in Jayahari et al. work, stainless steel 304 sheet metal is drawn using warm deep drawing at three different temperatures [16]. In this study, effects of many parameters on this process have been investigated. Results of experiments, which were performed at three different temperatures and strain rates, were compared with each other by using punch load. In the study of Reddy et al. results of experimental and numerical analyses of the square cup drawn processes have been compared with respect to punch force, thickness distribution and dome height for three different materials that are aluminum, AISI 304 and brass [17]. In FE simulation, Hill48 yield criterion has been used. To draw sheet metal, the needed punch force was found more for AISI 304 when compared to other two materials. Thickness variation is nearly same for all materials; however, only slight variation can be seen for aluminum. The maximum stress was found higher for AISI 304 than for other two materials.

Laurent et al. have studied on effects of temperature and friction coefficients on deep

drawing process of AA5754-O alloy sheet [5]. Both numerical and experimental results are compared. All experiments and analyses have been carried out at temperatures from room temperature to 200°C. By using coupled thermo-mechanical FE model, FEA has been carried out and in these analyses, different yield criteria such as von Mises and Hill48 were used, and blank was modeled with heated die and blank holder. Punch force decreased greatly by temperature of above 150°C.

Fakir et al. studied HFQ process for AA5754-O material numerically [6]. Good correlation was obtained between simulated and experimentally formed shape with respect to thickness distribution. Moreover, effects of forming temperature and forming speed on the thickness distribution of the HFQ part. It was observed that higher forming speed is more beneficial for HFQ forming since it led to less thinning and more uniform shape. For these results, analyses and experiments were carried out at temperature of 200°C, 350°C and 480°C and at speeds of 250 mm/s, 500 mm/s and 750 mm/s. Temperature of 480°C is SHT temperature. For FE model, the used initial blank shape was rectangular and for HFQ process, to include deformation and heat transfer mechanisms, 8-node thermally coupled brick elements (C3D8T) were used. Zheng et al. [18] have investigated two different aluminum alloys that are AA6082 and AA7075. HFQ process was carried out with respect to time and temperature ranging from 250°C to 400°C. For AA7075 material, normalized stress level for ageing at 400°C was found highest however, ageing at 350°C was the lowest during 10s holding time. This situation was related to coarse precipitation. Moreover, to form the AA6082 material easily, holding time was increased above 10s. Ying et al. have investigated Interfacial-Heat-Transfer-Coefficient (IHTC) between aluminum alloy and cylindrical die for AA7075-T6. In this study, Beck's and heat balance methods were compared. Surface roughness, contact pressure and surface lubrication affect the IHTC. In order to verify the IHTC attained by heat transfer model, the U-type model test was applied. In this U-type test, pressing pressure, which is the normal pressure on the model, was about 10 MPa and temperature data from the blank was collected by using K-type thermocouples. For simulation, COMSOL Multi-physics was used. Temperature history results were compared with the experimental results. It was observed that, when the contact pressure was in the range between 30-80 MPa, the IHTC increases with increasing contact pressure,

when contact pressure is high and roughness is small, IHTC decreases with increasing surface roughness and when the heat conductivity of the lubricant is larger than air, IHTC increases since contact area and heat transfer efficiency increase. Fan et al. have studied on hot forming quenching process of 6A02 aluminum alloy sheet [19]. While used dies were at room temperature in most of the studies related to HFQ process, temperature of the dies were ranging from 50°C to 350°C in this study. Up to 250°C, important decrease of strength of material was not obtained. With increasing temperature from 250°C to 350°C, tensile and yield stress of the material decreased. The first step of the experiment was heating the sheet metal up to SHT. After that sheet metal was placed into warm dies quickly and formed into the required shape. Then the formed part was held about 5-10s in warm die to reduce its temperature to the forming-die temperature and then removed for air cooling at the room temperature. Final step was aging of the formed part to get the full strength. It was concluded that temperature of the forming-dies can be increased to 250°C for HFQ integrated forming process of 6A02 aluminum alloy sheet to obtain enough strength and formability.



## CHAPTER 3

### CONSTITUTIVE MODELS AND FORMULATION OF THERMAL PROBLEMS

For most of the materials, there are two modes of behavior under loading. Elastic behavior is the mechanical behavior during which the materials return to initial dimensions upon release of the load. After yield point, plastic behavior of the materials start and part of the deformation on the specimen is permanent. This plastic deformation does not disappear upon release the load.

Stress states can be calculated using Hooke's Law up to yield point for linear elastic response. However, after initial yield, plastic deformation starts and stress increases nonlinearly.

The relationship among the stresses which predict the yielding of a material is called yield criterion. There are many different yield criteria to express stress states. Yield criteria can be isotropic or anisotropic. During process, if material has same material properties in all directions, it is called isotropic yielding. However, for most of the process, the material does not have same behavior in all directions. This type of material is defined as anisotropic material.

The other important issue is hardening model in sheet metal forming process. The material becomes stronger after getting worked upon during plastic deformation. Hardening rules basically determine the behavior of the yield surface. Yield strength of the material increases after plastic working which is called work or strain hardening. In isotropic work hardening, yield strength enhances uniformly in all direction and yield surface gets stretched out uniformly all around. When yield surface remains same shape and size but it translates in the stress space, this

type of hardening model is called kinematic hardening model. There is another work hardening which includes both isotropic and kinematic hardening rules called combined hardening model. In this hardening rule, yield surface of material expands and translates.

For plastic deformation, constitutive equations, which define the relation between stress and strain, must include three typical properties that are hardening rule, flow rule and yield function.

Flow rule is about the relationship between stresses and strains in plastic region and relates increment of plastic deformation to increment of stresses. General form of the flow rule is given in as:

$$d\varepsilon_{ij}^p = d\lambda \frac{\partial Q}{\partial \sigma_{ij}} \quad (3.1)$$

where  $d\lambda$  is called plastic multiplier,  $\varepsilon_{ij}^p$  is plastic strain,  $\sigma_{ij}$  is stress tensor and function  $Q$  is the plastic potential.

The yield criterion is a scalar function related to stress and internal variables. It is used for calculation of yield stress of a material under any stresses. General function of the yield criteria is

$$f(\sigma, \xi) = 0 \quad (3.2)$$

where  $\xi$  corresponds history dependent scalar and tensor internal variable.

### 3.1 Von Mises Yield Criteria with Isotropic Hardening Rule

Isotropic hardening expresses the expanding of yield surface which stays in the same shape.

$$f = F(J_2', J_3') - K(\alpha) \quad (3.3)$$

where  $J_2'$  and  $J_3'$  are the invariants of the deviatoric stress tensor and  $K$  is a function of  $\alpha$  which characterizes the hardening. When  $F(J_2', J_3')$  is assumed to be von Mises

yield function,

$$f = J_2' - \frac{1}{3}\sigma_y^2 \quad (3.4)$$

where  $J_2'$  is the second invariant of the stress deviator and  $\sigma_y$  is yield strength as a function of  $\alpha$ . In cartesian form, the von Mises yield surface is expressed as,

$$(\sigma_{33} - \sigma_{22})^2 + (\sigma_{11} - \sigma_{33})^2 + (\sigma_{11} - \sigma_{22})^2 + 6(\sigma_{23}^2 + \sigma_{13}^2 + \sigma_{12}^2) = 2\bar{\sigma}^2 \quad (3.5)$$

In plastic flow, using the consistency as below,

$$df = 0 \quad (3.6)$$

$$df = \frac{\partial f}{\partial \sigma_{ij}} d\sigma_{ij} - \frac{\partial f}{d\bar{\varepsilon}^P} d\bar{\varepsilon}^P = 0 \quad (3.7)$$

For von Mises yield criterion,

$$\frac{\partial f}{\partial \sigma_{ij}} = \frac{3}{2} \frac{\sigma_{ij}}{\bar{\sigma}} \quad (3.8)$$

Then,

$$\frac{3}{2} \frac{\sigma_{ij}}{\bar{\sigma}} d\sigma_{ij} - \frac{\partial f}{d\bar{\varepsilon}^P} d\bar{\varepsilon}^P = 0 \quad (3.9)$$

$$d\bar{\varepsilon}^P = \frac{\frac{3}{2} \frac{\sigma_{ij}}{\bar{\sigma}} d\sigma_{ij}}{\frac{\partial f}{d\bar{\varepsilon}^P}} \quad (3.10)$$

By using general flow rule, simple relation between  $d\lambda$  and  $d\bar{\varepsilon}^P$ :

$$d\bar{\varepsilon}^P = \sqrt{\frac{2}{3} d\lambda \frac{\partial f}{\partial \sigma_{ij}} d\lambda \frac{\partial f}{\partial \sigma_{ij}}} = d\lambda \sqrt{\frac{2}{3} \frac{3}{2} \frac{\sigma_{ij}}{\bar{\sigma}} \frac{3}{2} \frac{\sigma_{ij}}{\bar{\sigma}}} = d\lambda \sqrt{\frac{\frac{3}{2} \sigma_{ij} \sigma_{ij}}{\bar{\sigma}^2}} \quad (3.11)$$

$d\lambda$  used in Eq. 3.11 can be expressed as in Eq. 3.12.

$$d\lambda = \frac{\frac{3}{2} \frac{\sigma_{ij}}{\bar{\sigma}} d\sigma_{ij}}{\frac{\partial f}{d\bar{\varepsilon}^P}} \quad (3.12)$$

By combining Eq. 3.8, Eq. 3.1 and Eq. 3.12, and obtained Eq. 3.13 gives increment of plastic strain.

$$d\varepsilon_{ij}^P = \frac{9}{4} \frac{\sigma_{kl} d\sigma_{kl}}{\frac{\partial f}{d\bar{\varepsilon}^P} \bar{\sigma}^2} \sigma_{ij} \quad (3.13)$$

### 3.2 Von Mises Yield Criteria with Kinematic Hardening Rule

When yield surface stays in same shape and size but it translates in the space, this type of hardening model is called kinematic hardening model. In this hardening model, Bauschinger effect is considered, because resistance of material for each loading in opposite direction reduces.

$$f = f(\sigma_{ij}, \alpha_{ij}) = \bar{\sigma}(\sigma_{ij} - \alpha_{ij}) - \sigma_s \quad (3.14)$$

For this hardening model, von Mises yield criterion can be written as in Eq. the above equation,  $\alpha_{ij}$  is second order tensor and called as backstress and  $\sigma_s$  is the initial yield stress. Eq. 3.16 and Eq. 3.17 represent for Prager and Ziegler formulas. Note that in ABAQUS, Prager-Ziegler linear kinematic model is used. Moreover,  $c^{(k)}$  is a constant.

$$\alpha_{ij} = \alpha_{ij}(\varepsilon_{kl}^P) \quad (3.15)$$

Prager equation is

$$d\alpha_{ij} = c^{(k)} d\varepsilon_{ij}^P \quad (3.16)$$

Whereas Ziegler equation is defined as

$$d\alpha_{ij} = d\mu(\sigma_{ij} - \alpha_{ij}) \quad (3.17)$$

here

$$d\mu = d\mu(\varepsilon_{kl}^p) \quad (3.18)$$

Writing backstress in terms of plastic strain

$$\alpha_{ij} = c^{(k)} \varepsilon_{ij}^p \quad (3.19)$$

and

$$\alpha_{kk} = c^{(k)} \varepsilon_{kk}^p = 0 \quad (3.20)$$

By using the consistency condition  $df = 0$  and then differentiation of  $f$  and fundamental normality rule give

$$df = \frac{\partial f}{\partial \sigma_{ij}} d\sigma_{ij} - \frac{\partial f}{\partial \sigma_{ij}} \frac{\partial \alpha_{ij}}{\partial \varepsilon_{kl}^p} \varepsilon_{kl}^p = \frac{\partial f}{\partial \sigma_{ij}} d\sigma_{ij} - \frac{\partial f}{\partial \sigma_{ij}} \frac{\partial \alpha_{ij}}{\partial \varepsilon_{kl}^p} d\lambda \frac{\partial f}{\partial \sigma_{kl}} \quad (3.21)$$

and

$$d\lambda = \frac{\frac{\partial f}{\partial \sigma_{mn}} d\sigma_{mn}}{\frac{\partial f}{\partial \sigma_{ij}} \frac{\partial \alpha_{ij}}{\partial \varepsilon_{kl}^p} \frac{\partial f}{\partial \sigma_{kl}}} \quad (3.22)$$

Finally, the plastic strain increment is obtained from the flow equation.

$$d\varepsilon_{kl}^p = d\lambda \frac{\partial f}{\partial \sigma_{ij}} = \frac{\frac{\partial f}{\partial \sigma_{mn}} d\sigma_{mn}}{\frac{\partial f}{\partial \sigma_{pq}} \frac{\partial \alpha_{pq}}{\partial \varepsilon_{kl}^p} \frac{\partial f}{\partial \sigma_{kl}}} \frac{\partial f}{\partial \sigma_{ij}} \quad (3.23)$$

### 3.3 Von Mises Yield Criteria with Combined Hardening Rule

Combined hardening rule is the combination of both isotropic and kinematic hardening rules. In this hardening rule, yield surface of the material both expands and translates. General form of combined hardening rule is shown below

$$f(\sigma_{ij}, K_i) = f_0(\sigma_{ij} - \alpha_{ij}) - K \quad (3.24)$$

where  $K$  and  $\alpha_{ij}$  are scalar hardening parameters. The combined hardening rule can be corresponded to use with von Mises yield criterion as

$$(\sigma_{ij} - \alpha_{ij})(\sigma_{ij} - \alpha_{ij}) = \frac{2}{3} \bar{\sigma}^2 \quad (3.25)$$

### 3.4 Hill48 Yield Criterion with Isotropic Hardening Rule

Hill48 is an anisotropic yield criterion and function of it is a quadratic function as given below

$$2f(\sigma_{ij}) = F(\sigma_{33}-\sigma_{22})^2 + G(\sigma_{11}-\sigma_{33})^2 + H(\sigma_{22}-\sigma_{11})^2 + 2L(\sigma_{23})^2 + 2M(\sigma_{31})^2 + 2N(\sigma_{12})^2 - 1 \quad (3.26)$$

where the constants can be determined as

$$2F = \frac{1}{Z^2} + \frac{1}{Y^2} - \frac{1}{X^2} \quad (3.27)$$

$$2G = \frac{1}{Z^2} + \frac{1}{X^2} - \frac{1}{Y^2} \quad (3.28)$$

$$2H = \frac{1}{Y^2} + \frac{1}{X^2} - \frac{1}{Z^2} \quad (3.29)$$

$$2L = \frac{1}{R^2} \quad (3.30)$$

$$2M = \frac{1}{S^2} \quad (3.31)$$

$$2N = \frac{1}{T^2} \quad (3.32)$$

It should be defined that  $X$ ,  $Y$  and  $Z$  are tensile yield stresses in  $x$ ,  $y$  and  $z$  axis; moreover,  $R$ ,  $S$  and  $T$  are yield stresses for pure shear stresses with respect to orthogonal planes of anisotropy  $yz$ ,  $xz$  and  $xy$ .

In formulation of Hill48 yield criteria, Lankford parameters can also be used. A Lankford parameter is represented by  $r_{\Theta}$  which is equal to ratio of width to thickness strain and  $\Theta$  shows the angle from rolling direction. Then using Lankford parameters in  $0^\circ$ ,  $45^\circ$  and  $90^\circ$

$$r_0 = \frac{H}{G} \quad (3.33)$$

$$r_{45} = \frac{N}{F+G} - \frac{1}{2} \quad (3.34)$$

$$r_{90} = \frac{H}{F} \quad (3.35)$$

$$r = \frac{d\varepsilon_w^p}{d\varepsilon_t^p} \quad (3.36)$$

$$r_\theta = \frac{\frac{\partial F(\sigma_{ij})\sin^2\theta}{\partial\sigma_{xx}} + \frac{\partial F(\sigma_{ij})\cos^2\theta}{\partial\sigma_{yy}} - 2\frac{\partial F(\sigma_{ij})\sin\theta\cos\theta}{\partial\sigma_{xy}}}{\frac{\partial F(\sigma_{ij})}{\partial\sigma_{xx}} + \frac{\partial F(\sigma_{ij})}{\partial\sigma_{yy}}} \quad (3.37)$$

The yield criterion can be written as

$$\sigma_{xx}^2 - \frac{2r_0}{1+r_0}\sigma_{xx}\sigma_{yy} + \frac{r_0(1+r_{90})}{r_{90}(1+r_0)}\sigma_{yy}^2 + \frac{r_0+r_{90}}{r_{90}(1+r_{90})}(2r_{45}+1)\sigma_{xy}^2 = \sigma_Y^2 \quad (3.38)$$

### 3.5 Johnson Cook Model with von Mises Yield Criteria and Isotropic Hardening Rule

This plasticity model [20] describes the flow stress depending on strain, strain rate and temperature as given below

$$\sigma = (A + B\varepsilon^n)(1 + C\ln(\frac{\dot{\varepsilon}}{\dot{\varepsilon}_{ref}}))(1 - (\frac{T - T_{ref}}{T_m - T_{ref}})^m) \quad (3.39)$$

$$\varepsilon^* = \frac{\dot{\varepsilon}}{\dot{\varepsilon}_{ref}} \quad (3.40)$$

$$T^* = \frac{T - T_{ref}}{T_m - T_{ref}} \quad (3.41)$$

In this model,  $A$ ,  $B$ ,  $C$ ,  $n$  and  $m$  are constant parameters, and  $\varepsilon$ ,  $\dot{\varepsilon}$ ,  $\dot{\varepsilon}_{ref}$ ,  $T$ ,  $T_m$  and  $T_{ref}$  correspond strain and temperature dependent parameters. Johnson Cook model is available in Abaqus package program.

### 3.6 YLD2003-8P Yield Criteria

This yield criterion has a plane stress yield function and it contains eight anisotropy parameters which are  $a_1, \dots, a_8$ .

$$|\sigma_1'|^m + |\sigma_2'|^m + |\sigma_1'' - \sigma_2''|^m = 2Y_{ref}^m \quad (3.42)$$

where  $Y_{ref}$  is reference yield stress of used material and  $m$  is material constant depends on the material crystal structure;  $m$  is either 6 or 8 for BCC and FCC crystal structures, respectively. Moreover, for von Mises yield criteria, values of eight anisotropy parameters are same and equal to 1, and  $m=2$ . The stress values  $\sigma_1'$ ,  $\sigma_2'$ ,  $\sigma_1''$  and  $\sigma_2''$  can be written as

$$\sigma_1' = \frac{a_8\sigma_{11} + a_1\sigma_{22}}{2} + \sqrt{\left(\frac{a_2\sigma_{11} - a_3\sigma_{22}}{2}\right)^2 + a_4\sigma_{21}\sigma_{12}} \quad (3.43)$$

$$\sigma_2' = \frac{a_8\sigma_{11} + a_1\sigma_{22}}{2} - \sqrt{\left(\frac{a_2\sigma_{11} - a_3\sigma_{22}}{2}\right)^2 + a_4\sigma_{21}\sigma_{12}} \quad (3.44)$$

$$\sigma_1'' = \frac{\sigma_{11} + \sigma_{22}}{2} + \sqrt{\left(\frac{a_5\sigma_{11} - a_6\sigma_{22}}{2}\right)^2 + a_7\sigma_{21}\sigma_{12}} \quad (3.45)$$

$$\sigma_2'' = \frac{\sigma_{11} + \sigma_{22}}{2} - \sqrt{\left(\frac{a_5\sigma_{11} - a_6\sigma_{22}}{2}\right)^2 + a_7\sigma_{21}\sigma_{12}} \quad (3.46)$$

where

$$\sigma_{11} = Y_\varphi \cos^2 \varphi \quad (3.47)$$

$$\sigma_{22} = Y_\varphi \sin^2 \varphi \quad (3.48)$$

$$\sigma_{21} = \sigma_{11} = Y_\varphi \sin^2 \varphi \cos^2 \varphi \quad (3.49)$$

$$f(a_i, \sigma) = \bar{\sigma}(a_i, \sigma) - Y_{ref} \leq 0 \quad (3.50)$$

For this yield function, the equivalent stress is,

$$\bar{\sigma}(a_i, \sigma) = \left( \frac{|\sigma_1'|^m + |\sigma_2'|^m + |\sigma_1'' - \sigma_2''|}{2} \right)^{1/m} \quad (3.51)$$

The directional r value is,

$$r_\varphi = - \frac{\sin^2 \varphi \left( \frac{\partial f}{\partial \sigma_{11}} \right) - \sin 2\varphi \left( \frac{\partial f}{\partial \sigma_{12}} \right) + \cos^2 \varphi \left( \frac{\partial f}{\partial \sigma_{22}} \right)}{\left( \frac{\partial f}{\partial \sigma_{11}} \right) + \left( \frac{\partial f}{\partial \sigma_{22}} \right)} \Bigg|_{\sigma_\varphi} \quad (3.52)$$

where  $\varphi$  is the angle from rolling direction. The equibiaxial r-value is defined as:

$$r_b = \frac{\left( \frac{\partial f}{\partial \sigma_{22}} \right)}{\left( \frac{\partial f}{\partial \sigma_{11}} \right)} \Bigg|_{\sigma_b} \quad (3.53)$$

in the above equation  $\sigma_b$  is balanced biaxial yield stress. Then the following equations can be written for different directions.

$$\bar{\sigma}(\sigma_0, a_1, \dots, a_8) - Y_{ref} = 0 \quad (3.54)$$

$$\bar{\sigma}(\sigma_{45}, a_1, \dots, a_8) - Y_{ref} = 0 \quad (3.55)$$

$$\bar{\sigma}(\sigma_{90}, a_1, \dots, a_8) - Y_{ref} = 0 \quad (3.56)$$

$$r_0(\sigma_0, a_1, \dots, a_8) - r_0^{exp} = 0 \quad (3.57)$$

$$r_{45}(\sigma_{45}, a_1, \dots, a_8) - r_{45}^{exp} = 0 \quad (3.58)$$

$$r_{90}(\sigma_{90}, a_1, \dots, a_8) - r_{90}^{exp} = 0 \quad (3.59)$$

$$r_b(\sigma_b, a_1, \dots, a_8) - r_b^{exp} = 0 \quad (3.60)$$

The normality rule given as

$$\Delta \varepsilon_{ij}^p = \Delta \lambda \frac{\partial f}{\partial \sigma_{ij}} \quad (3.61)$$

$$f = \frac{\bar{\sigma}^m}{Y_{ref}^m} - 1 = \frac{\dot{\sigma}}{Y_{ref}^m} - 1 \quad (3.62)$$

$$\dot{\sigma} = \frac{|\sigma_1'|^m + |\sigma_2'|^m + |\sigma_1'' - \sigma_2''|^m}{2} \quad (3.63)$$

General form of the derivative can be obtained as in following:

$$\frac{\partial f}{\partial \sigma_{ij}} = \frac{\partial f}{\partial \dot{\sigma}} \left[ \frac{\partial \dot{\sigma}}{\partial \sigma_1'} \frac{\partial \sigma_1'}{\partial \sigma_{ij}} + \frac{\partial \dot{\sigma}}{\partial \sigma_2'} \frac{\partial \sigma_2'}{\partial \sigma_{ij}} + \frac{\partial \dot{\sigma}}{\partial \sigma_1''} \frac{\partial \sigma_1''}{\partial \sigma_{ij}} + \frac{\partial \dot{\sigma}}{\partial \sigma_2''} \frac{\partial \sigma_2''}{\partial \sigma_{ij}} \right] \quad (3.64)$$

$$\frac{\partial f}{\partial \dot{\sigma}} = \frac{1}{Y_{ref}^m} \quad (3.65)$$

$$\frac{\partial f}{\partial Y} = -m \frac{\dot{\sigma}}{Y_{ref}^{m+1}} \quad (3.66)$$

$$\frac{\partial \dot{\sigma}}{\partial \sigma_1'} = \frac{1}{2} m |\sigma_1'|^{m-1} a \begin{cases} \sigma_1' > 0 \Rightarrow a = 1 \\ \sigma_1' < 0 \Rightarrow a = -1 \end{cases} \quad (3.67)$$

$$\frac{\partial \dot{\sigma}}{\partial \sigma_2'} = \frac{1}{2} m |\sigma_2'|^{m-1} b \begin{cases} \sigma_2' > 0 \Rightarrow b = 1 \\ \sigma_2' < 0 \Rightarrow b = -1 \end{cases} \quad (3.68)$$

$$\frac{\partial \dot{\sigma}}{\partial \sigma_1''} = \frac{1}{2} m |\sigma_1'' - \sigma_2''|^{m-1} \quad (3.69)$$

$$\frac{\partial \delta}{\partial \sigma_2''} = \frac{1}{2} m |\sigma_1'' - \sigma_2''|^{m-1} \quad (3.70)$$

$$\frac{\partial \sigma_1'}{\partial \sigma_{11}} = \frac{1}{2} a_8 + \frac{1}{2} \left[ \left( \frac{a_2 \sigma_{11} - a_3 \sigma_{22}}{2} \right)^2 + a_4^2 \sigma_{12}^2 \right]^{-1/2} \left( \frac{a_2^2 \sigma_{11} - a_3 a_2 \sigma_{22}}{2} \right) \quad (3.71)$$

$$\frac{\partial \sigma_1'}{\partial \sigma_{22}} = \frac{1}{2} a_1 + \frac{1}{2} \left[ \left( \frac{a_2 \sigma_{11} - a_3 \sigma_{22}}{2} \right)^2 + a_4^2 \sigma_{12}^2 \right]^{-1/2} \left( \frac{a_3^2 \sigma_{11} - a_3 a_2 \sigma_{11}}{2} \right) \quad (3.72)$$

$$\frac{\partial \sigma_1'}{\partial \sigma_{12}} = \frac{1}{2} \left[ \left( \frac{a_2 \sigma_{11} - a_3 \sigma_{22}}{2} \right)^2 + a_4^2 \sigma_{12}^2 \right]^{-1/2} (2a_4^2 \sigma_{12}) \quad (3.73)$$

$$\frac{\partial \sigma_2'}{\partial \sigma_{11}} = \frac{1}{2} a_8 - \frac{1}{2} \left[ \left( \frac{a_2 \sigma_{11} - a_3 \sigma_{22}}{2} \right)^2 + a_4^2 \sigma_{12}^2 \right]^{-1/2} \left( \frac{a_2^2 \sigma_{11} - a_3 a_2 \sigma_{22}}{2} \right) \quad (3.74)$$

$$\frac{\partial \sigma_2'}{\partial \sigma_{22}} = \frac{1}{2} a_1 - \frac{1}{2} \left[ \left( \frac{a_2 \sigma_{11} - a_3 \sigma_{22}}{2} \right)^2 + a_4^2 \sigma_{12}^2 \right]^{-1/2} \left( \frac{a_3^2 \sigma_{11} - a_3 a_2 \sigma_{11}}{2} \right) \quad (3.75)$$

$$\frac{\partial \sigma_2'}{\partial \sigma_{12}} = \frac{1}{2} \left[ \left( \frac{a_2 \sigma_{11} - a_3 \sigma_{22}}{2} \right)^2 + a_4^2 \sigma_{12}^2 \right]^{-1/2} (2a_4^2 \sigma_{12}) \quad (3.76)$$

$$\frac{\partial \sigma_1''}{\partial \sigma_{11}} = \frac{1}{2} + \frac{1}{2} \left[ \left( \frac{a_5 \sigma_{11} - a_6 \sigma_{22}}{2} \right)^2 + a_7^2 \sigma_{12}^2 \right]^{-1/2} \left( \frac{a_5^2 \sigma_{11} - a_6 a_5 \sigma_{22}}{2} \right) \quad (3.77)$$

$$\frac{\partial \sigma_1''}{\partial \sigma_{22}} = \frac{1}{2} + \frac{1}{2} \left[ \left( \frac{a_5 \sigma_{11} - a_6 \sigma_{22}}{2} \right)^2 + a_7^2 \sigma_{12}^2 \right]^{-1/2} \left( \frac{a_5^2 \sigma_{22} - a_6 a_5 \sigma_{11}}{2} \right) \quad (3.78)$$

$$\frac{\partial \sigma_1''}{\partial \sigma_{12}} = \frac{1}{2} \left[ \left( \frac{a_5 \sigma_{11} - a_6 \sigma_{22}}{2} \right)^2 + a_7^2 \sigma_{12}^2 \right]^{-1/2} (2a_7^2 \sigma_{12}) \quad (3.79)$$

$$\frac{\partial \sigma_2''}{\partial \sigma_{22}} = \frac{1}{2} - \frac{1}{2} \left[ \left( \frac{a_5 \sigma_{11} - a_6 \sigma_{22}}{2} \right)^2 + a_7^2 \sigma_{12}^2 \right]^{-1/2} \left( \frac{a_5^2 \sigma_{22} - a_6 a_5 \sigma_{11}}{2} \right) \quad (3.80)$$

$$\frac{\partial \sigma_2''}{\partial \sigma_{11}} = \frac{1}{2} - \frac{1}{2} \left[ \left( \frac{a_5 \sigma_{11} - a_6 \sigma_{22}}{2} \right)^2 + a_7^2 \sigma_{12}^2 \right]^{-1/2} \left( \frac{a_5^2 \sigma_{11} - a_6 a_5 \sigma_{22}}{2} \right) \quad (3.81)$$

$$\frac{\partial \sigma_2''}{\partial \sigma_{12}} = -\frac{1}{2} \left[ \left( \frac{a_5 \sigma_{11} - a_6 \sigma_{22}}{2} \right)^2 + a_7^2 \sigma_{12}^2 \right]^{-1/2} (2a_7^2 \sigma_{12}) \quad (3.82)$$

Yield function and Equations 3.71-3.82 are solved for  $\varphi=0^\circ$ ,  $\varphi=45^\circ$  and  $\varphi=90^\circ$  to get necessary anisotropic constants.

The increment plastic multiplier is obtained from consistency condition.

$$\Delta \lambda = \frac{f + \frac{df}{d\sigma_{ij}} C_{ijkl} \Delta \varepsilon_{kl}}{\frac{df}{d\sigma_{ij}} C_{ijkl} \frac{df}{d\sigma_{kl}} - \frac{df}{dY} \frac{dY}{d\varepsilon_{eq}^P} \frac{\sigma_{kl}}{Y} \frac{df}{d\sigma_{kl}}} \quad (3.83)$$

$$\varepsilon(a_1, \dots, a_8) = \left( \frac{\bar{\sigma}_b - Y_{ref}}{Y_{ref}} \right)^2 + \sum_{i=1}^3 \left( \frac{\bar{\sigma}_{\phi_i} - Y_{ref}}{Y_{ref}} \right)^2 + \left( \frac{r_b - r_b^{exp}}{r_b^{exp}} \right)^2 + \sum_{i=1}^3 \left( \frac{r_{\phi_i} - r_{\phi_i}^{exp}}{r_{\phi_i}^{exp}} \right)^2 = \min \quad (3.84)$$

### 3.7 Formulation of Thermal Problems

There are three different types of heat transfer mechanisms which are conduction, convection and radiation.

$$Q_t = \frac{\lambda_t A}{L} (T_1 - T_2) \Delta t \quad (3.85)$$

$$\dot{q} = \frac{Q_t}{A \Delta t} = \frac{\lambda_t}{L} (T_1 - T_2) \quad (3.86)$$

$$\dot{q} = \alpha_c (T_1 - T_2) \quad (3.87)$$

where  $Q_t$ ,  $A$ ,  $\dot{q}$ ,  $\lambda_t$  and  $\Delta t$  are heat energy, area of heat transfer, heat flux density, thermal conductivity of the material and change of time, respectively.

## CHAPTER 4

### FINITE ELEMENT ANALYSIS

#### 4.1 Finite Element Method

Different numerical methods are used to solve the most of the engineering problems. Although there are a lot of numerical methods, FEM is one of the best known numerical methods, and this method is used for solving partial differential equation and integral equations simplified from complicated problems.

Finite element method starts the analysis to obtain approximate solutions of boundary value problems in engineering by dividing the domain to a number of smaller domains called as finite elements that have simpler geometries and smaller dimensions. Each element connects with each other by associated nodes. The boundary value problems correspond to field problems, and the field symbolizes a physical entity and field variables that are the dependent variables of interest governed by the differential equations. Moreover, the boundary conditions can describe values of displacement, force, heat flux and temperature [21].

#### 4.2 Finite Element Analysis

In this study, FE analyses of the cylindrical, hemispherical and square cup deep drawings processes and deep drawing of a complex shaped part were carried out for different temperatures by using the ABAQUS software. Moreover, local heating of the circular and complex shaped blanks were also simulated.

The available models such as isotropic, kinematic and combined hardening and Hill48

models in the Abaqus software were directly used. Moreover, the von Mises yield criterion was performed with these three hardening rules. A subroutine was prepared to conduct the simulations with YLD2003 yield criterion. Deep drawing process has nonlinear characteristics, therefore; a nonlinear analysis is used with the Lagrangian formulation [22]. For homogeneous heating analysis, elasto-plastic analysis is used, however; for local heating simulations, coupled thermal-stress analysis models are carried out.

### 4.3 Finite Element Models

The cylindrical, square and complex shaped parts were modeled and analyzed with a finite element analyses package (ABAQUS) at different temperatures and considering different yield criteria and hardening models. Local heating processes was also analyzed for circular and complex shaped parts.

#### 4.3.1 Cylindrical Deep Drawing

Dimensions of the tools of the cylindrical deep drawing are presented in Table 4.1. The tools and the blank are shown in Figures 4.1 and 4.2, respectively. The quarter of the cup which has been simulated as shown in Figure 4.3 and includes 2016 finite elements. S4R 4 node shell elements with reduced integration are selected to form the mesh. Size of the mesh elements were determined by considering time of analysis and getting best results. The die, blank holder and punch were modeled as rigid bodies, and only sheet metal was defined as deformable body.

Table 4.1: Dimensions of the tools of the cylindrical cup deep drawing [1]

Diameter of Blank (mm)	230
Diameter of Punch (mm)	110
Diameter of Punch Shoulder (mm)	10
Diameter of Die (mm)	113
Diameter of Die Shoulder (mm)	15

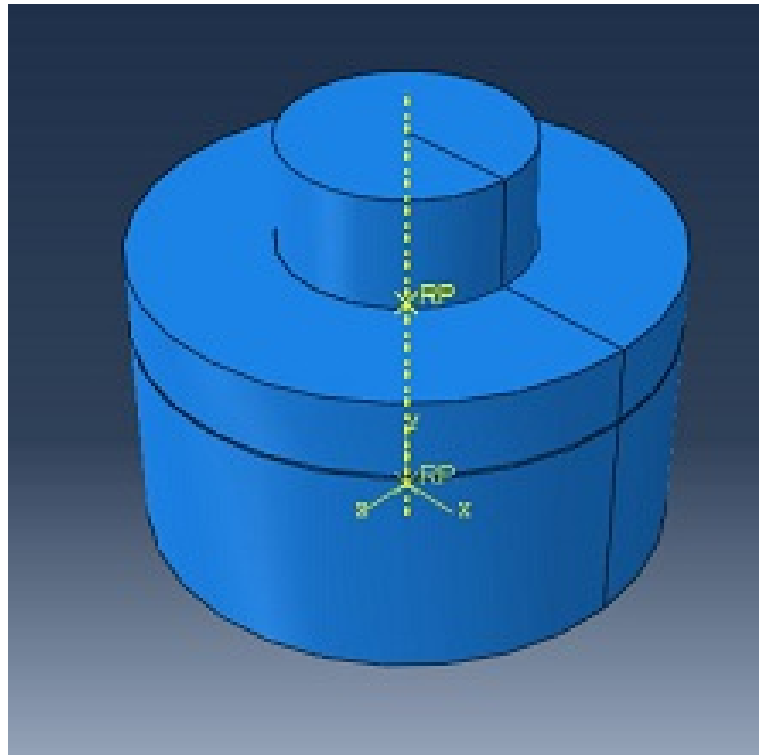


Figure 4.1: FE modeling of cylindrical deep drawing

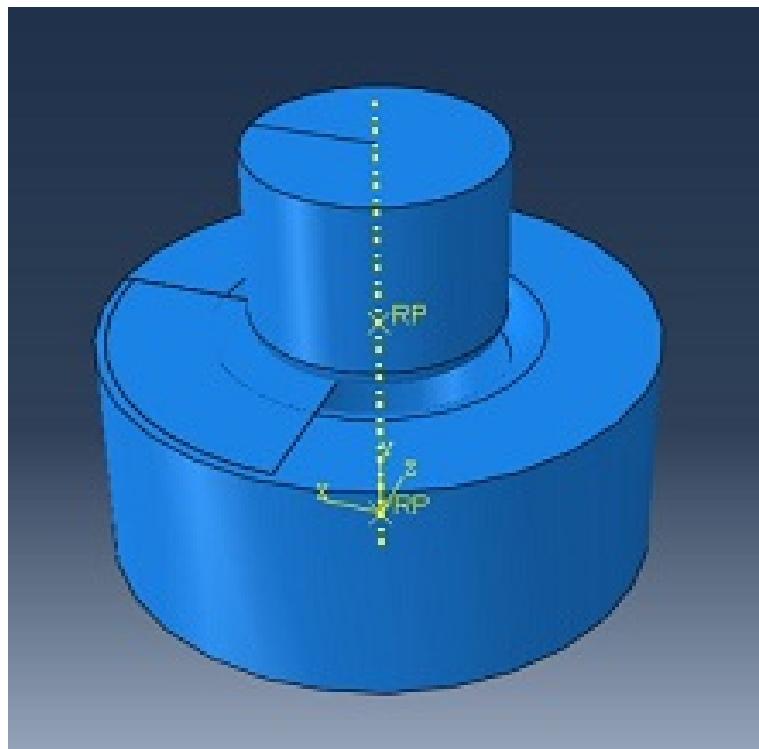


Figure 4.2: FE modeling of cylindrical deep drawing without blank holder

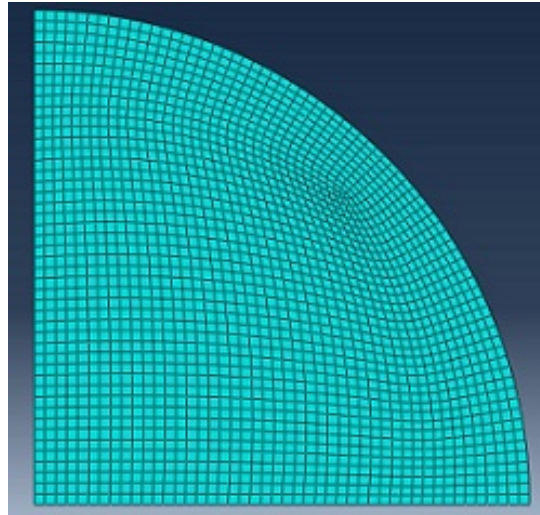


Figure 4.3: Mesh Modeling of quarter circular blank (Cylindrical)

In cylindrical cup drawing, AA5754-O aluminum and SS304 sheet metal alloys were modeled. Blank holder force was taken 10000 N and friction coefficients between tools and blank were used as 0.06 and 0.12 [1].

### 4.3.2 Hemispherical Deep Drawing

Dimensions of the tools of the hemispherical cup deep drawing are shown in Table 4.2. The tools and blank are shown in Figures 4.4 and 4.5, respectively. The quarter cup model shown in Figure 4.6 includes 763 finite elements. S4R 4 node shell elements with reduced integration are selected to form the mesh. The die, blank holder and punch were modeled as rigid bodies, and only sheet metal was defined as deformable body. In deep drawn hemispherical cup model, blank holder force was taken as 900 N and friction coefficients between drawing tools are used as 0.06 [2].

Table 4.2: Dimensions of the tools of the hemispherical cup deep drawing [2]

Diameter of Blank (mm)	110
Diameter of Punch (mm)	50
Diameter of Die (mm)	53
Diameter of Die Shoulder (mm)	13.5

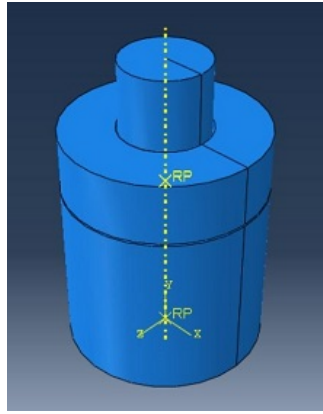


Figure 4.4: FE modeling of hemispherical deep drawing

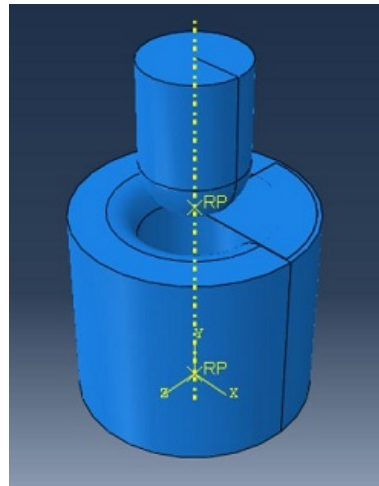


Figure 4.5: FE modeling of hemispherical deep drawing without blank holder

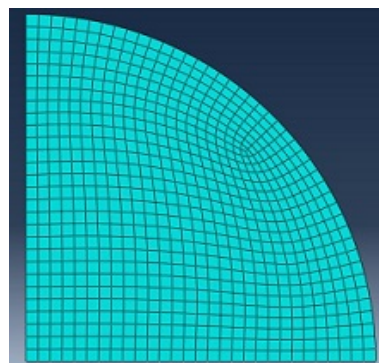


Figure 4.6: Mesh modeling of quart. of circular blank (Hemispherical)

### 4.3.3 Square Deep Drawing

Dimensions of the tools of the square deep drawing are shown in Table 4.3. The tools and blank are shown in Figure 4.7. The quarter cup model shown in Figure 4.8 includes 1600 finite elements. S4R 4 node shell elements with reduced integration are selected to form the mesh. The die, blank holder and punch were modeled as rigid bodies, and only sheet metal was defined as deformable body.

Table 4.3: Dimensions of the tools of the square cup deep drawing [2]

Blank Dimension (mm)	80 x 80
Punch Dimension (mm)	40 x 40
Punch Shoulder Diameter (mm)	12
Die Dimension (mm)	42 x 42
Die Shoulder Diameter (mm)	4.5

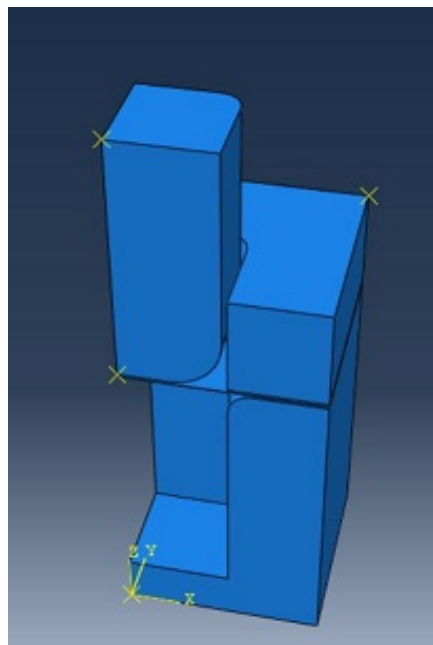


Figure 4.7: FE modeling of square deep drawing

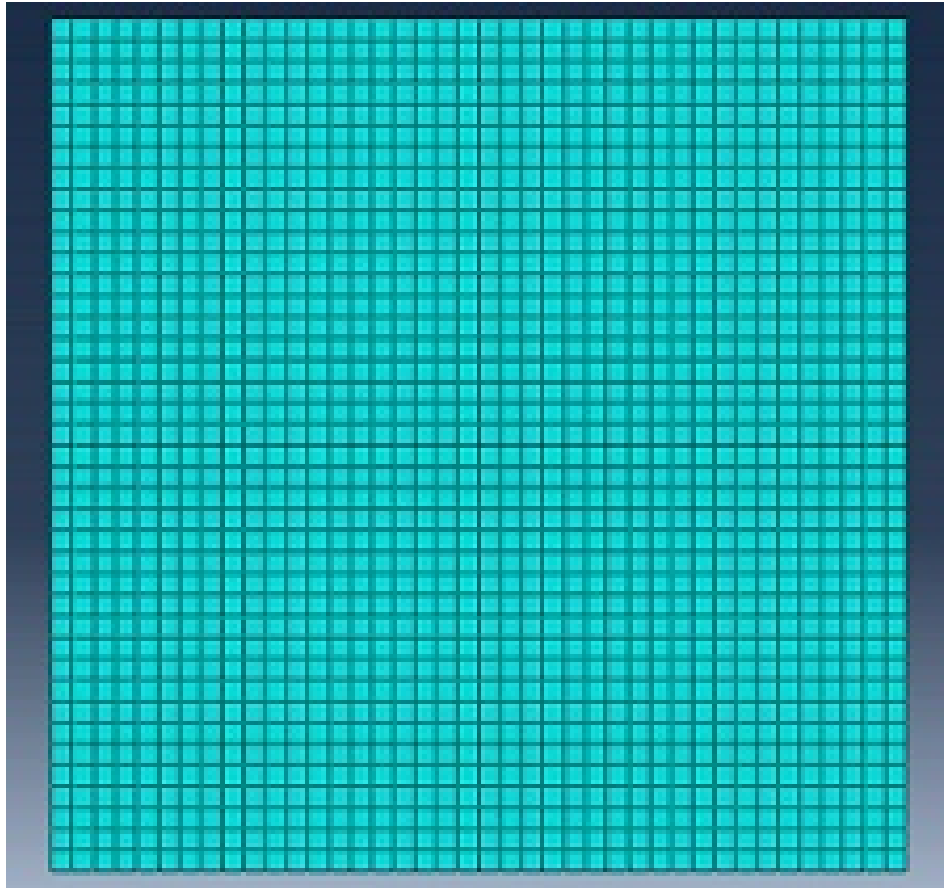


Figure 4.8: Mesh modeling of quarter of square blank

In square cup drawn model, blank holder force was taken as 900 N and friction coefficients between drawing tools were used as 0.06 [2].

#### **4.3.4 Local Heating of Cylindrical Cup Drawing**

The blank, punch and die are shown in Figure 4.9 used for local heating. For the tools and blank, thermal material properties were defined since temperature-displacement analyses have been carried out in this part. This deep drawing problem involves significant heating due to the inelastic deformation of the material. Moreover, contact conditions include the heat conducted between surfaces which depends on the contact area between them and transmitted pressure. Blank has 2760 mesh elements named as C3D8RT as shown in Figure 4.10. Different initial temperature values were defined at the different regions of the blank. Blank holder force was taken as 25000 N.

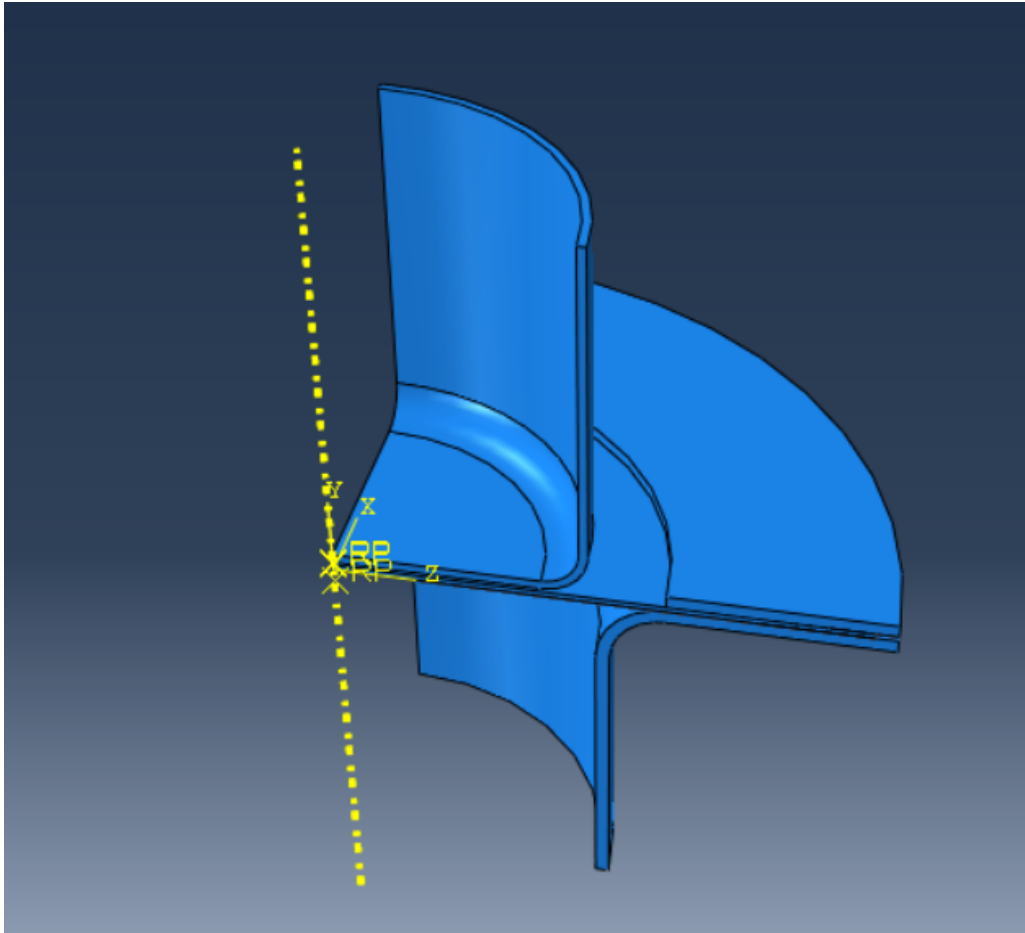


Figure 4.9: FE modeling of cylindrical deep drawing

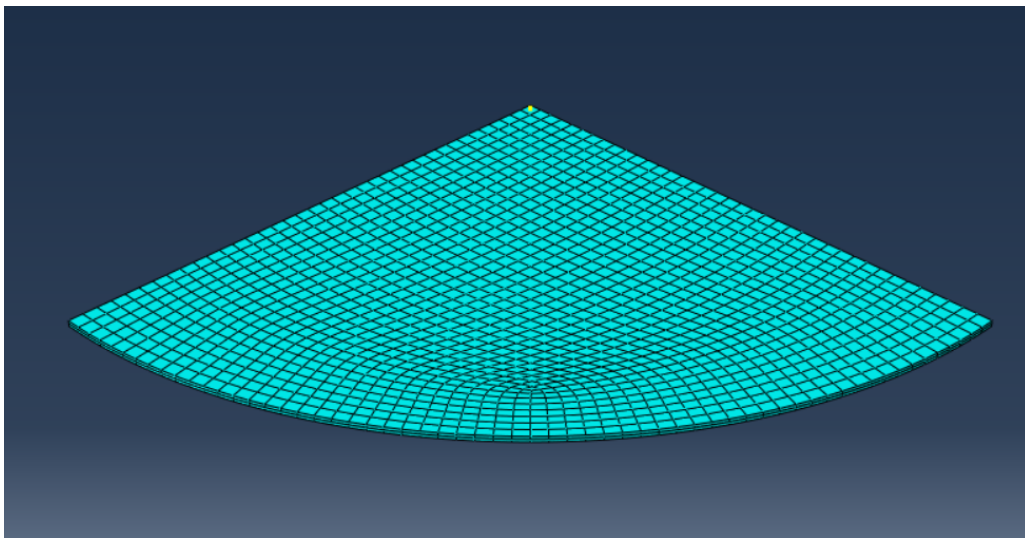


Figure 4.10: Mesh modeling of cylindrical deep drawing

### 4.3.5 Local Heating of Complex Shape in Deep Drawing Process and HFQ

Local heating of blank and HFQ process were simulated for a sheet metal part made of AA5754-O. The HFQ process was investigated by two steps. In the first step, general forming process is carried out as the top punch forms sheet metal towards the bottom die. This first step continues up to contacting the bottom die with sheet metal. After that second step starts on the other hand forming of the central features of the sheet metal part starts. In this step blank holder force is exerted also by spring fixed to the bottom die. Stages of the process are demonstrated in Figure 4.11.

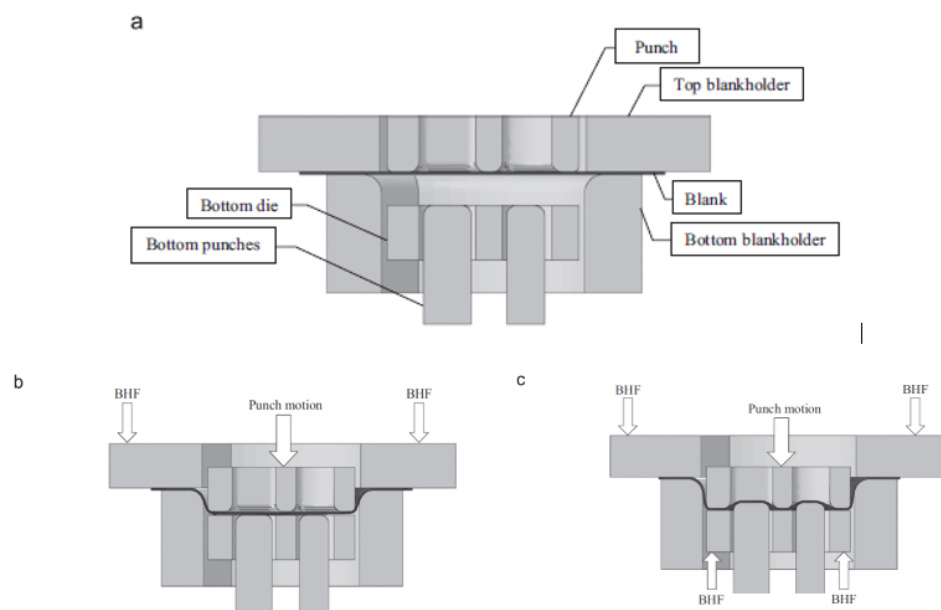


Figure 4.11: (a) Initial section of the blank and tools, (b) 1st stage of the process in where BHF is applied top BH, and (c) 2nd stage of the process in where sheet metal contacts with bottom die and BHF is also applied by gas springs. [6]

For sheet material, explicit, 8-node thermally coupled brick elements (C3D8T) are used to represent the deformation and heat transfer mechanisms and for the other tools, 4-node thermally coupled tetrahedron elements (C3D4T) are used. All tools and blank modelled as deformable bodies since heat transfer occurs between them. While C3D8T mesh elements are used for homogeneous heating of the rectangular blank, C3D4T mesh elements are used for local heating of the rectangular blank.

Created FE model of HFQ process in ABAQUS includes six different parts which are rectangular blank, top punch, top blank holder, bottom punch, bottom die and bottom blank holder respectively shown in Figure 4.13-4.18 and assembly model shown in Figure 4.12. Dimensions of the rectangular blank are  $200 \times 65 \times 1.5 \text{ mm}^3$  [6].

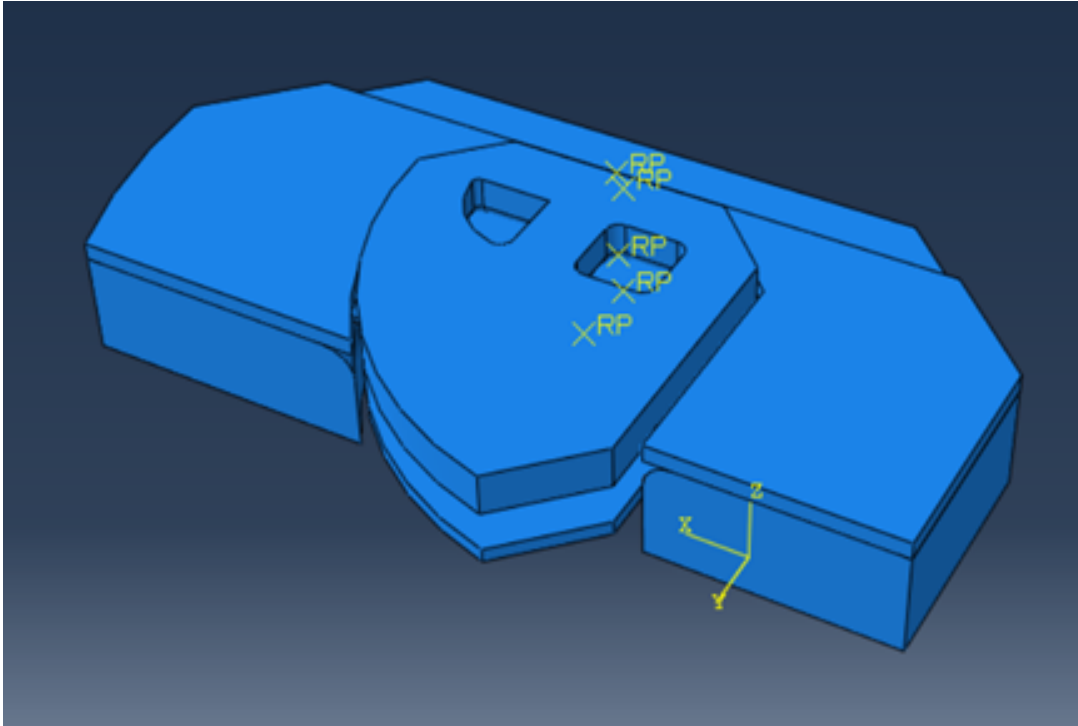


Figure 4.12: Assembly modeling of deep drawing of complex shape.

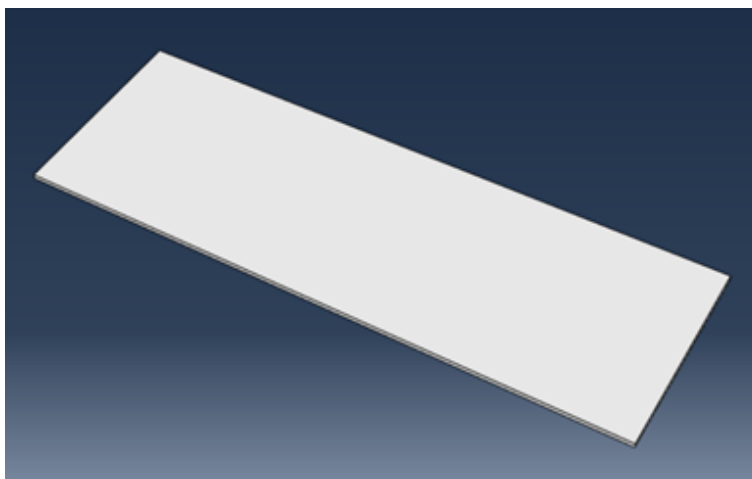


Figure 4.13: Modeling of rectangular blank.

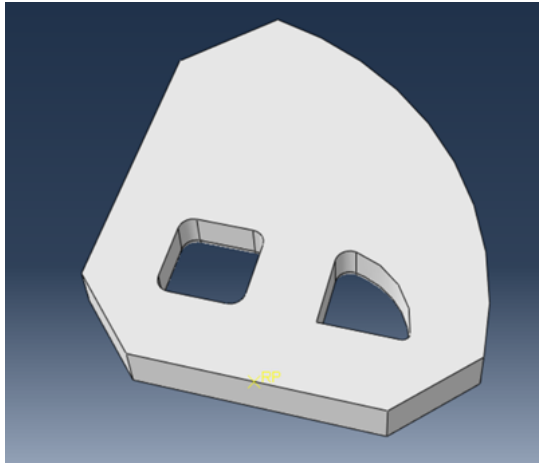


Figure 4.14: Modeling of top punch.

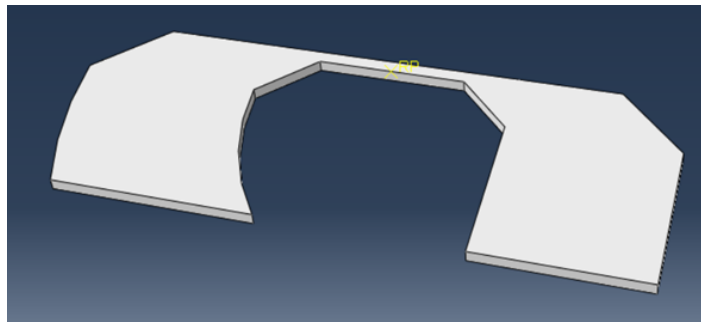


Figure 4.15: Modeling of top blank holder.

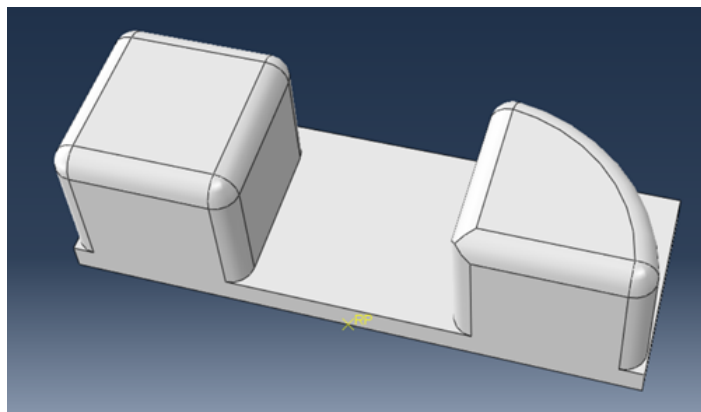


Figure 4.16: Modeling of bottom punch.

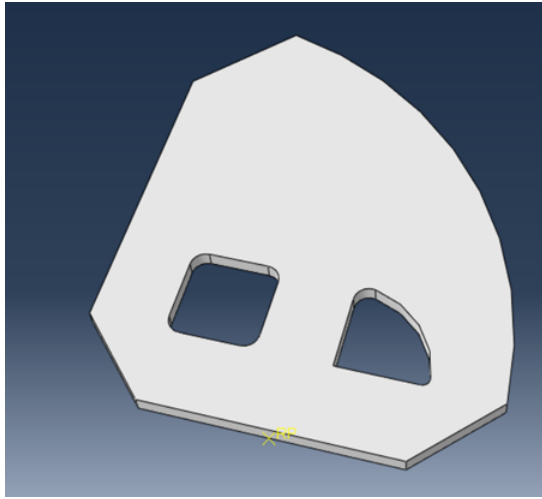


Figure 4.17: Modeling of bottom die.

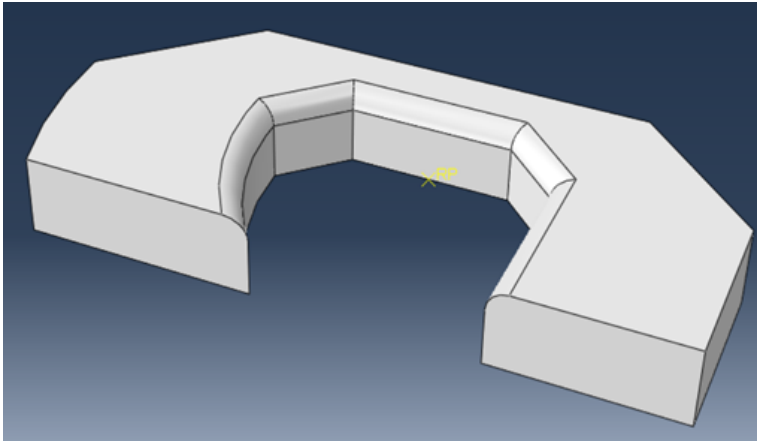


Figure 4.18: Modeling of bottom blank holder.

## CHAPTER 5

### MATERIAL DATA

In this study, AA5754-O and SS304 sheet materials were used for cylindrical, hemispherical, square deep drawing processes. AA5754-O sheet material was also used for local heating processes of circular and complex shaped parts. In local heating processes, XC38CrMoV5 and H13 steel materials were used as tool materials.

#### 5.1 AA5754 and Tool Materials

##### 5.1.1 Properties and Parameters of AA5754 for Cylindrical, Hemispherical and Square Deep Drawing

Mechanical properties and density, Johnson Cook and Lankford parameters are presented in Tables 5.1, 5.2 and 5.3, respectively.

Table 5.1: Mechanical properties and density of AA5754 [1]

Young Modulus E (GPa)	194
Poisson's Ratio	0.22
Density (kg/m <sup>3</sup> )	2700

Table 5.2: Johnson Cook Parameters of AA5754 [3]

A (MPa)	B (MPa)	C	n	m	$\dot{\epsilon}$ (s <sup>-1</sup> )
28.13	278.67	0.00439	0.183	2.527	0.1

Table 5.3: Lankford Parameters of AA5754 [4]

$\Theta$	$r_{\Theta}$
0°	0.85
45°	0.67
90°	0.7

True stress-strain curves for AA5754 material at room temperature, 175°C and 250°C that were obtained from study of Winklhofer et al. are shown in Figure 5.1.

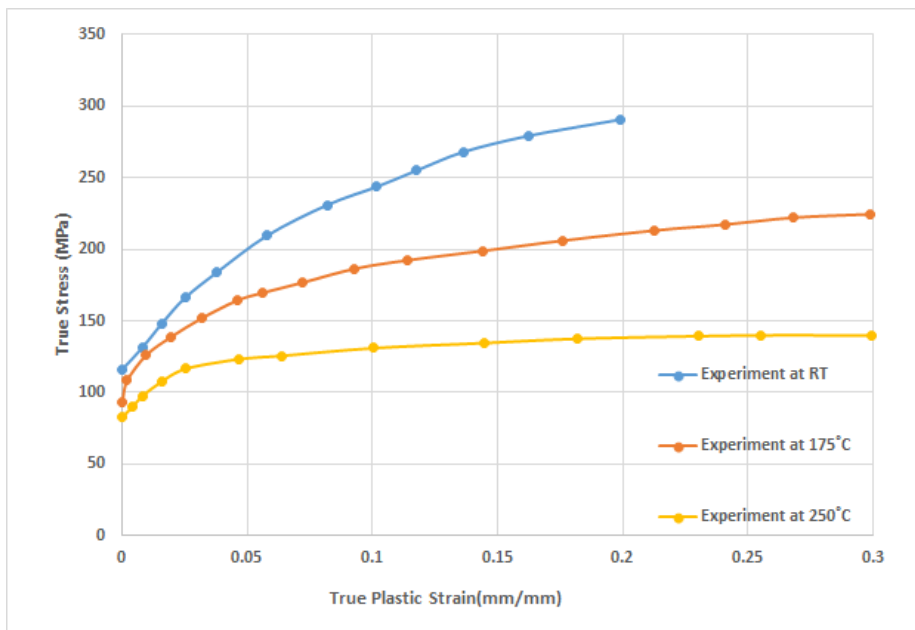


Figure 5.1: True stress-strain curve of AA5754-O at room temperature, 175°C and 250°C [1].

### 5.1.2 Properties and Parameters of AA5754 and Tool Material for Circular Blank of Local Heating Process

In local heating process of circular blank made of AA5754, thermal and mechanical properties of XC38CrMoV5 tool material that were taken from study of Laurent et al. are presented in Table 5.4.

Table 5.4: Thermal and mechanical properties of blank and tool material [1] and [5]

	Blank Material	Tool Material
Property	AA5754-O	XC38CrMoV5
Density	2700 kg/m <sup>3</sup>	8150 kg/m <sup>3</sup>
Young's Modulus	71000*10 <sup>6</sup> N/m <sup>2</sup>	215000 *10 <sup>6</sup> N/m <sup>2</sup>
Poisson's ratio	0.33	0.3
Thermal expansion coefficient	2.4*10 <sup>-5</sup> 1/K	1.9*10 <sup>-5</sup> 1/K 1/K
Heat capacity	920 J/kgK	500 J/kgK
Heat conduction	121 W/mK	25 W/mK

### 5.1.3 Properties and Parameters of AA5754 and Tool Material for HFQ Process

FEA of HFQ and deep drawing processes of complex shaped blank were carried out at 200°C, 350°C and HFQ temperature of 480°C at a speed of 250mm/s. 480°C is the SHT temperature of AA5754-O. The thermal and mechanical properties and density of AA5754-O sheet and H13 tool steel materials that were taken from study of Fakir et al. are presented in Table 5.5.

Table 5.5: Material and thermal properties of blank and tools [6].

	Blank Material	Tool Material
Property	AA5754	H13 Tool Steel
Thermal Conductivity (W/mK)	147*10 <sup>6</sup>	38*10 <sup>6</sup>
Specific Heat (J/mK)	9.60*10 <sup>2</sup>	4.70*10 <sup>2</sup>
Density (kg/m <sup>3</sup> )	2700	7800
Poisson's Ratio	0.33	0.3
Young Modulus (MPa)	-	2.1*10 <sup>5</sup>

## 5.2 SS304 Material

Mechanical properties and Lankford parameters of SS304 are presented in Tables 5.6 and 5.7 for cylindrical, hemispherical and square deep drawing processes. Johnson Cook model parameters for SS304 material were taken from study of Chagas and Machado [23].

Table 5.6: Mechanical Parameters of SS304 [2]

Young Modulus E (GPa)	194
Poisson's Ratio	0.22
$\nu$	339
Ultimate Stress (MPa)	675
K (MPa)	1325
n	0.31

Table 5.7: Lankford Parameters of SS304 [2]

$\Theta$	$r_{\Theta}$
0°	0.72
45°	1.19
90°	0.33

## CHAPTER 6

### RESULTS AND DISCUSSION

Firstly, results of FEA of cylindrical, hemispherical and square deep drawing processes were expressed with respect to variations of the thickness strains, punch force and rim shapes with different temperature values for AA5754 and SS304 sheet materials in this section of the thesis. For these three types of the deep drawing processes, used blanks had uniform temperature values and temperature values were kept constant during analyses.

After that results of analyses of the locally heated cylindrical cup deep drawing are presented for AA5754 with respect to thickness strain and temperature variations. Different temperatures were given to the inner and flange regions of the blank. Results of the analyses of the local heating of the circular blank that are compared with each other and results of the homogeneous heated blank.

Maximum cup height that could be reached without failure was investigated by using Johnson Cook Failure Criterion for local heating process of circular blank. For these purposes, von Mises yield criterion with isotropic hardening rules was also used.

Lastly, results of the analyses of the HFQ process on complex shape at different temperatures and locally heated complex shape are presented with respect to thickness strain variations and rim shapes for AA5754 sheet materials.

#### **6.1 Results of Cylindrical Deep Drawing for AA5754**

In this section, obtained results from FE analyses of cylindrical deep drawing are compared with each others and experimental results taken from study of Fakir et al.

[6]. It was decided that which yield criterion gave the best approximate results to the experimental results. Von Mises yield criterion with isotropic, kinematic and combined hardening rules, Johnson Cook model, Hill48 and YLD2003-8p yield criteria have been used at room temperature, 175°C and 250°C for 80 mm punch travel. Thickness strain distribution from center of blank and variation of punch force with respect to punch displacements at different temperatures are shown in Figures 6.1-6.18. Moreover, rim shapes of the deep drawn cylindrical cup for all used yield criteria and temperature values are shown in Figures 6.19-6.23.

### **6.1.1 Thickness Strain Distributions on Cylindrical Cup Deep Drawing for AA5754**

Thickness strain distributions of the deep drawn cylindrical cup with 80 mm punch travel at room temperature are shown in Figure 6.1 for all yield criteria. Except Hill48 and von Mises yield criteria with kinematic hardening rule, other models gave close results to experimental result for all part of the blank. Results of the thickness strain distributions of the Hill48 and von Mises yield criteria with kinematic hardening rule approximates the experimental results only at the flange region. The closest result to the experimental result was obtained from YLD2003-8p yield criterion for all regions of the drawn blank and the results, which were obtained from von Mises yield criterion with kinematic hardening rule, deviates significantly from experimental results.

Thickness strain distributions of deep drawn cylindrical cup for 80 mm punch travel at 175°C are shown in Figure 6.2. These thickness strain distributions show almost same trend with results at room temperature. The experimental result gave more uniform result than the results of the FEA at the bottom bend radius region. Results of thickness strain distribution of the Von-Mises yield criterion with kinematic hardening rule is significantly different from results of the experiment and other models at the region under the punch. At this region, Hill48 yield criterion gave better result than the Von-Mises yield criterion with kinematic hardening rule. YLD2003 yield criterion gave the best result for this case.

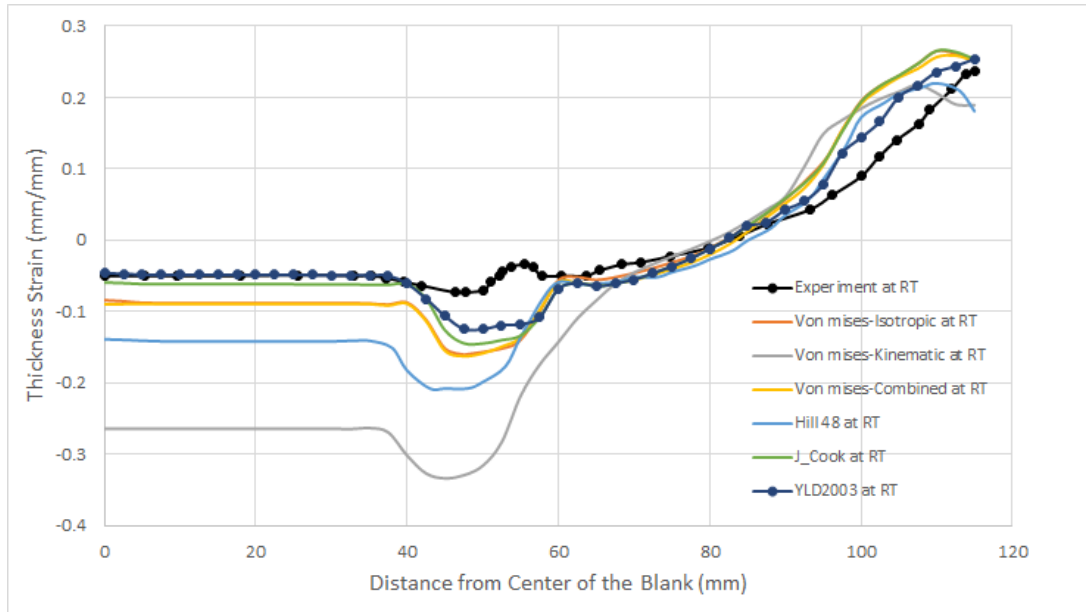


Figure 6.1: Thickness strain distributions for different models and experiment at room temperature (AA5754-O, cylindrical, 80 mm punch travel)

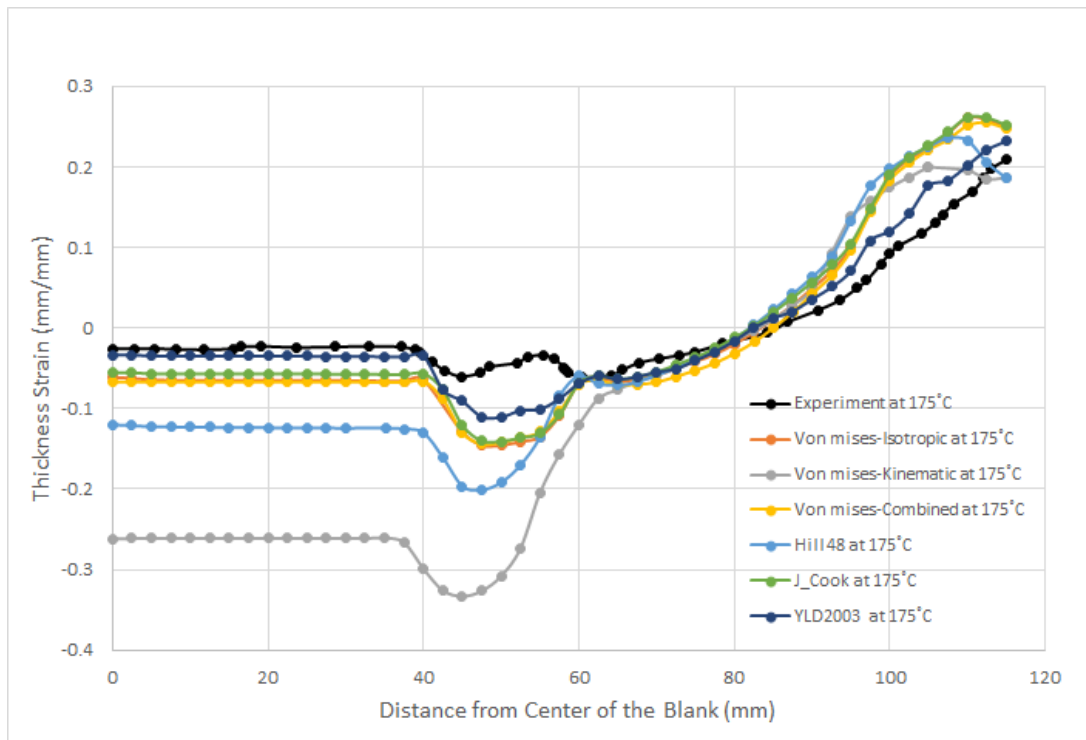


Figure 6.2: Thickness strain distributions for different models and experiment at 175°C (AA5754-O, cylindrical, 80 mm punch travel)

Thickness strain distributions of the deep drawn cylindrical cup at 250°C are shown in Figure 6.3 for all mentioned yield criteria. Except von Mises yield criterion with kinematic hardening rule, other yield criteria have close results to experimental result for all parts of the blank. Result of the YLD2003-8p yield criterion is in better agreement with experimental result for all parts of the blank. While result of thickness strain distribution of the Von-Mises yield criterion with kinematic hardening rule is significantly different from results of the experiment and other models at the region under the punch, this model gives a good result at the flange region. Hill48 yield criterion gives better result at 250°C than room temperature and 175°C for the region under the punch. Hill48 yield criterion gives better result at 250°C than room temperature and 175°C for the region under the punch.

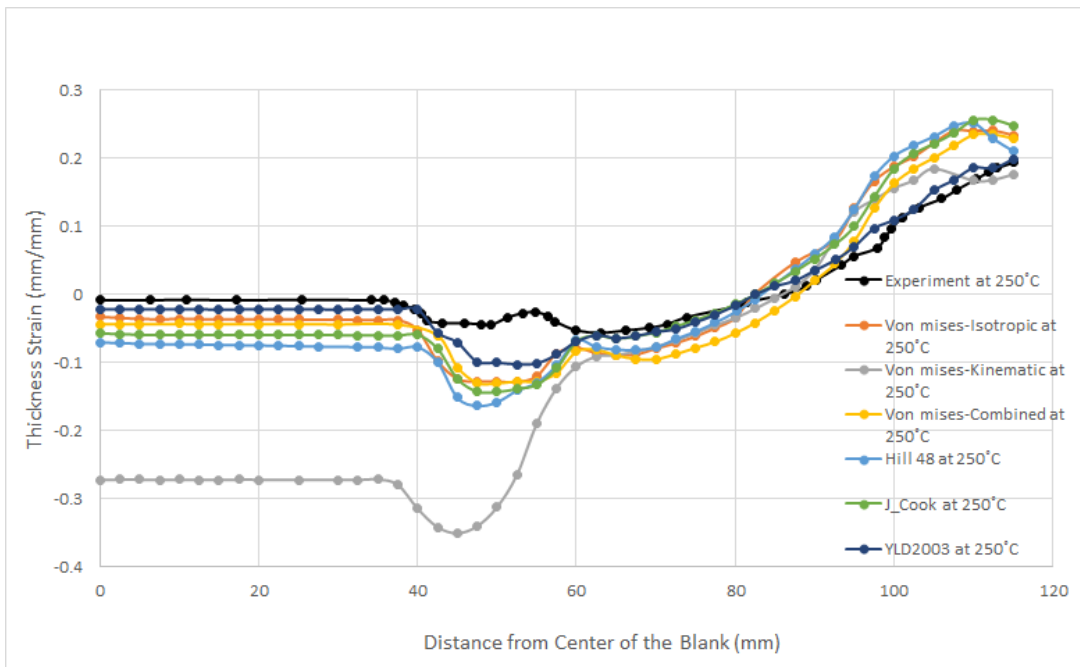


Figure 6.3: Thickness strain distributions for different models and experiment at 250°C (AA5754-O, cylindrical, 80 mm punch travel)

In Figures 6.4-6.9 the effects of the temperature on thickness strain distributions of deep drawn cylindrical cup are shown at room temperature, 175°C and 250°C for experimental data and mentioned yield criteria.

Figure 6.4 shows the thickness strain distribution of experimental results obtained from cylindrically deep drawn cup at room temperature, 175°C and 250°C. At the

punch region of the blank, thickness strain of the blank made of AA5754 sheet material decreases with increasing temperature from room temperature to 250°C. Except for small region of the wall region, at wall and flange regions of the blank, differences of thickness strain have become less than the punch region for different temperature values, however; thickness strain decreases with increasing temperature at these regions. Whereas blank has got thinning at punch and wall regions of the blank, thickenings of the blank are seen at the flange region.

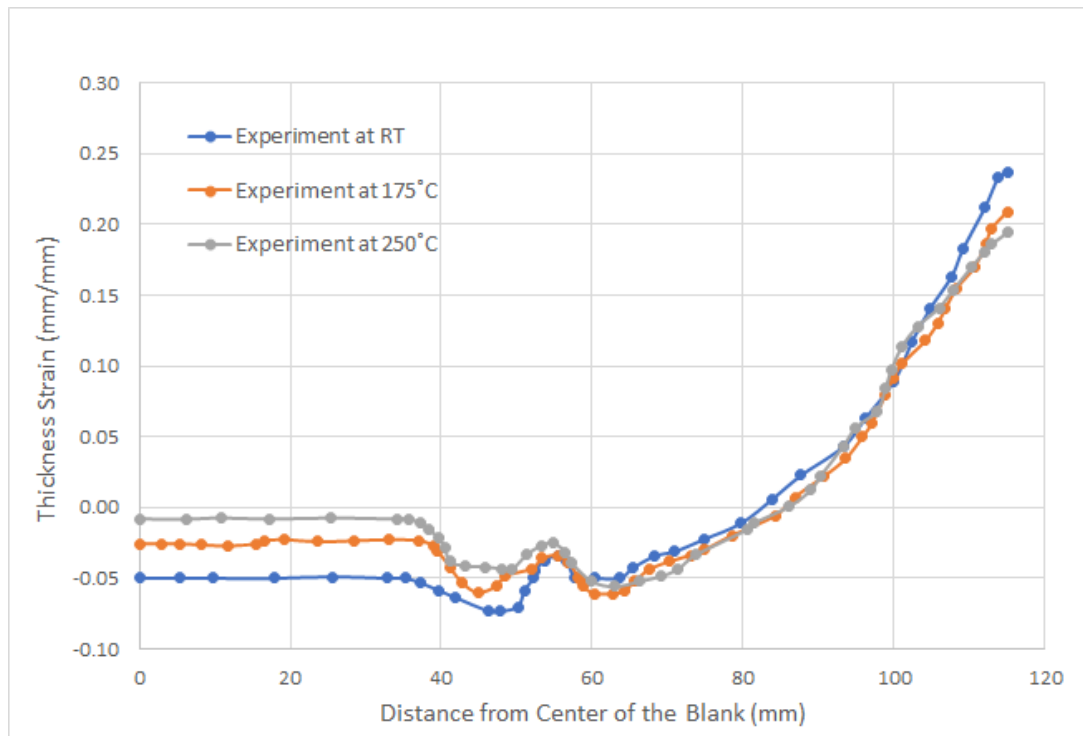


Figure 6.4: Effect of temperature on thickness strain distributions for experiments with different temperatures. [1] (AA5754-O, cylindrical, 80 mm punch travel).

In Figure 6.5, the results of the thickness strain distribution of deep drawn cylindrical cup at temperature values of room temperature, 175°C and 250°C for von-Mises yield criterion with isotropic hardening rule are presented. Whereas thickness strain and thinning of the sheet decrease with increasing temperature for the region under the punch and bend radius area, at small part of the cup wall region, thickness strain and thinning of the sheet increases with increasing temperature. There are not significant variations between values of thickness strain of blank at different temperatures in the flange region, however at the small parts of the flange region, it can be seen that

thickness strain increases with decreasing temperature.

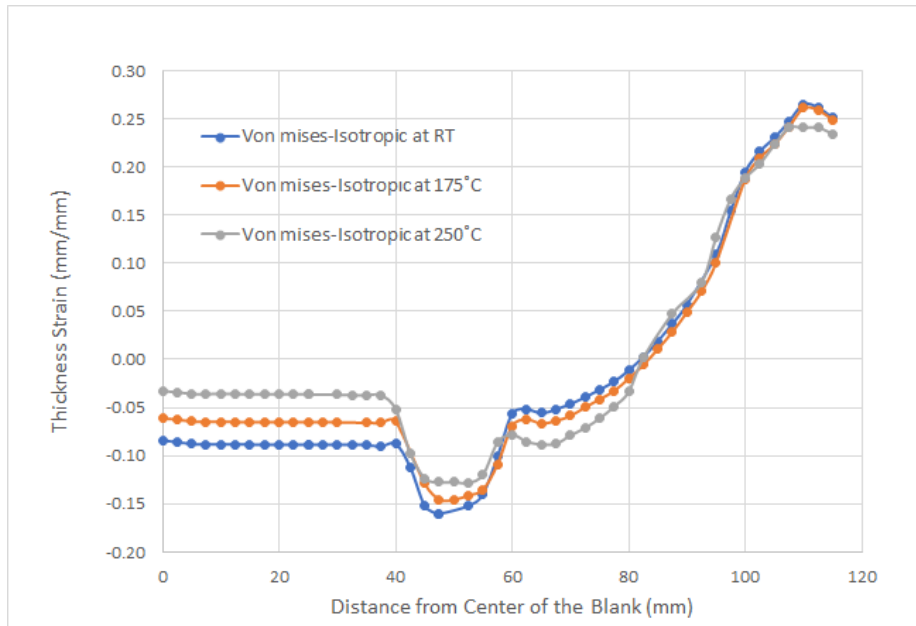


Figure 6.5: Effect of temperature on thickness strain distributions on von Mises-Isotropic (AA5754-O, cylindrical, 80 mm punch travel)

In Figure 6.6, the results of the thickness strain distribution of deep drawn cylindrical cup at temperature values of room temperature, 175°C and 250°C for von-Mises yield criterion with kinematic hardening rule are presented. At the region under the punch and the bend radius area, there is very little differences between results of thickness strain of the cup at different temperatures from room temperature to 250°C and, thickness strain increases with increasing temperature values. At the flange region of the sheet metal, values of thickness strain decrease with increasing temperature. The highest values of the thickness strain have been observed from analyses of Von-Mises yield criterion with kinematic hardening rule as about -0.35.

In Figure 6.7, the results of the thickness strain distribution of deep drawn cylindrical cup at temperature values of room temperature, 175°C and 250°C for von-Mises yield criterion with combined hardening rule are presented. Whereas thickness strain and thinning of the sheet decrease with increasing temperature for the region under the punch and the bend radius area, thickness strain and thinning of the sheet increases with increasing temperature at small part of the cup wall region. Thickness strain

values and thickening of the sheet decrease with increasing temperature at the flange region of the blank.

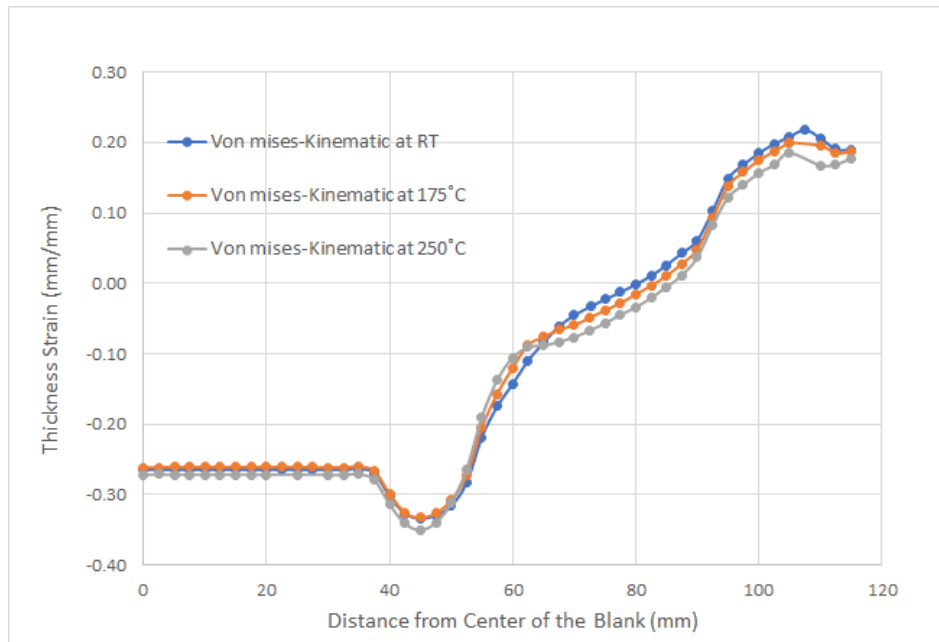


Figure 6.6: Effect of temperature on thickness strain distributions on von Mises-Kinematic (AA5754-O, cylindrical, 80 mm punch travel)

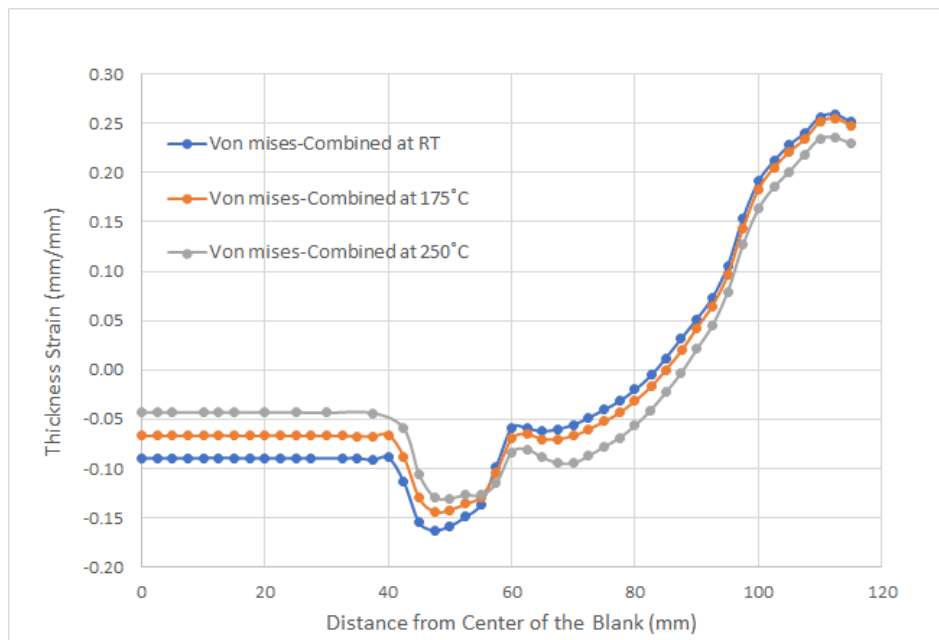


Figure 6.7: Effect of temperature on thickness strain distributions on von Mises-Combined (AA5754-O, cylindrical, 80 mm punch travel)

In Figure 6.8, the results of the thickness strain distribution of deep drawn cylindrical cup at temperature values of room temperature, 175°C and 250°C for Hill48 yield criterion with isotropic hardening rule are presented. Whereas thickness strain and thinning of the sheet decrease with increasing temperature for the region under the punch and the bend radius area, thickness strain and thinning of the sheet increases with increasing temperature at small part of the cup wall region. At the flange region, thickness strain values increase with increasing temperature. While results of thickness strain distribution are close each other at the region under the punch for analyses at room temperature and 175°C, results of thickness strain distribution are close each other at the flange region for analyses at 175°C and 250°C. The sheet material does not show same properties in all direction, since Hill48 yield criterion is anisotropic. Thickness strain variations at different directions are presented in Figures A.1 and A.2.

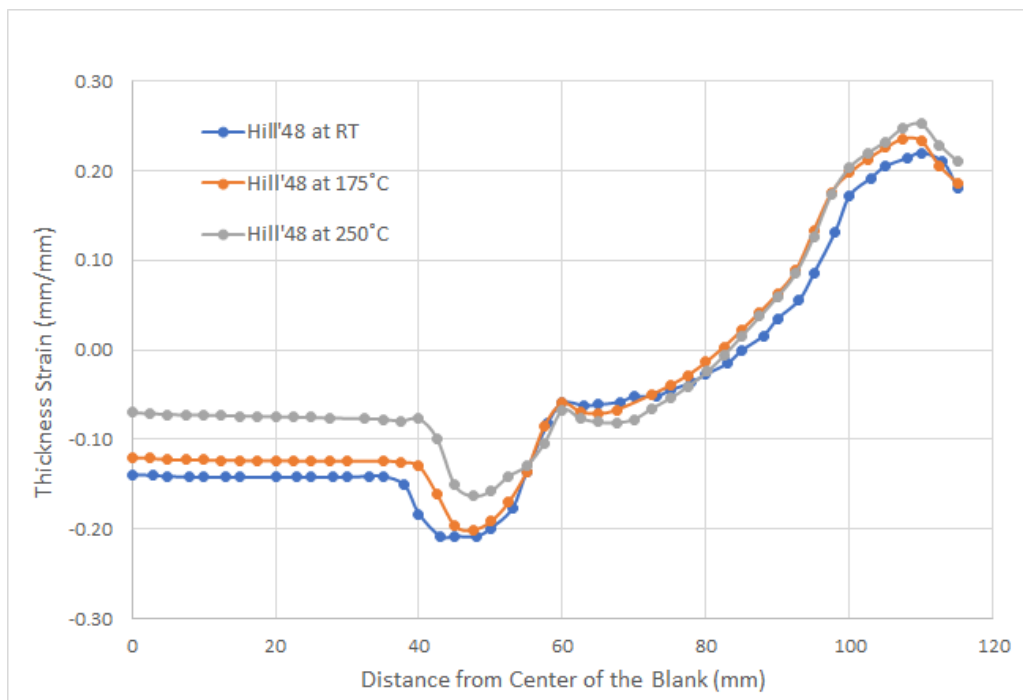


Figure 6.8: Effect of temperature on thickness strain distributions on Hill48 criteria (AA5754-O, cylindrical, 80 mm punch travel)

In Figure 6.9, the results of the thickness strain distribution of deep drawn cylindrical cup are shown at temperature values of room temperature, 175°C and 250°C for

YLD2003 yield criterion. Thickness strain and thinning of the sheet decrease with increasing temperature for the region under the punch and the bend radius area. At the cup wall region, there are not any significant thickness strain variations between results of analyses at different temperatures. At the flange region, thickness strain values decrease with increasing temperature.

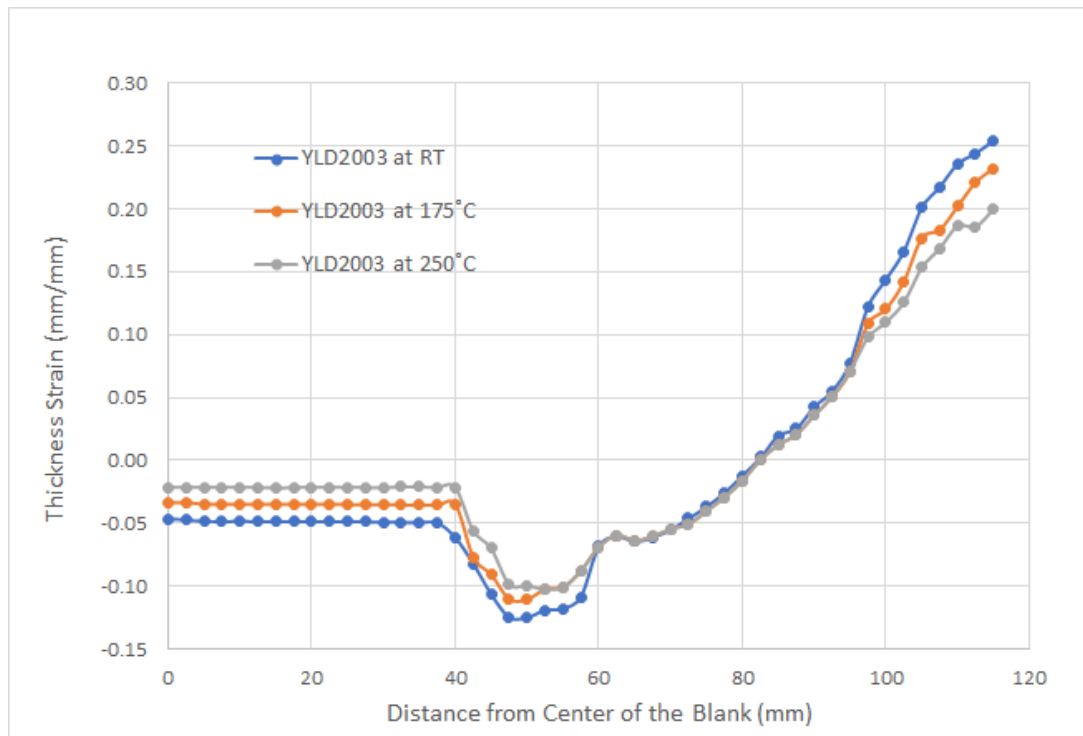


Figure 6.9: Effect of temperature on thickness strain distributions on YLD2003-8P Yield Criteria (AA5754-O, cylindrical, 80 mm punch travel)

According to these results, YLD2003 yield criterion gives the most uniform results with respect to thickness strain distribution in all used yield criteria. For all used yield criteria, at the region under the punch and the bend radius area, thickness strain values and hence thinning of the sheet decrease with increasing temperature, moreover; at these regions, the results, which deviate considerably from experiment, were obtained from von-Mises yield criteria with kinematic hardening rule. At the flange region, the highest thinning values were obtained from von-Mises yield criteria with combined hardening rule and Johnson-Cook model.

### **6.1.2 Variation of Punch Force with Punch Displacement on Cylindrical Cup Deep Drawing for AA5754**

In Figures 6.10-6.12, variation of punch force with punch displacement are shown for temperature values of room temperature, 175°C and 250°C respectively. The maximum punch displacement was taken as 80 mm. In Figures 6.13-6.18, variation of punch force with punch displacement are shown respectively for von-Mises yield criterion with isotropic hardening rule, von-Mises yield criterion with kinematic hardening rule, von-Mises yield criterion with combined hardening rule, Hill48 yield criterion and YLD2003 yield criterion at room temperature, 175°C and 250°C for a cup height of 60 mm.

Variations of punch forces with punch travel for AA5754 sheet material by using all yield criteria at room temperature are shown in Figure 6.10. Von-Mises yield criterion with isotropic hardening and combined hardening rules give higher punch forces than other models up to 45 mm cylindrical punch travel. After 45 mm cylindrical punch travel, von-Mises yield criterion with kinematic hardening rule results in higher punch forces than other yield criteria. Whereas punch force increased until 70 mm punch travel for von-Mises yield criterion with kinematic hardening rule, punch force increase was observed until 40 mm punch travel for the other yield criteria. Von-Mises yield criterion with kinematic hardening rule and YLD2003 yield criteria predicted lower punch force values up to 28 mm punch travel than other models. YLD2003 yield criterion has predicted minimum punch force values throughout the whole punch travel.

Variations of punch forces with punch travel for AA5754 sheet material by using all yield criteria at 175°C are shown in Figure 6.11. Von-Mises yield criterion with isotropic hardening and combined hardening rules and Johnson-Cook model resulted at higher punch forces than other models up to 52 mm punch travel. Von-Mises yield criterion with kinematic hardening rule has indicated higher punch forces than other yield criteria after 52 mm punch travel. Whereas the maximum punch force was observed at 68 mm of punch travel for von-Mises yield criterion with kinematic hardening rule, the maximum punch force values were obtained at 38 mm of punch travel for the other models. Von-Mises yield criterion with kinematic hardening rule

and YLD2003 yield criteria predicted lower punch forces values up to 35 mm of punch travel. YLD2003 yield criterion gave the minimum punch force throughout the whole punch travel.

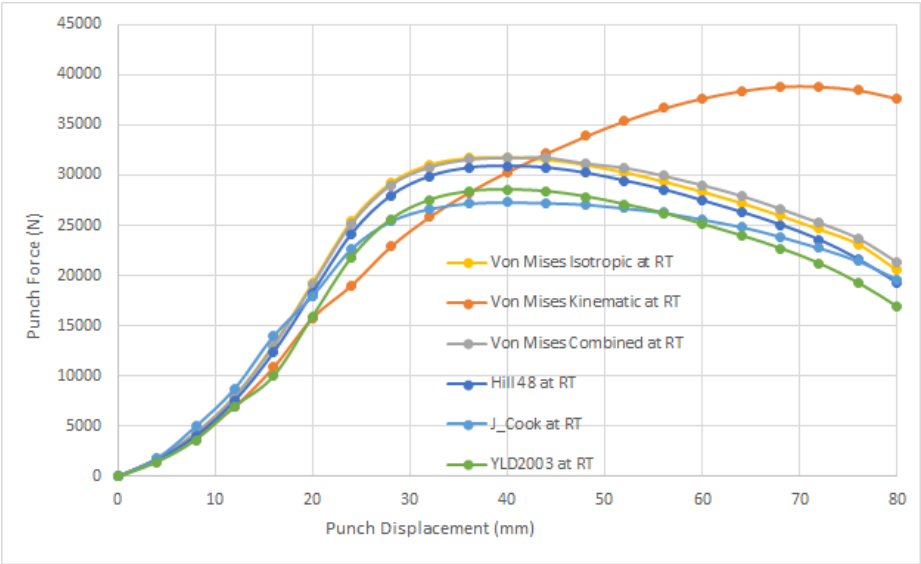


Figure 6.10: Punch force vs cylindrical punch displacement at room temperature for different models (AA5754-O)

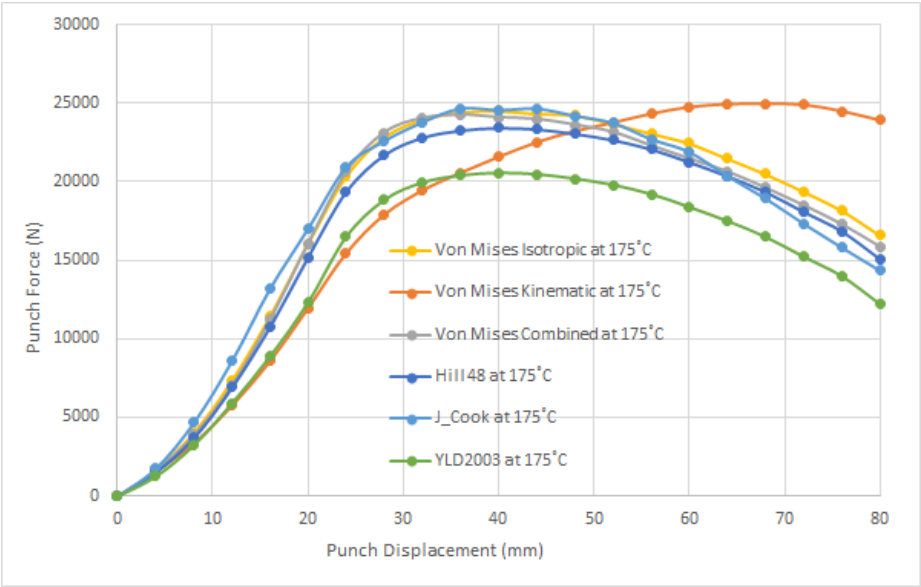


Figure 6.11: Punch force vs cylindrical punch displacement at 175°C for different models (AA5754-O)

Variations of punch forces with punch travel for AA5754 sheet material by using all yield criteria at 250°C are shown in Figure 6.12. Johnson-Cook model has predicted higher punch force than other models up to 50 mm of cylindrical punch travel. After 50 mm cylindrical punch travel, von-Mises yield criterion with kinematic hardening rule gave the highest punch force. Whereas punch force increases until 60 mm of punch travel for von-Mises yield criterion with kinematic hardening rule, punch force increase was observed until 35 mm of punch travel for the other yield criteria. Von-Mises with kinematic hardening rule and YLD2003 yield criteria predicted lower punch force values up to 28 mm punch travel values and then YLD2003 yield criterion gave the least punch force value in all models.

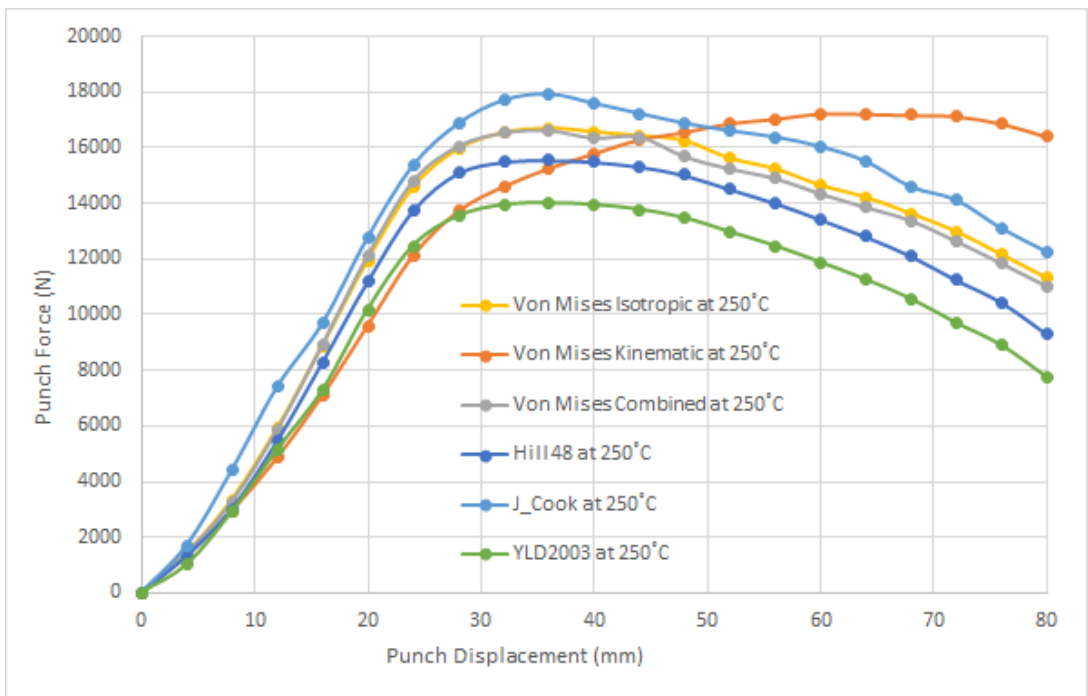


Figure 6.12: Punch force vs cylindrical punch displacement at 250°C for different models (AA5754-O)

Variations of the punch forces with punch displacements at room temperature, 175°C and 250°C for Von-Mises yield criterion with isotropic, kinematic and combined hardening rules, Hill48, Johnson Cook model and YLD2003 yield criteria are shown in Figures 6.13-6.18 respectively. The forming process is carried out more easily When the process temperature of the blank is increased since strength of

material decreases and ductility of the material increases with increasing temperature. Therefore, the punch force decreased when the temperature of the blank is increased as in Figures 6.13-6.18.

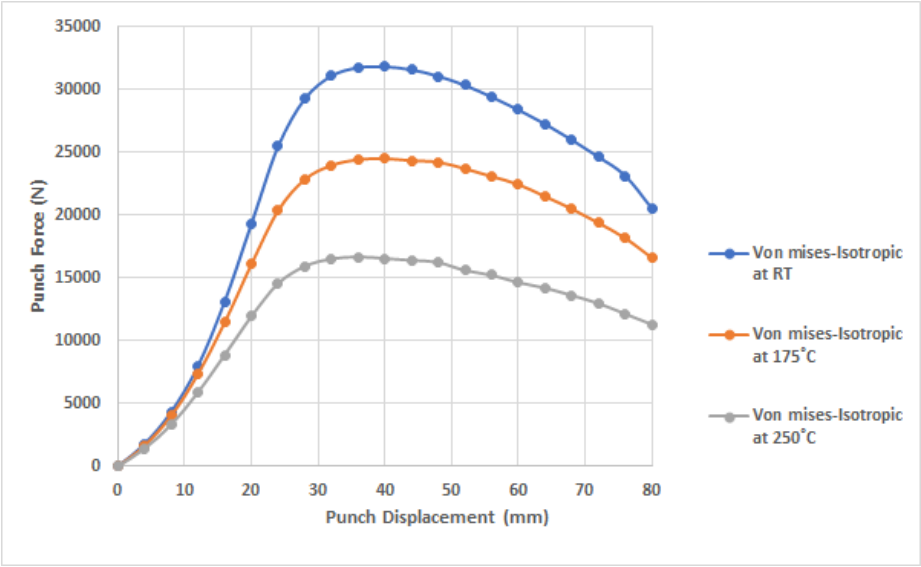


Figure 6.13: Punch force vs cylindrical punch displacement at different temperatures for von Mises-Isotropic (AA5754-O)

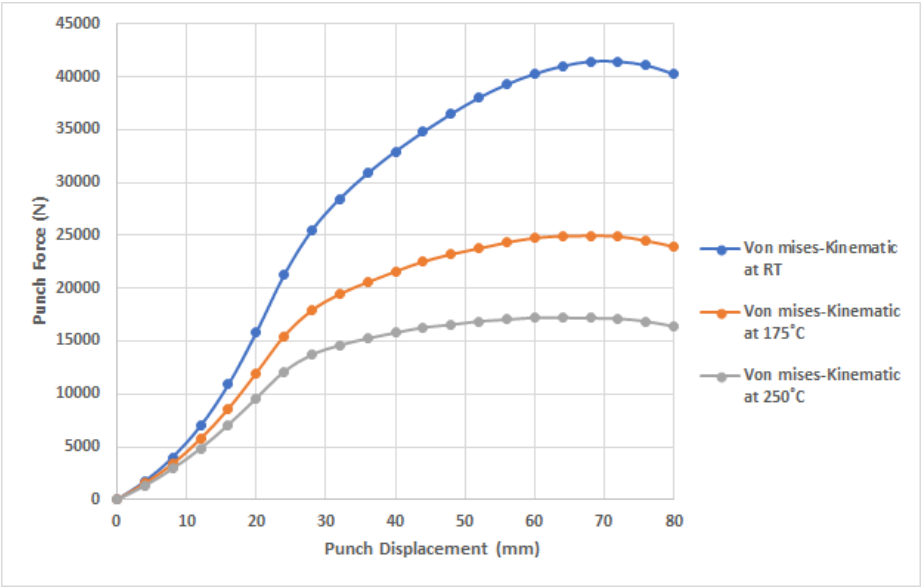


Figure 6.14: Punch force vs cylindrical punch displacement at different temperatures for von Mises-Kinematic (AA5754-O)

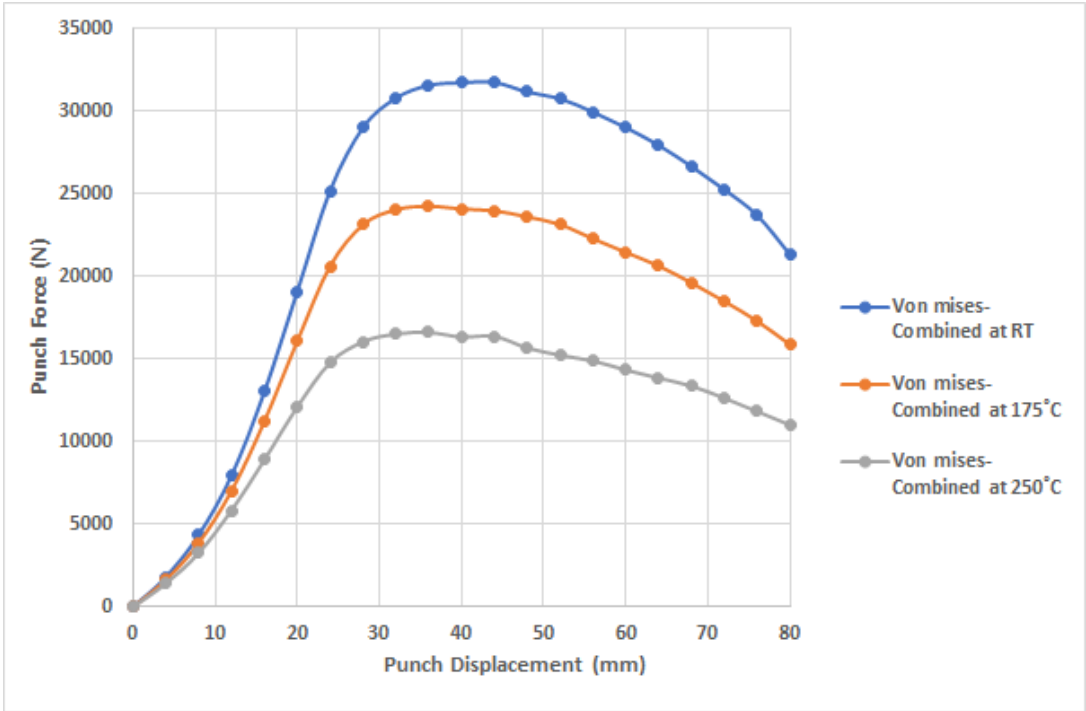


Figure 6.15: Punch force vs cylindrical punch displacement at different temperatures for von Mises-Combined (AA5754-O)

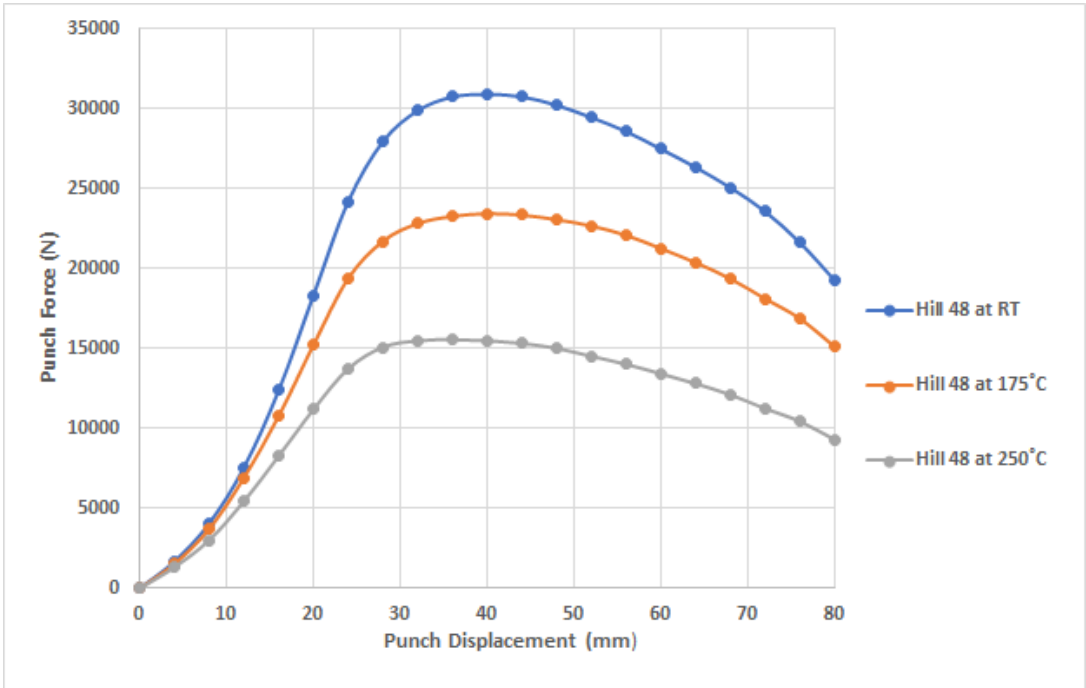


Figure 6.16: Punch force vs cylindrical punch displacement at different temperatures for Hill48 Criterion (AA5754-O)

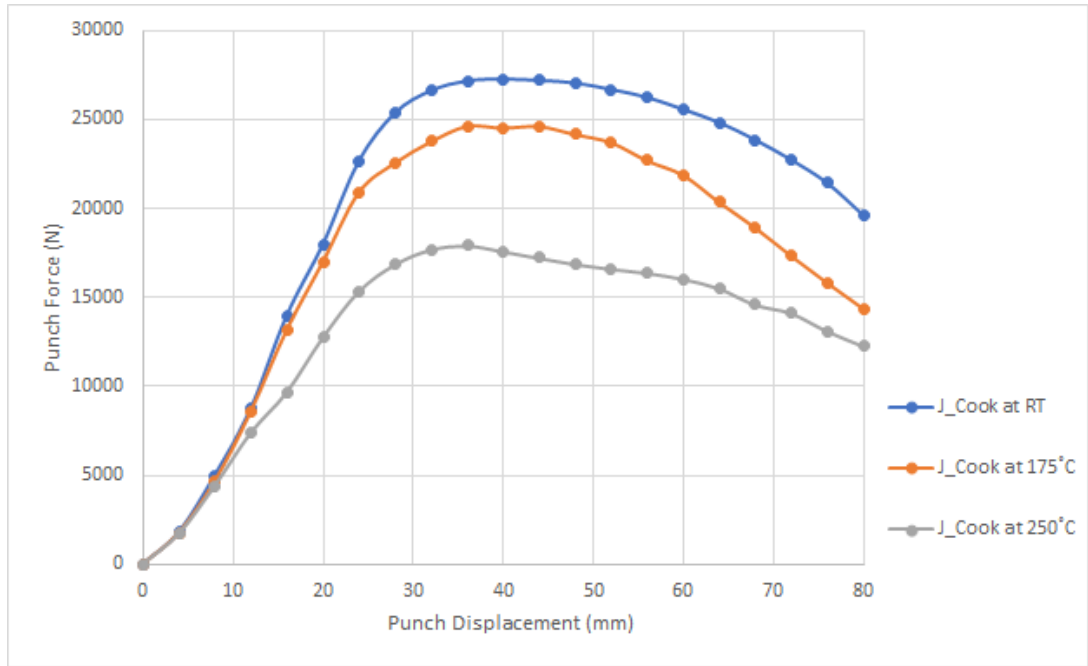


Figure 6.17: Punch force vs cylindrical punch displacement at different temperatures for Johnson Cook Model (AA5754-O)

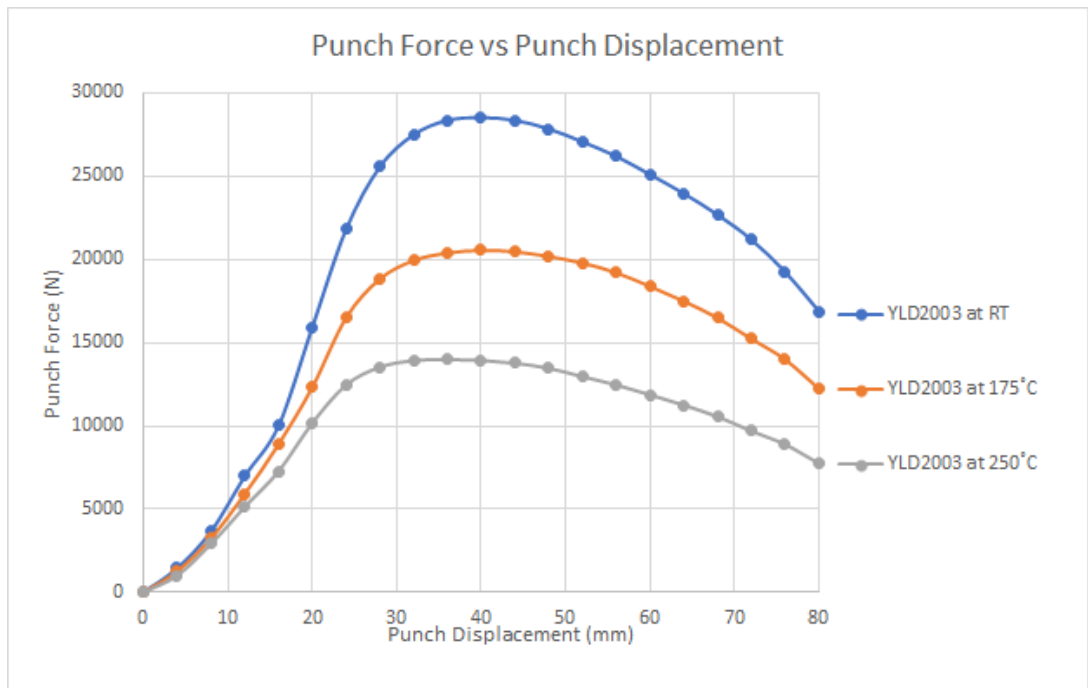


Figure 6.18: Punch force vs cylindrical punch displacement at different temperatures for YLD2003-8P Yield Criterion (AA5754-O)

It is observed that for all used models the differences between values of punch forces for different temperatures become apparent after about 10 mm punch travel and then differences of punch force values for different temperature increase with increasing punch travel until sheet material loses its strength due to instabilities.

### 6.1.3 Rim Shape of Cylindrical Cup Deep Drawing for AA5754

In this section, rim shapes of the undeformed and deformed blanks are shown in Figures 6.19-6.23 determined for all yield criteria at room temperature, 175°C and 250°C. Radius of the undeformed blank is 115 mm. By comparing these five figures, variations of the rim shapes are observed. Although the differences are not significant, it can be seen that radius of the rim shape of the deformed blank becomes smaller with decreasing temperature. The predicted flow of the blank into the die cavity is larger for Hill48 and YLD2003 yield criteria. Variations of the radius value increased at the middle of the edge of the quarter rim shape.

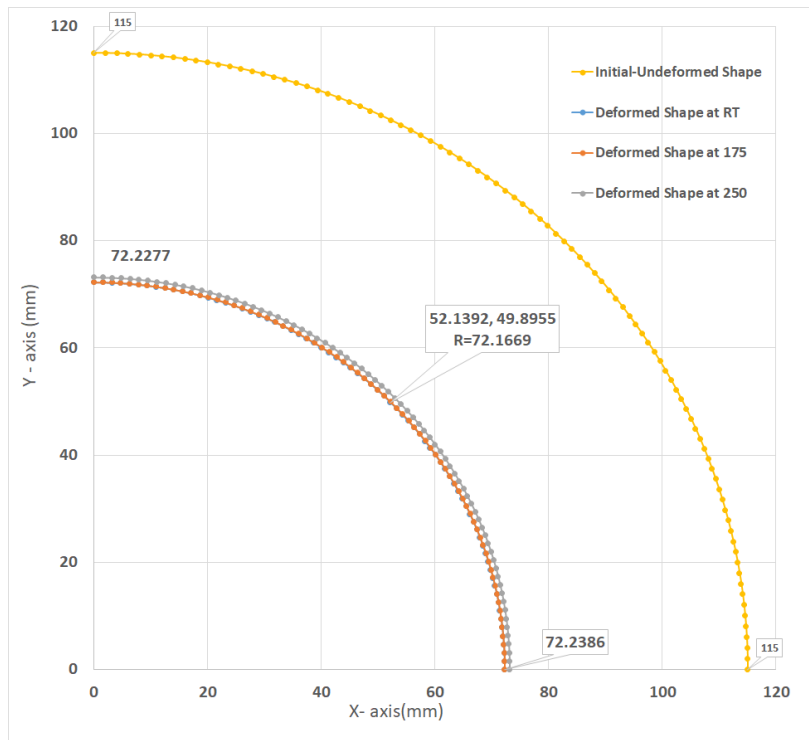


Figure 6.19: Rim shapes of the undeformed blank and deep drawn cylindrical cup at different temperatures. (AA5754-O, VonMises-Isotropic)

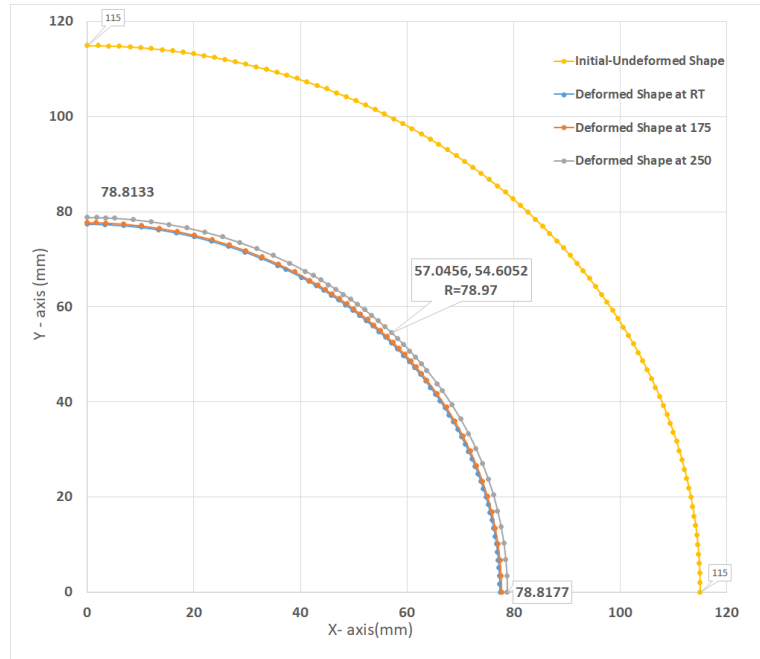


Figure 6.20: Rim shapes of the undeformed blank and deep drawn cylindrical cup at different temperatures. (AA5754-O, VonMises-Kinematic)

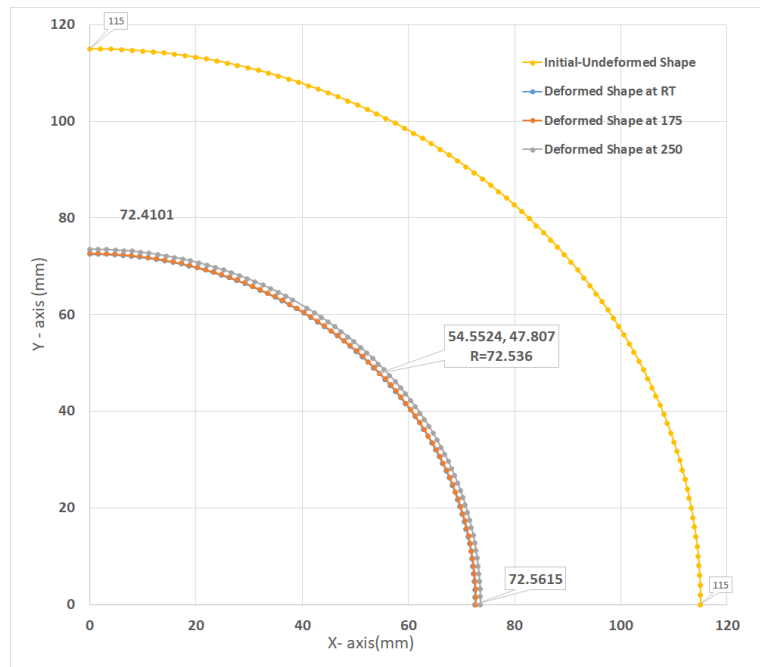


Figure 6.21: Rim shapes of the undeformed blank and deep drawn cylindrical cup at different temperatures. (AA5754-O, VonMises-Combined)

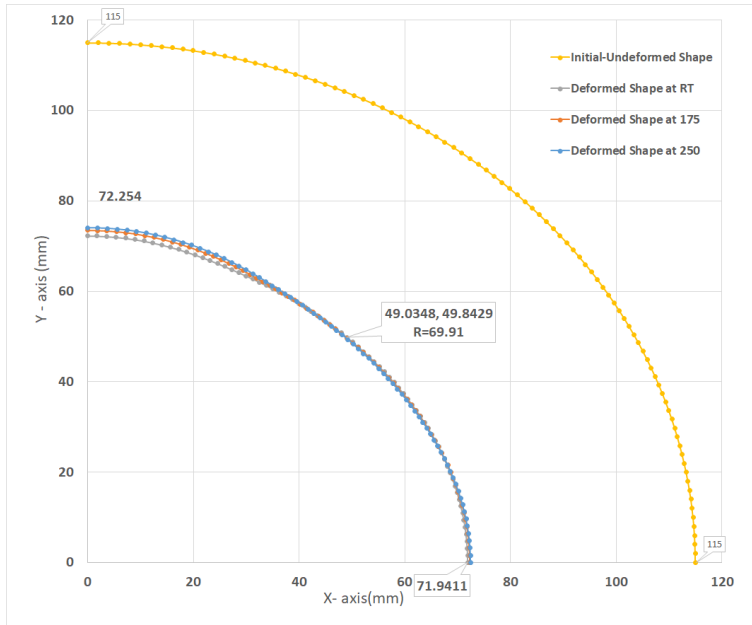


Figure 6.22: Rim shapes of the undeformed blank and deep drawn cylindrical cup at different temperatures. (AA5754-O, Hill48)

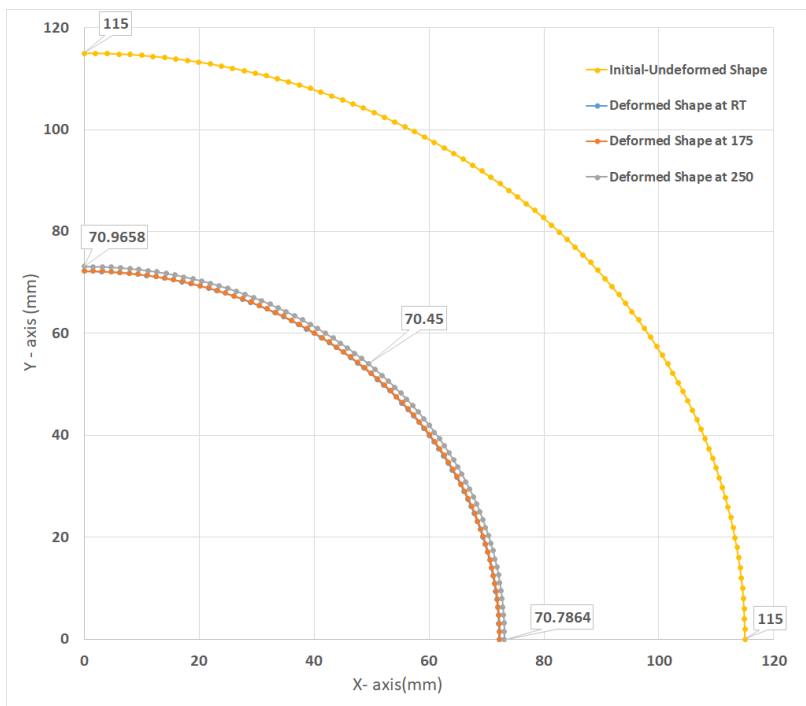


Figure 6.23: Rim shapes of the undeformed blank and deep drawn cylindrical cup at different temperatures. (AA5754-O, YLD2003)

## **6.2 Results of Cylindrical Deep Drawing for SS304**

By compared the results of FEA of the cylindrical deep drawing process, YLD2003-8p yield criterion gave the best approximate results to the experimental results for AA5754. Therefore, it was decided that only YLD2003 yield criterion was used at different temperature values for cylindrical deep drawing of SS304 sheet material. The parameters of temperature, punch travel, friction coefficients and dimensions of the blank and tools are same as for AA5754 sheet material.

### **6.2.1 Thickness Strain Distribution on Cylindrical Cup Deep Drawing for SS304**

Results of thickness strain distribution of deep drawn SS304 sheet material is presented in Figure 6.24 for YLD2003-8p with 80 mm punch travel. Thickness strain decreased with increasing temperature at the region under the punch and bend radius area. There were slight differences between thickness strain values at 175°C and 250°C at the region under the punch and bend radius area. The differences between thickness strain values of blank at different temperatures were not significant at the flange region. More uniform shape was obtained at elevated temperatures with respect to thickness strain.

### **6.2.2 Variation of Punch Force with Punch Displacement on Cylindrical Cup Deep Drawing for SS304**

Variations of the punch forces with punch displacement for SS304 sheet material are shown in Figure 6.25 at room temperature, 175°C and 250°C. Punch forces were lower at elevated temperatures than room temperature. The punch forces at 175°C and 250°C were close to each other. It is observed that 75°C of temperature difference is small to effect the strength of SS304 sheet material.

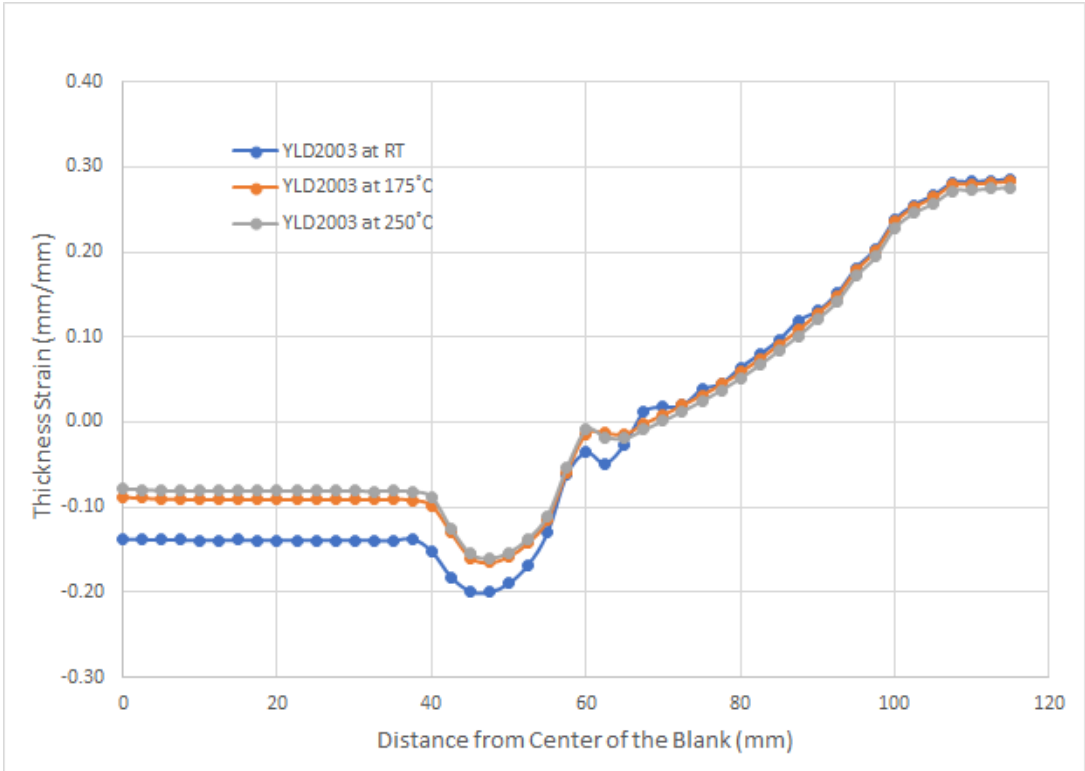


Figure 6.24: Effect of temperature on thickness strain distributions for YLD2003-8P Yield Criteria (SS304, cylindrical, 80 mm punch travel)

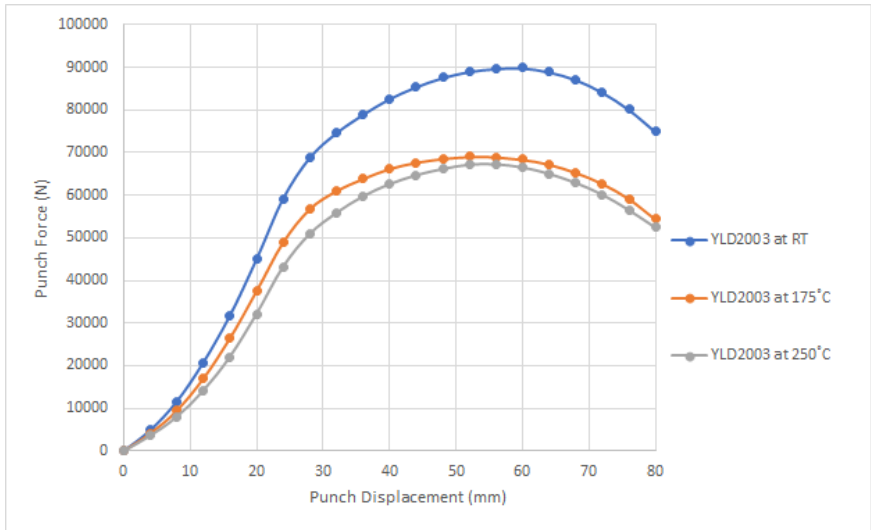


Figure 6.25: Punch force vs cylindrical punch displacement at different temperatures for YLD2003-8P Yield Criteria (SS304)

### 6.2.3 Rim Shapes of Cylindrical Cup Deep Drawing for SS304

In Figure 6.26, rim shapes of drawn cylindrical cup are shown for SS304. Although the differences are not significant, the radius of the rim shape of the deformed blank becomes smaller with decreasing temperature.

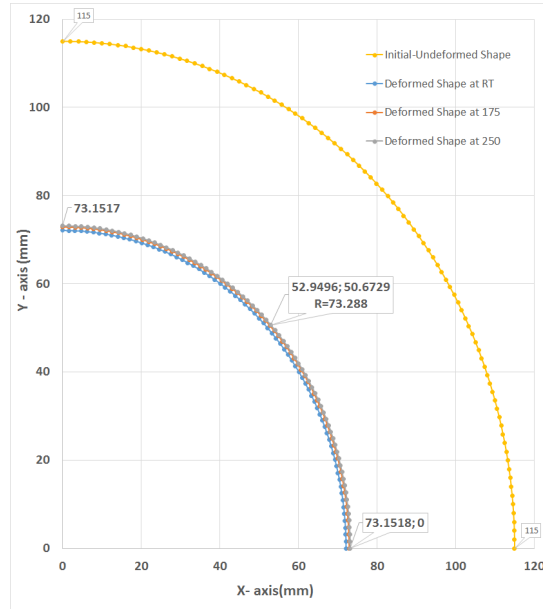


Figure 6.26: Rim shapes of the undeformed blank and deep drawn cylindrical cup at different temperatures. (SS304, YLD2003)

### 6.3 Results of Hemispherical Deep Drawing for SS304

Obtained results from FEA of hemispherical deep drawing and experimental results taken from study of Cogun and Darendeliler [2] were compared with each other. Von Mises yield criterion with isotropic, kinematic and combined hardening rules, Johnson Cook model, Hill48 and YLD2003-8p yield criteria have been used at room temperature, 300°C and 600°C for 45 mm punch travel and experimental result is available only at room temperature for thickness strain distribution. Thickness strain distribution from center of blank and variation of punch force with respect to punch displacement at different temperatures are shown in Figures 6.27-6.42. Moreover, rim shapes of the deep drawn hemispherical cup for all used yield criteria and temperature values are shown in Figures 6.43-6.47.

### 6.3.1 Thickness Strain Distribution on Hemispherical Cup Deep Drawing for SS304

Thickness strain distributions of the hemispherical deep drawing with 45 mm depth of punch at room temperature are shown in Figure 6.27 for all yield criteria and experiment. YLD2003 yield criterion agreed well with experimental results and this criterion gave more uniform results for all region of the cup when it is compared with other models. For the region under the punch, there was small deviation between Von Mises yield criterion with kinematic, combined hardening rules and Johnson-Cook model and between Von Mises yield criterion with isotropic hardening rule and Hill48 yield criterion. At the flange region of the cup, all used models and experiment gave close results.

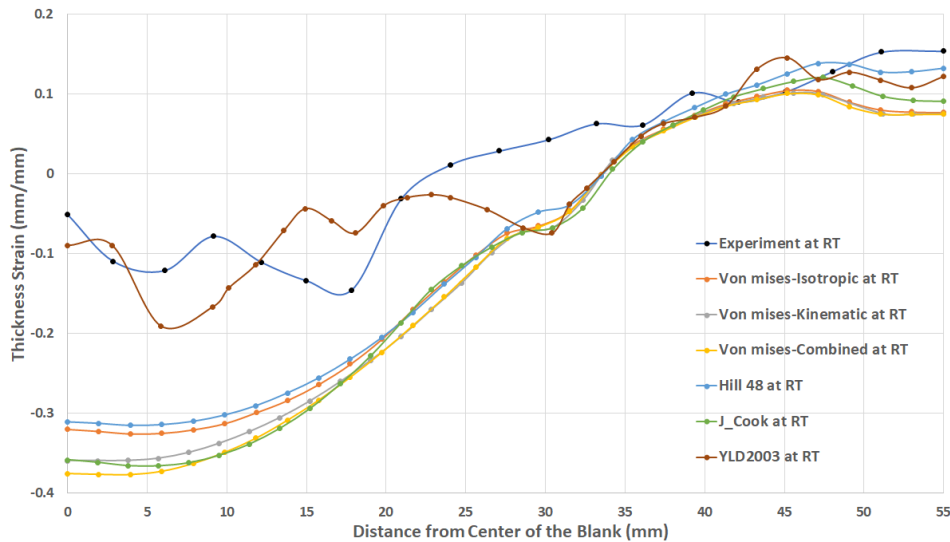


Figure 6.27: Thickness strain distributions for different models and experiment at room temperature (SS304, hemispherical, 45 mm punch travel)

Thickness strain distributions of the hemispherical deep drawing with 45 mm depth of punch at 300°C are shown in Figure 6.28 for all yield criteria. When YLD2003 yield criterion is compared with other models, it gave more uniform results for the region under the punch and wall of the cup. For the region under the punch, there were small deviations between Von Mises yield criterion with kinematic, combined hardening rules and Johnson-Cook model and between Von Mises yield criterion with

isotropic hardening rule and Hill48 yield criterion. At the flange region, Von Mises with combined hardening rule and Hill48 yield criteria gave more uniform results than other models. Whereas the thinning of the cup was observed at the cup wall area and the region under the punch, thickening of the cup was seen at the flange region.

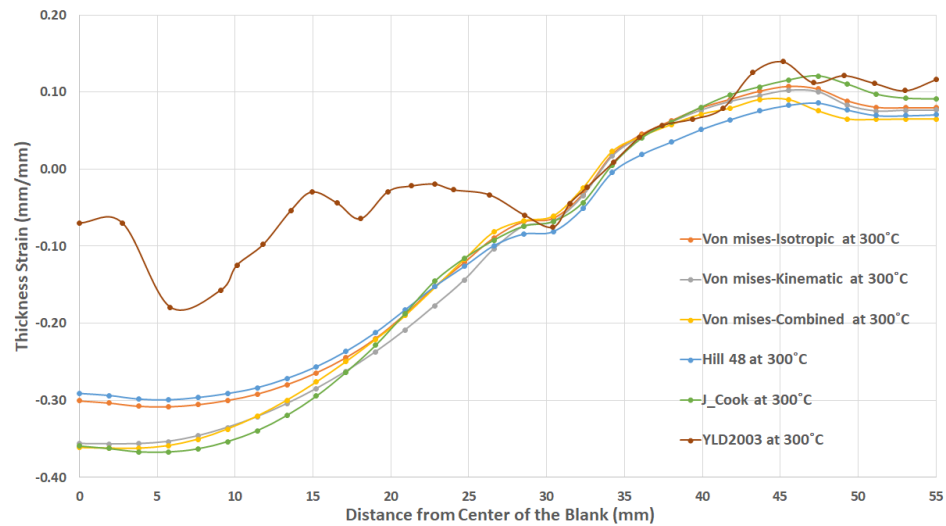


Figure 6.28: Thickness strain distributions for different models at 300°C (SS304, hemispherical, 45 mm punch travel)

Thickness strain distributions of the hemispherical deep drawing with 45 mm depth of punch at 600°C are shown in Figure 6.29 for all yield criteria. When YLD2003 yield criterion was compared with other models, it gave more uniform results for the region under the punch and wall of the cup. For the region under the punch, there were small deviations between Von Mises yield criterion with kinematic, combined hardening rules and Johnson-Cook model and, between von Mises with isotropic hardening rule and Hill48 yield criteria. At the flange region, von Mises with combined hardening rule and Hill48 yield criteria gave more uniform results. At the region under the punch and cup wall, the thinning of the cup was observed and thickening of the cup is seen at the flange region.

The results of the thickness strain distribution at room temperature, 300°C and 600°C showed same trend for all used models.

In Figure 6.30, the thickness strain distributions of hemispherical deep drawing

process at room temperature, 300°C and 600°C are presented for von-Mises yield criterion with isotropic hardening rule. Thickness strain and thinning of the sheet decrease with increasing temperature for the region under the punch. At the flange region of the cup, the thickening of the sheet was observed and there was not deviation between thickness strain values for at room temperature, 300°C and 600°C. The obtained results were close to each other at the cup wall region.

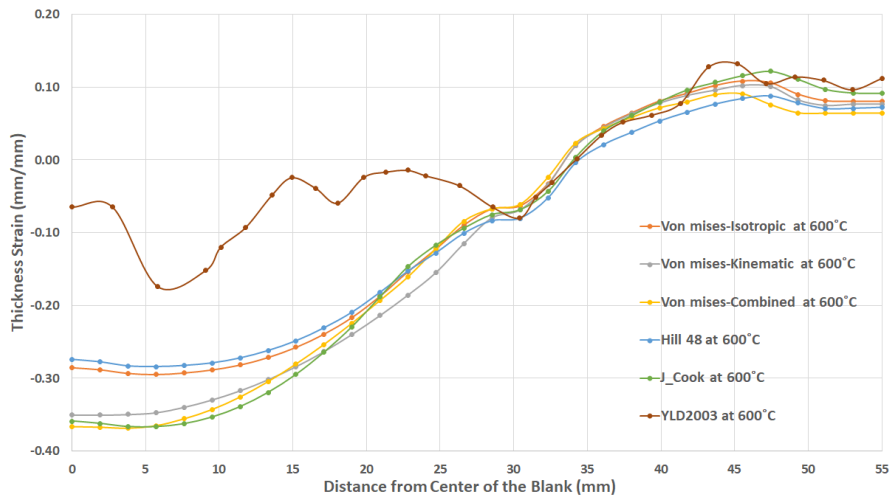


Figure 6.29: Thickness strain distributions for different models at 600°C (SS304, hemispherical, 45 mm punch travel)

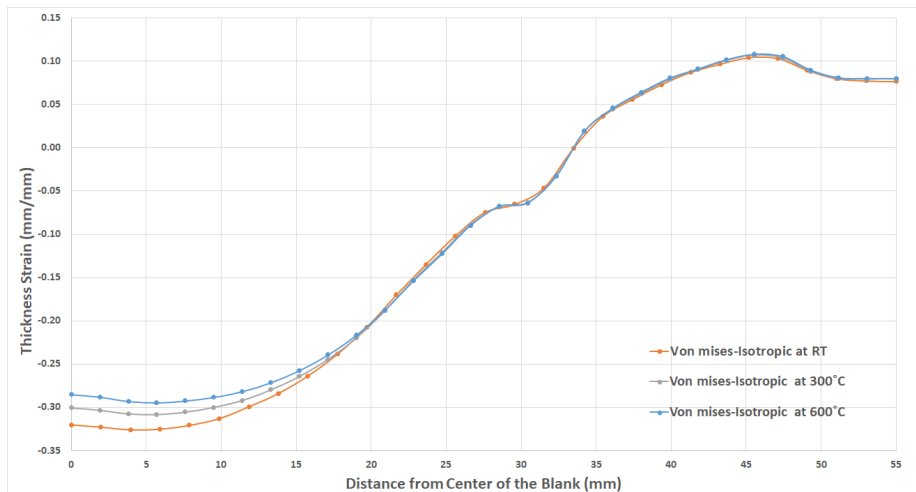


Figure 6.30: Effect of temperature on thickness strain distributions for von Mises-Isotropic (SS304, hemispherical, 45 mm punch travel)

In Figure 6.31, the thickness strain distributions of deep drawn hemispherical cup at temperature values of room temperature, 300°C and 600°C for von-Mises yield criterion with kinematic hardening rule are presented. Thickness strain and thinning of the sheet decreased with increasing temperature for the region under the punch and the cup wall region. At the flange region of the cup, thickening of the sheet was observed and there was not deviations between thickness strain values for these three temperature values.

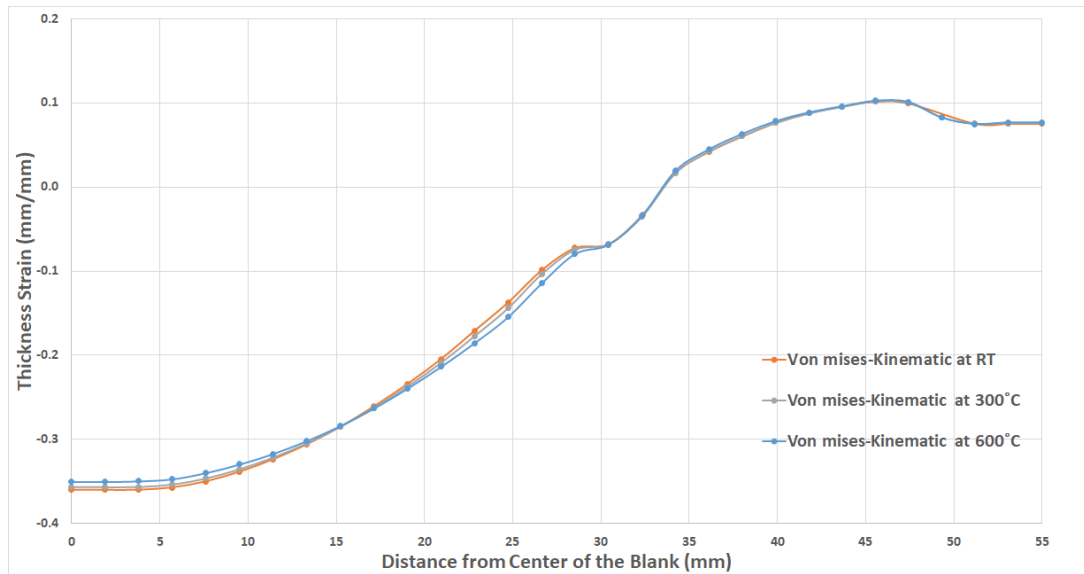


Figure 6.31: Effect of temperature on thickness strain distributions for von Mises-Kinematic (SS304, hemispherical, 45 mm punch travel)

In Figure 6.32, the thickness strain distributions of deep drawn hemispherical cup at temperature values of room temperature, 300°C and 600°C for von-Mises yield criterion with combined hardening rule are presented. Thickness strain and thinning of the sheet decreased with increasing temperature for the region under the punch and the cup wall region but thickness strain values were slightly lower at 300°C than 600°C. At the flange region of the cup, thickening of the sheet was observed. The more uniform shape was obtained at 600°C.

In Figure 6.33, thickness strain distributions of deep drawn hemispherical cup at temperature values of room temperature, 300°C and 600°C for Hill48 yield criterion with isotropic hardening rule are presented. Thickness strain and thinning of the sheet

decreased with increasing temperature for the region under the punch. More uniform shape was observed at 600°C for the region under the punch. At the small region of the cup wall, thinning of the sheet was observed. At the flange region, thickness strain and thickening of the sheet decreased with increasing temperature. There were not significant differences between thickness strains at 300°C and 600°C.

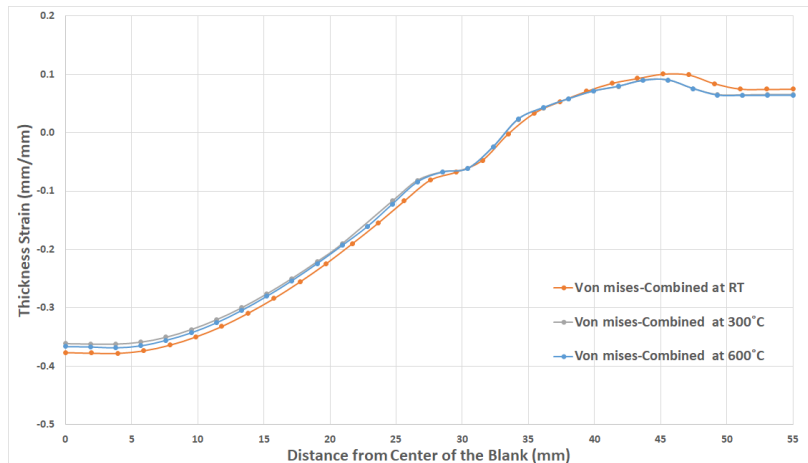


Figure 6.32: Effect of temperature on thickness strain distributions for von Mises-Combined (SS304, hemispherical, 45 mm punch travel)

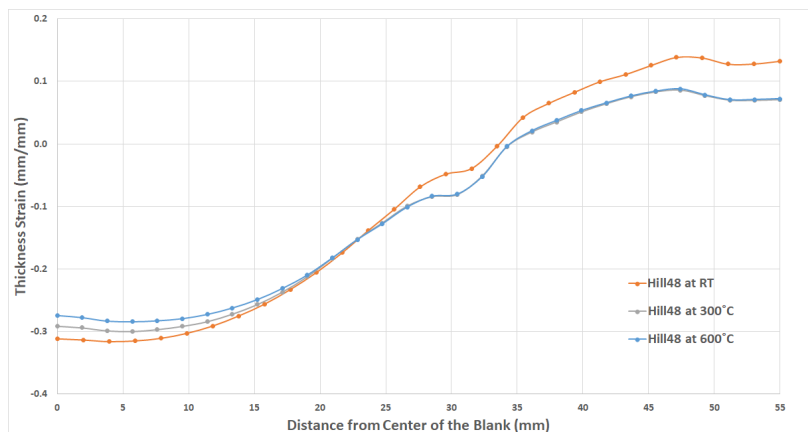


Figure 6.33: Effect of temperature on thickness strain distributions for Hill48 (SS304, hemispherical, 45 mm punch travel)

In Figure 6.34, the thickness strain distributions of deep drawn hemispherical cup at temperature values of room temperature, 300°C and 600°C for YLD2003-8p yield criterion are presented. Thickness strain and thinning of the sheet decreased

with increasing temperature for the region under the punch. More uniform results were obtained at 600°C for the region under the punch, moreover there were small deviations between thickness strains for 300°C and 600°C. At the small region of the cup wall, thinning of the sheet was observed. At the flange region, thickness strain and thickening of the sheet decreased with increasing temperature.

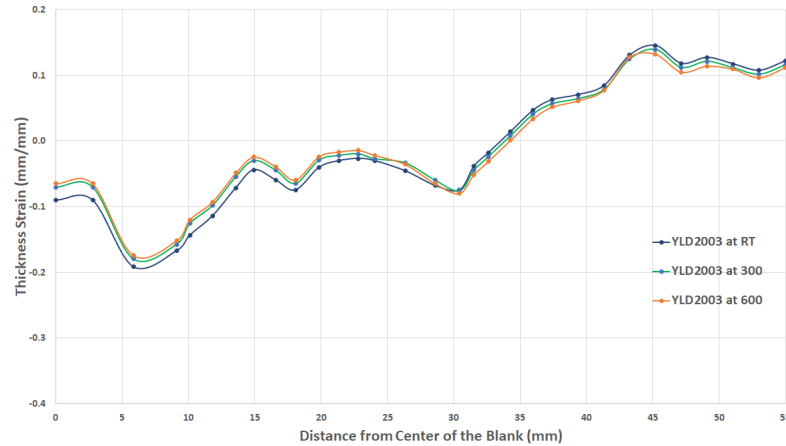


Figure 6.34: Effect of temperature on thickness strain distributions for YLD2003 (SS304, hemispherical, 45 mm punch travel)

### 6.3.2 Variation of Punch Force with Punch Displacement on Hemispherical Cup Deep Drawing for SS304

In Figures 6.35-6.37, variations of punch force with punch displacement are shown at room temperature, 300°C and 600°C respectively for 45 mm punch travel. In Figures 6.38-6.42, effects of temperature on variations of punch force with punch displacement are shown for von-Mises yield criterion with isotropic hardening rule, von-Mises yield criterion with kinematic hardening rule, von-Mises yield criterion with combined hardening rule, Hill48 yield criterion and YLD2003 yield criterion respectively with 45 mm punch travel.

Variations of punch forces with punch travel for SS304 sheet material are shown in Figure 6.35 at room temperature by using all yield criteria. YLD2003 yield criterion predicted the highest punch forces in all used yield criteria. The lowest punch forces were obtained from kinematic hardening rule with von Mises yield criterion.

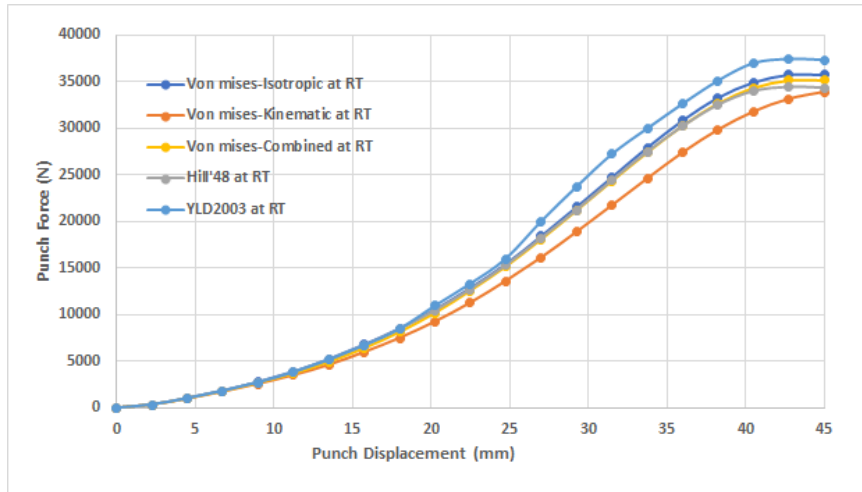


Figure 6.35: Punch force vs hemispherical punch displacement at room temperature for different models (SS304)

Variations of punch forces with punch travel for SS304 sheet material are shown in Figure 6.36 at 300°C by using all yield criteria. YLD2003 yield criterion predicted the highest punch forces in all used yield criteria. The lowest punch force was obtained from kinematic hardening rule with von Mises yield criterion. There are slight differences between values of punch forces of YLD2003, Hill48 yield criteria and von Mises yield criterion with isotropic and combined hardening rules.

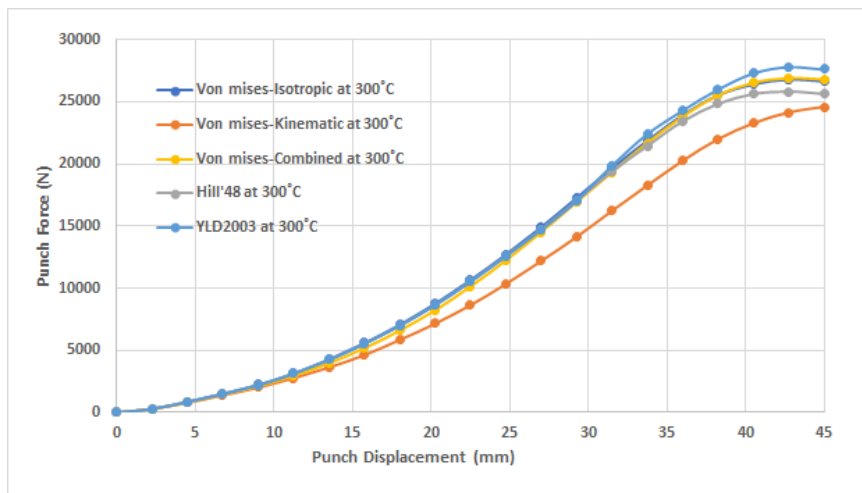


Figure 6.36: Punch force vs hemispherical punch displacement at 300°C for different models (SS304)

Variations of punch forces with punch travel for SS304 sheet material by using all yield criteria at 600°C are shown in Figure 6.37. Values of the punch forces are the highest for YLD2003 yield criterion in all used yield criteria. The lowest punch force values are obtained from kinematic hardening rule with von Mises yield criterion. There are slight differences between the values of punch forces of YLD2003, Hill48 and isotropic and combined hardening rules with von Mises yield criteria.

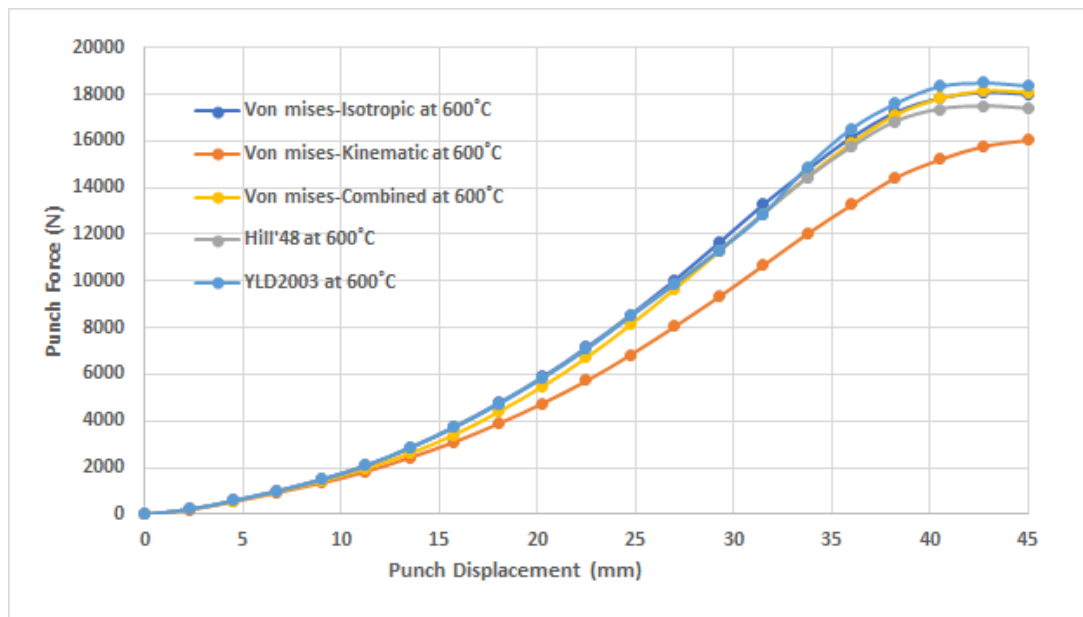


Figure 6.37: Punch force vs hemispherical punch displacement at 600°C for different models (SS304)

Effects of temperature variations on punch forces with punch displacement for von Mises yield criterion with isotropic, kinematic and combined hardening rules, Hill48, Johnson Cook model and YLD2003 yield criteria are shown in Figures 6.38-6.42.

It is observed that punch forces decrease with increasing temperature for all mentioned yield criteria, since strength of material decreases with increasing temperature. The differences of values of punch forces between analyses at room temperature, 300°C 600°C were about 9000 N at in temperature order for all mentioned yield criteria.

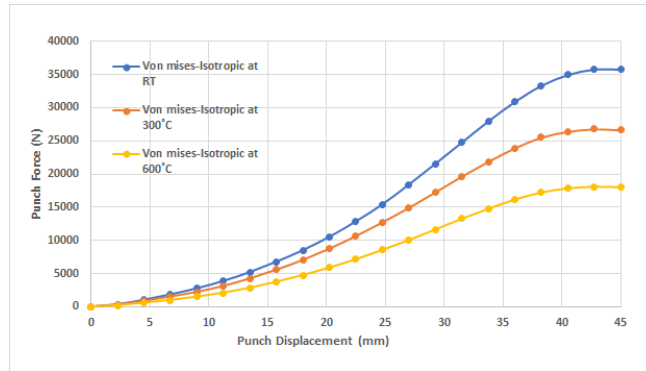


Figure 6.38: Punch force vs hemispherical punch displacement at different temperatures for von Mises-Isotropic (SS304)

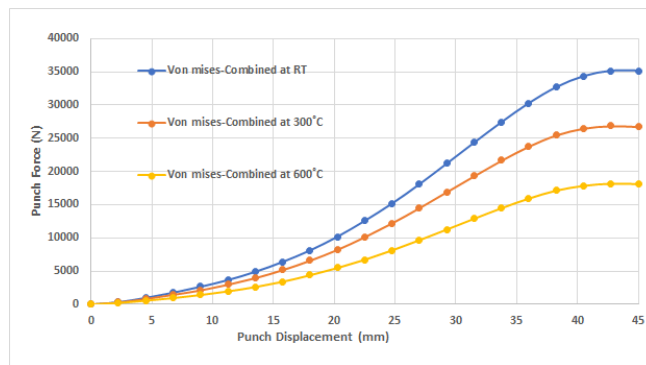


Figure 6.39: Punch force vs hemispherical punch displacement at different temperatures for von Mises-Combined (SS304)

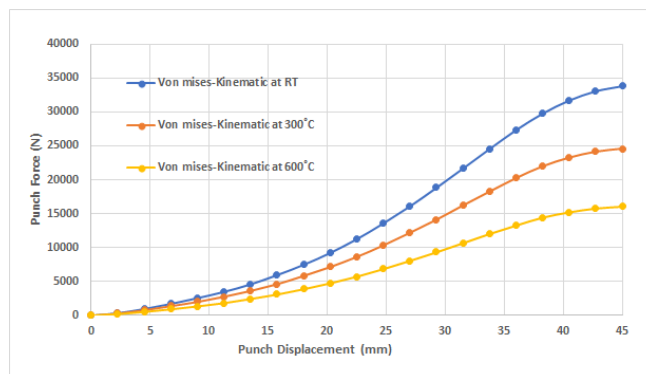


Figure 6.40: Punch force vs hemispherical punch displacement at different temperatures for von Mises-Kinematic (SS304)

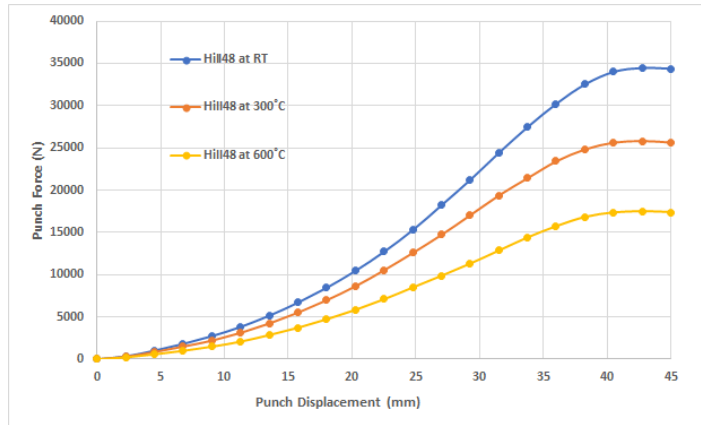


Figure 6.41: Punch force vs hemispherical punch displacement at different temperatures for Hill48 (SS304)

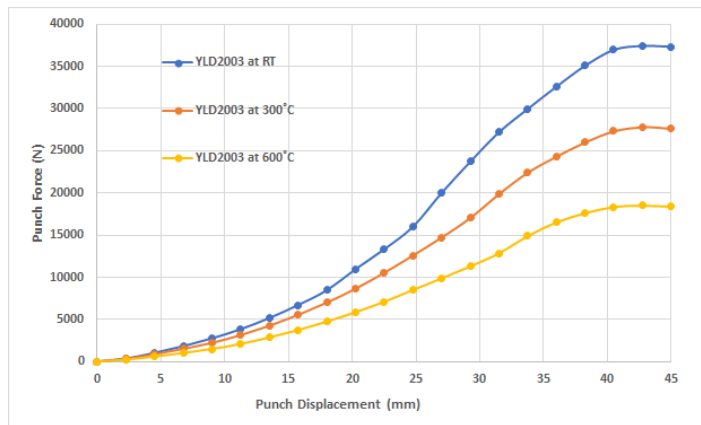


Figure 6.42: Punch force vs hemispherical punch displacement at different temperatures for YLD2003 (SS304)

### 6.3.3 Rim Shapes of Hemispherical Cup Deep Drawing for SS304

In this part, rim shapes of the undeformed and deformed blanks are shown in Figures 6.43-6.47 determined for all yield criteria separately at room temperature, 300°C and 600°C. Radius of the circular undeformed shape is 55 mm. By comparing these five figures, variations of the rim shapes are observed. Although the differences are not significant, it can be seen that radius of the rim shape of the deformed blank becomes smaller with decreasing temperature. The predicted flow of the blank into the die cavity is smaller for YLD2003 yield criterion. Variation of radius value increased at

the middle of the edge of the quarter rim shape.

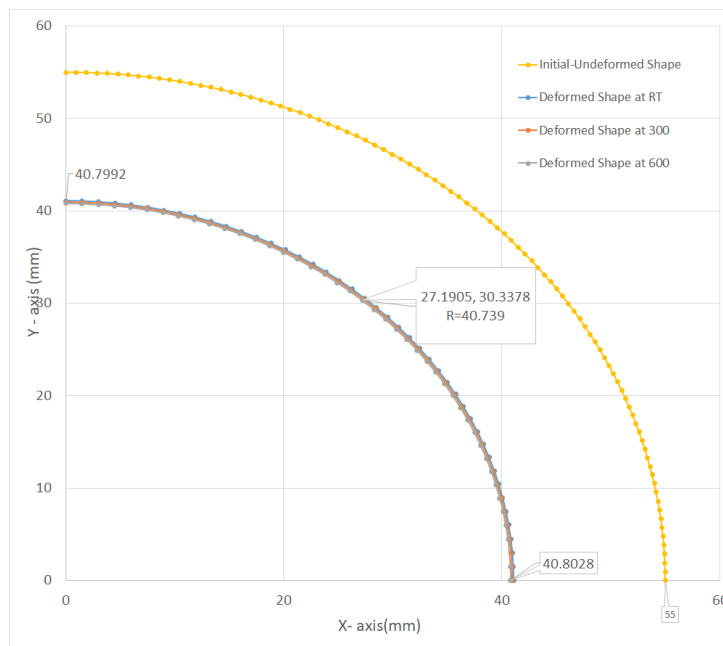


Figure 6.43: Rim shapes of the undeformed blank and deep drawn hemispherical cup at different temperatures. (SS304, VonMises-Isotropic)

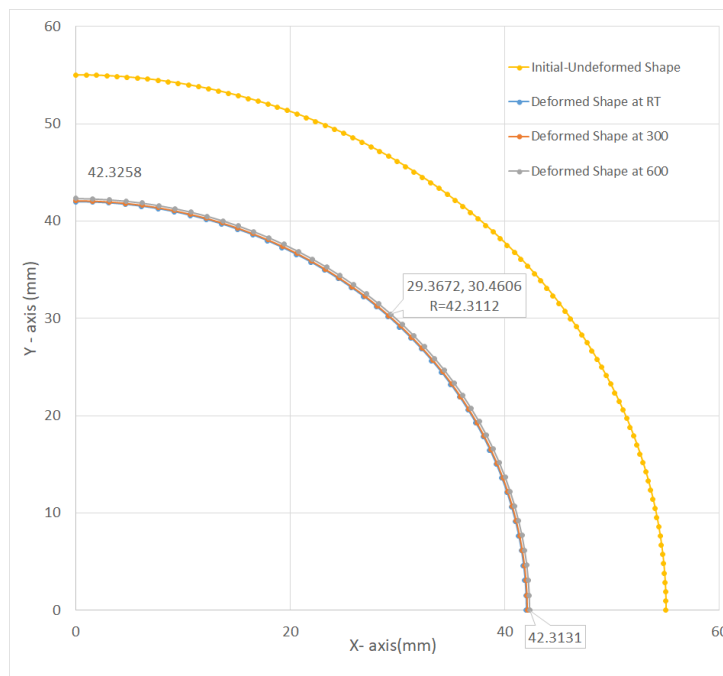


Figure 6.44: Rim shapes of the undeformed blank and deep drawn hemispherical cup at different temperatures. (SS304, VonMises-Kinematic)

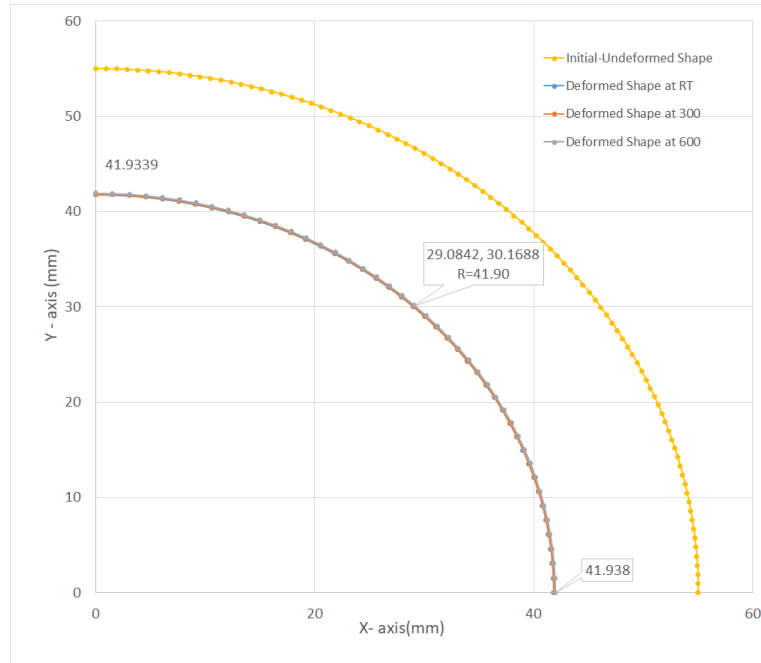


Figure 6.45: Rim shapes of the undeformed blank and deep drawn hemispherical cup at different temperatures. (SS304, VonMises-Combined)

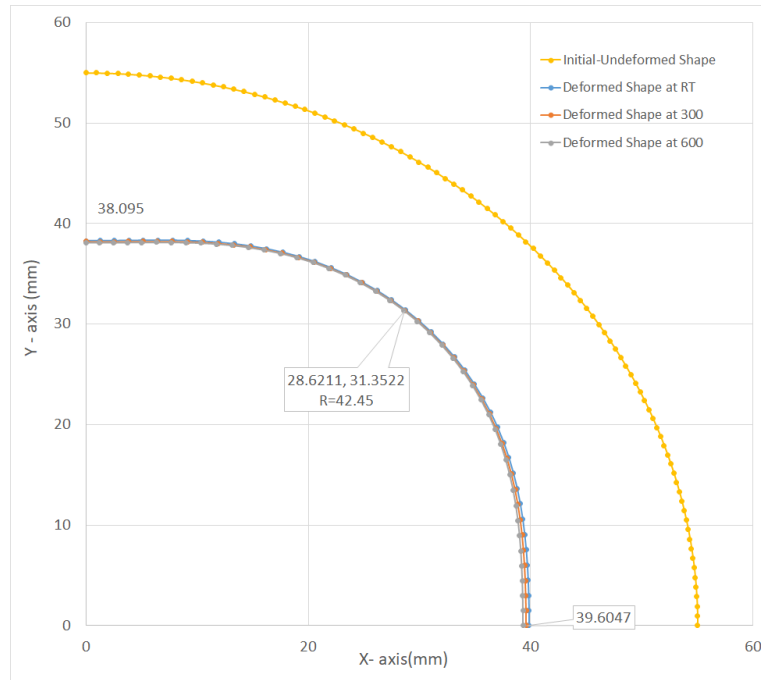


Figure 6.46: Rim shapes of the undeformed blank and deep drawn hemispherical cup at different temperatures. (SS304, Hill48)

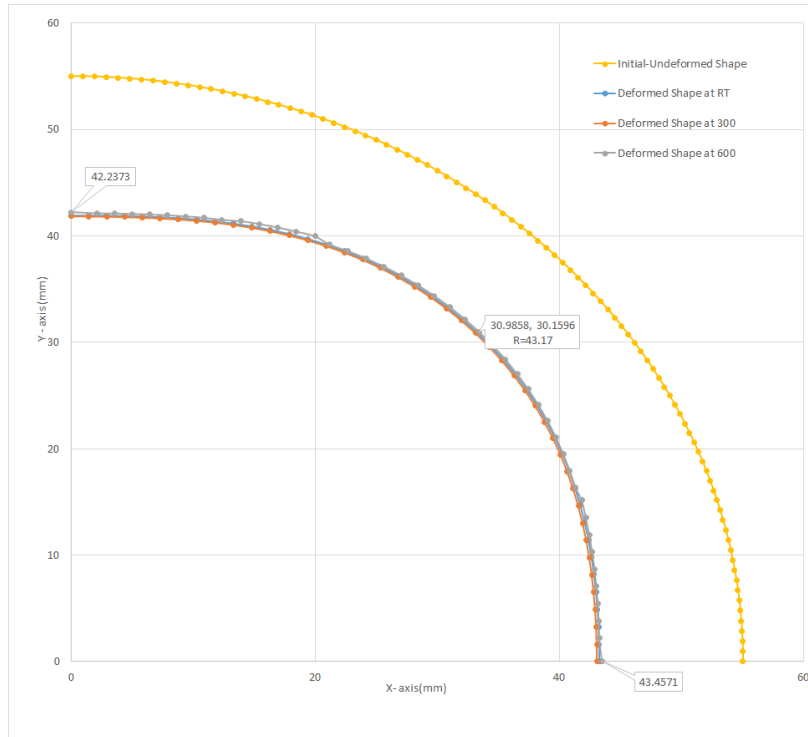


Figure 6.47: Rim shapes of the undeformed blank and deep drawn hemispherical cup at different temperatures. (SS304, YLD2003)

## 6.4 Results of Hemispherical Deep Drawing for AA5754

Since YLD2003-8p yield criterion gave the best approximate result to the experimental result in hemispherical deep drawing process for SS304 sheet material, only YLD2003-8p yield criterion was used with 25 mm punch travel at room temperature, 300°C and 520°C for AA5754. Since 600°C is the melting point of the AA5754 material, this temperature value was not used for analysis of AA5754 sheet material.

### 6.4.1 Thickness Strain Distribution on Hemispherical Cup Deep Drawing for AA5754

Results of the thickness strain distributions of the deep drawn hemispherical cup with 25 mm punch travel for YLD2003-8p yield criterion are shown in Figure 6.48. At the

region under the punch, thickness strains were more uniform at room temperature. Thickness strain values and thinning of the sheet increase with increasing temperature at that region. On the other hand, at the flange and cup wall regions, results of the thickness strains were close to each other. Thickness strains and thickening of the sheet decreased with increasing temperature at the flange region.

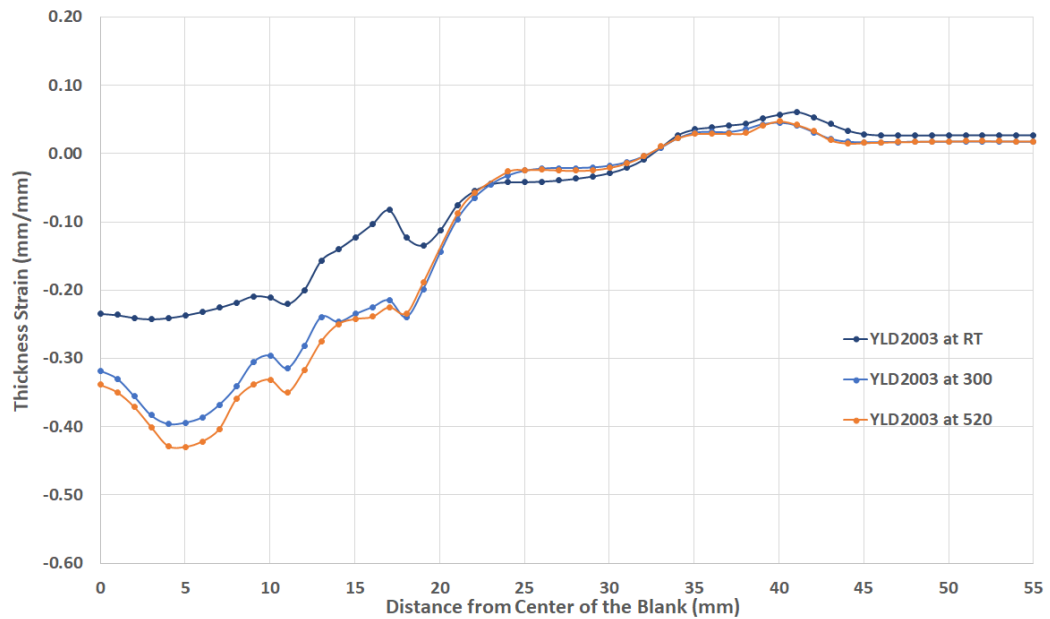


Figure 6.48: Effect of temperature on thickness strain distributions for YLD2003 (AA5754, hemispherical, 25 mm punch travel)

#### 6.4.2 Variation of Punch Force with Punch Displacement on Hemispherical Cup Deep Drawing for AA5754

In Figure 6.49, variations of punch force at room temperature, 300°C and 520°C are presented. Punch force decreased with increasing temperature. It is observed that magnitude of punch force is very low at 520°C, since 520°C is close to melting point of AA5754 and strength of material decreases.

Aluminum alloys are more ductile and weaker materials than steels, therefore it is observed that necessary punch force is lower for AA5754 than SS304.

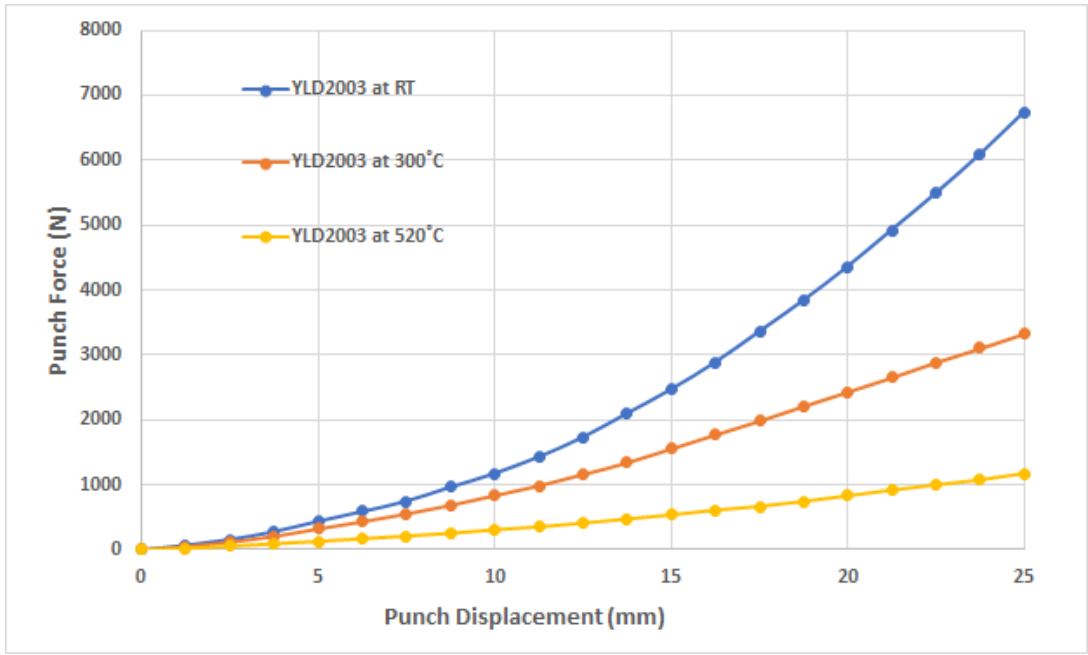


Figure 6.49: Punch force vs hemispherical punch displacement at different temperatures for YLD2003 (AA5754)

### 6.4.3 Rim Shapes of Hemispherical Cup Deep Drawing for AA5754

In this part, rim shapes of the undeformed and deformed blanks are shown in Figures 6.43-6.47 determined for all yield criteria separately at room temperature, 300°C and 600°C. Radius of the circular undeformed shape is 55 mm. By comparing these five figures, variations of the rim shapes are observed. Although the differences are not significant, it can be seen that radius of the rim shape of the deformed blank becomes smaller with decreasing temperature. The predicted flow of the blank into the die cavity is smaller for YLD2003 yield criterion. Variation of radius value increased at the middle of the edge of the quarter rim shape.

In Figure 6.50, rim shapes of deep drawn hemispherical cup are shown for AA5754 sheet material. It was observed that radius of the rim shape of the deformed blank became smaller with decreasing temperature. The differences of rim shapes were not significant at 300°C and 520°C. Since YLD2003 yield criterion is an anisotropic yield criterion, radius of a rim shape changes on the edge of the shape at any point.

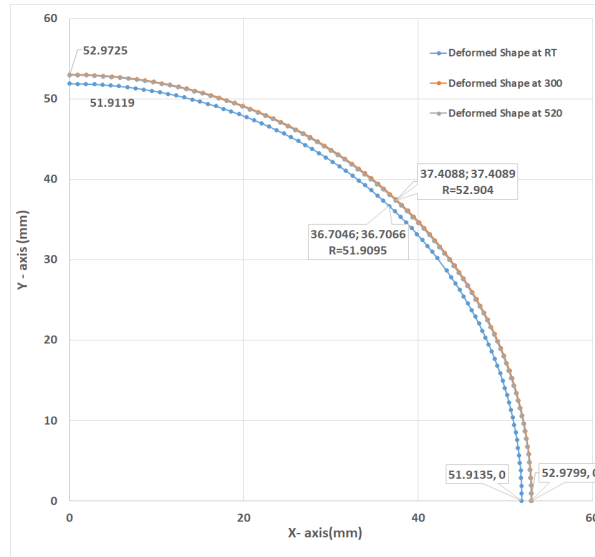


Figure 6.50: Rim shapes of the undeformed blank and deep drawn hemispherical cup at different temperatures. (AA5754, YLD2003)

## 6.5 Results of Square Deep Drawing for SS304

Obtained results from FE analyses of deep drawn square cup with experimental result taken from study of Cogun and Darendeliler [2] are presented in this section. Von Mises yield criterion with isotropic, kinematic and combined hardening rules, Johnson Cook model, Hill48 and YLD2003-8p yield criteria were used at room temperature, 300°C and 600°C for 25 mm punch travel value and experimental thickness strain distribution is available only at room temperature. Thickness strain distribution from center of blank and variation of punch force with respect to punch displacement at different temperatures are shown in Figures 6.51-6.66. Moreover, rim shapes of the deep drawn square cup for all mentioned yield criteria and temperatures are shown in Figures 6.67-6.71.

### 6.5.1 Thickness Strain Distribution on Square Cup Deep Drawing for SS304

Thickness strain distributions of the deep drawn square cup at room temperature are shown in Figure 6.51 for all mentioned yield criteria and experiment. At the region

under the punch, there were small deviations between the all used yield criteria and hardening rules. Thickness strain values of Hill48 yield criterion and von-Mises yield criterion with kinematic hardening rule were closer to thickness strain values of experiment than other models for the region under the square punch. At the bend radius and the nearby area, thinning of the sheet material was observed significantly except for YLD2003 yield criterion and experiment. Johnson-Cook model gave good results according to experimental result at the cup wall region. At the flange region of the cup, sheet materials got thickening and, YLD2003 yield criterion agrees well with experiment result.

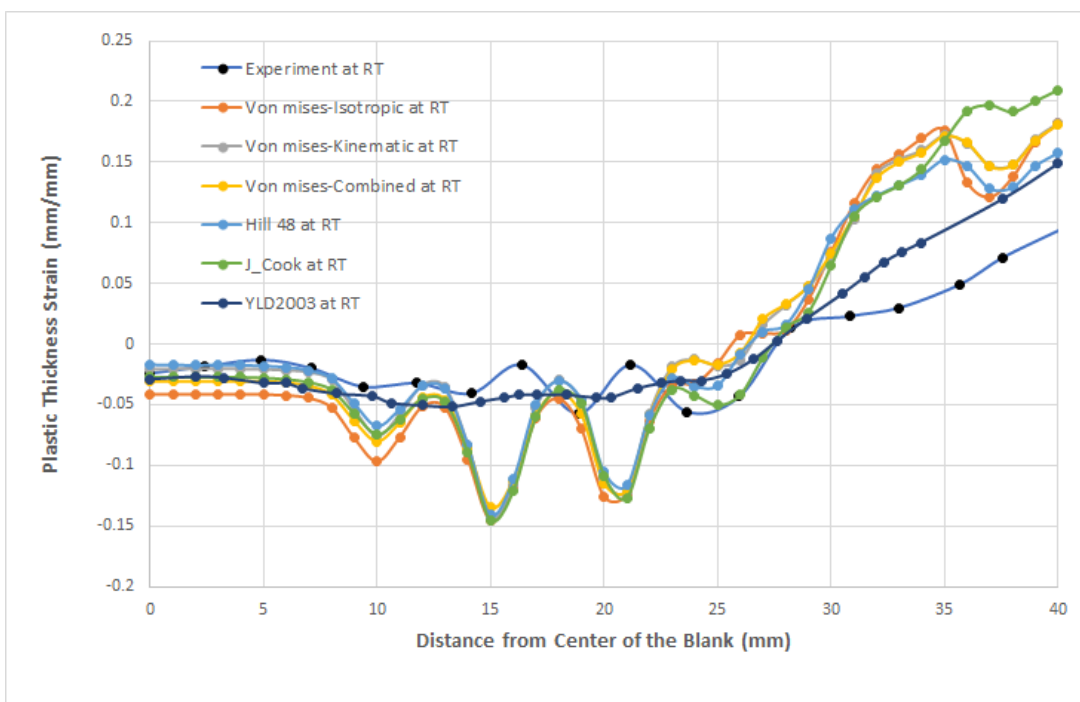


Figure 6.51: Thickness strain distributions for different models and experiment at room temperature (SS304, square, 25 mm punch travel)

Thickness strain distributions of the square deep drawing at 300°C are shown in Figure 6.52 for all mentioned yield criteria. At the region under the punch, there were small deviations between the all used yield criteria and hardening rules. YLD2003 Hill48 yield criterion and von-Mises yield criterion with combined hardening rule gave more uniform results at the region under the punch. At the bend radius and the nearby area, sheet material got thinner significantly except for YLD2003 yield

criterion. Von-Mises yield criterion with combined and kinematic hardening rules gave more uniform results and thinning was observed at the small part of the cup wall region. At the other part of the cup wall region, thickening of the sheet material was observed and YLD2003 gave more uniform results. At the flange region of the cup, thickening of the sheet materials was seen and, YLD2003 and Hill48 yield criteria gave more uniform results.

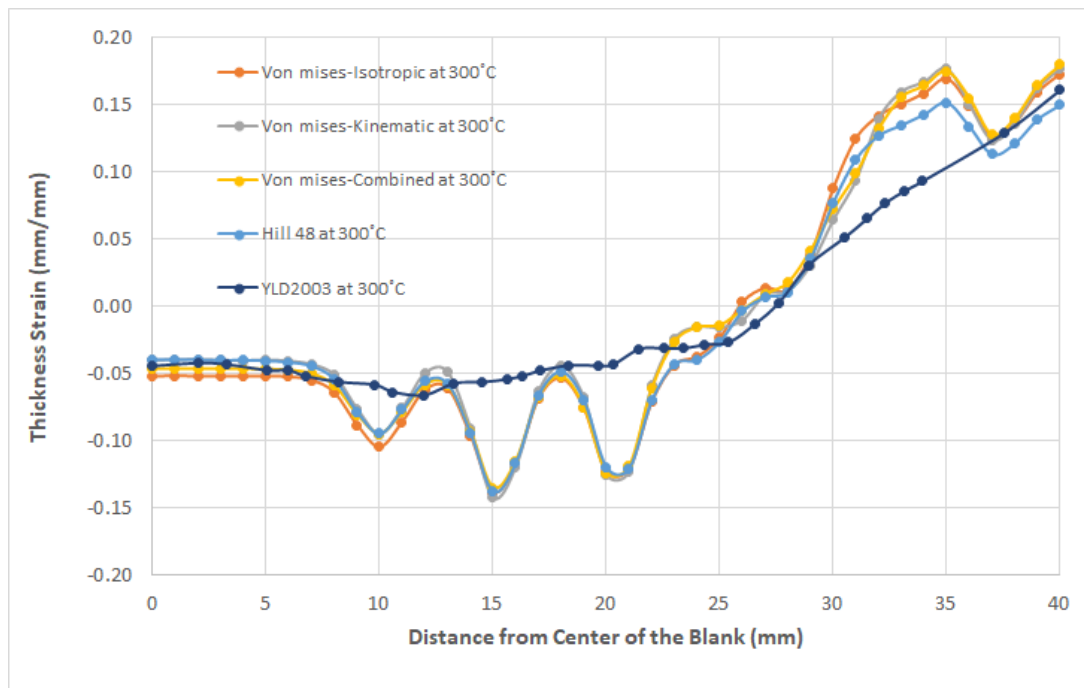


Figure 6.52: Thickness strain distributions for different yield criteria at 300°C (SS304, square, 25 mm punch travel)

Thickness strain distributions of the square deep drawing at 600°C are shown in Figure 6.53 for all mentioned yield criteria. At the region under the punch, there were small deviations between the all used yield criteria and hardening rules. YLD2003 and Hill48 yield criteria gave more uniform result at the region under the square punch. At the bend radius and the nearby area, thinning of the sheet material was observed significantly and, there were not significant deviation except for YLD2003 yield criterion. Von-Mises yield criterion with combined and kinematic hardening rules gave more uniform results and thinning of the sheet was observed at the small part of the cup wall region. At the other part of the cup wall region, thickening of the sheet material was seen and YLD2003 gave more uniform results. At the flange

region of the cup, sheet material has got thickening and, Hill48 yield criterion gave more uniform results.

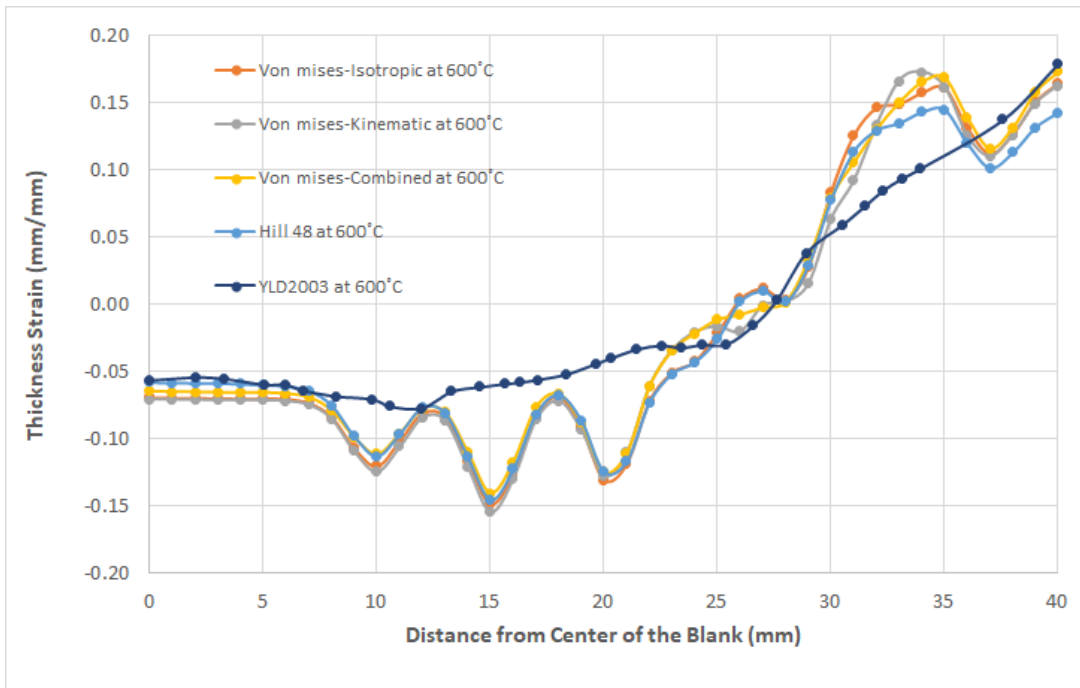


Figure 6.53: Thickness strain distributions for different yield criteria at 600°C (SS304, square, 25 mm punch travel)

As a result of Figures 6.51-6.53, YLD2003 yield criterion gave more uniform result for all temperature values, and agreed well with experimental results at room temperature.

In Figure 6.54, thickness strain distributions of deep drawn square cups are presented at room temperature, 300°C and 600°C for von-Mises yield criterion with isotropic hardening rule. Thickness strain and thinning of the sheet increased with increasing temperature at the region under the punch. Thinning of the blank increased dramatically at the bend radius and the nearby area. At most of the cup wall region, there were not significant deviations, however; at the flange region, thickness strain values and thickening of the sheet decreased with increasing temperature. Maximum thickening was observed at the flange region and, maximum thinning was seen at the bend radius and the nearby area.

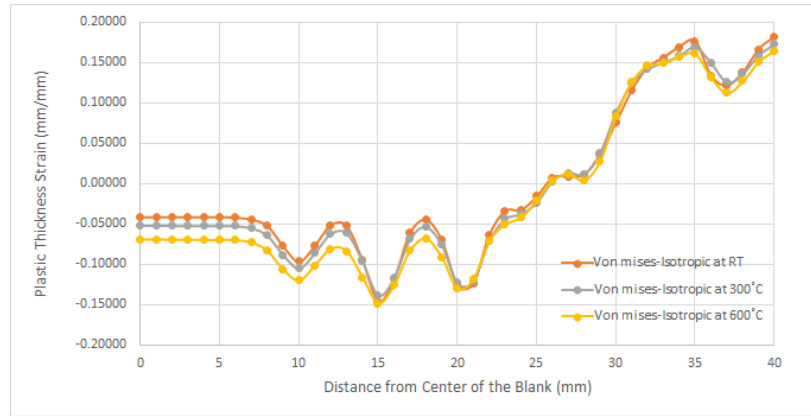


Figure 6.54: Effect of temperature on thickness strain distributions for von Mises-Isotropic (SS304, square, 25 mm punch travel)

In Figure 6.55, thickness strain distributions of deep drawn square cups at room temperature, 300°C and 600°C for von-Mises yield criterion with kinematic hardening rule are presented. Thickness strain and thinning of the sheet increase with increasing temperature at the region under the punch. Thinning of the sheet increased dramatically at the bend radius and the nearby area. More thinning was observed for kinematic hardening rule than isotropic hardening rules. At the thickening region of the cup wall and the flange region, thickness strain values and thickening decreased with increasing temperature. Maximum thickening was observed at the flange region and, maximum thinning is seen at the bend radius and the nearby area.

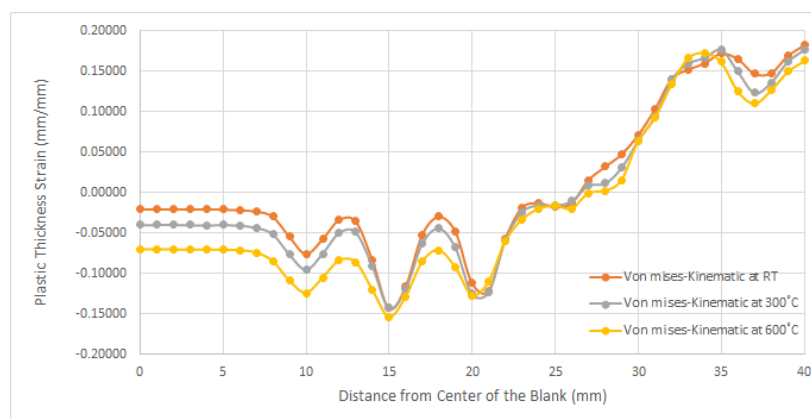


Figure 6.55: Effect of temperature on thickness strain distributions for von Mises-Kinematic (SS304, square, 25 mm punch travel)

In Figure 6.56, thickness strain distributions of deep drawn square cups at room temperature, 300°C and 600°C for von-Mises yield criterion with combined hardening rule are presented. Thickness strain and thinning of the sheet increased with increasing temperature at the region under the punch. Thinning increased dramatically at the bend radius and the nearby area. Thickness strain values of combined hardening rule were very close to thickness strain values of kinematic hardening rule for most of the region. At the thickening region of the cup wall and the flange region, thickness strain values and thickening of the sheet decreased with increasing temperature. Maximum thickening was observed at the flange region and, maximum thinning was seen at the bend radius and the nearby area.

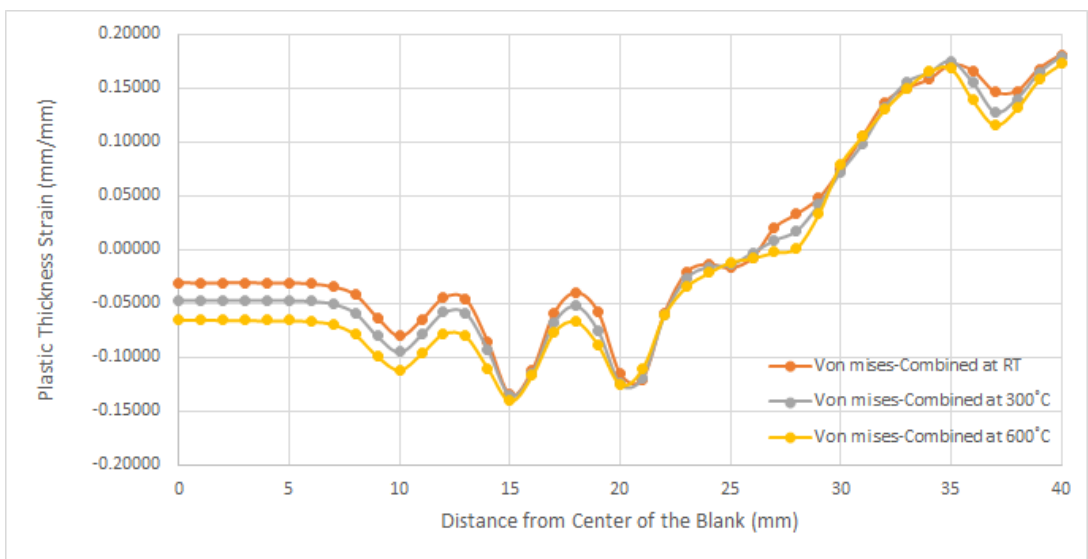


Figure 6.56: Effect of temperature on thickness strain distributions for von Mises-Combined (SS304, square, 25 mm punch travel)

In Figure 6.57, thickness strain distributions of deep drawn square cups at room temperature, 300°C and 600°C for Hill48 yield criterion are presented. Thickness strain and thinning of the sheet increased with increasing temperature at the region under the punch. Thinning of the sheet increased dramatically at the bend radius and the nearby area. At thickening region of the cup wall and the flange region, thickness strain values and thickening of the sheet decreased with increasing temperature. Maximum thickening was observed at the flange region and, maximum thinning was seen at the bend radius and the nearby area.

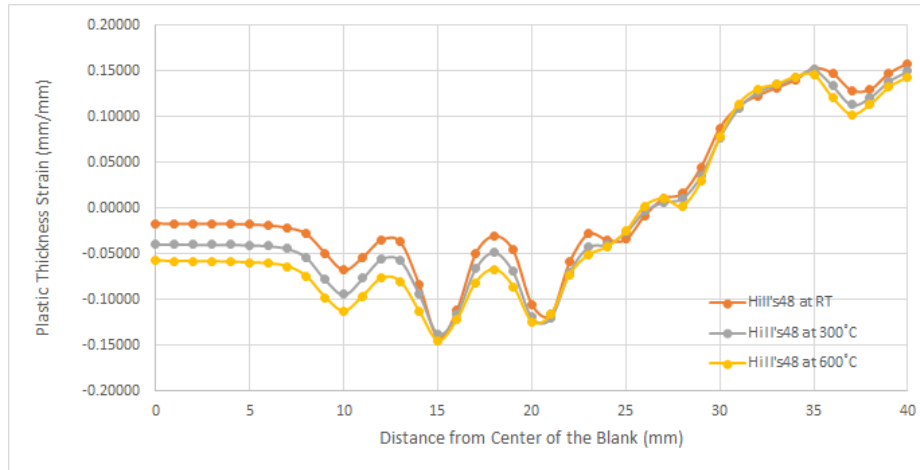


Figure 6.57: Effect of temperature on thickness strain distributions for Hill48 (SS304, square, 25 mm punch travel)

In Figure 6.58, thickness strain distributions of deep drawn square cups at room temperature, 300°C and 600°C for YLD2003 yield criterion are presented. Thickness strain and thinning of the sheet increased with increasing temperature at the region under the punch. Thinning of the sheet increased at the bend radius and the nearby area, however; this thinning of the blank is lower for YLD2003 yield criterion than other models. At the thickening region of the cup wall and the flange region, thickness strain values and thickening of the sheet decreased with increasing temperature.

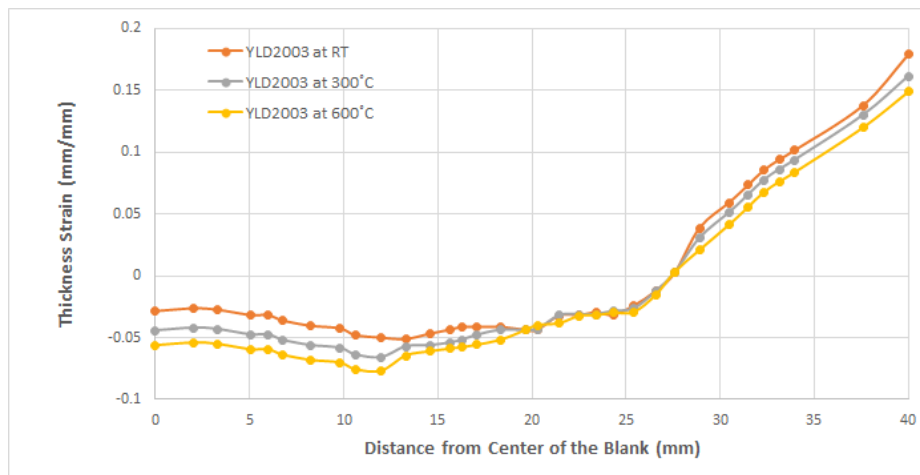


Figure 6.58: Effect of temperature on thickness strain distributions for YLD2003-8P Yield Criteria (SS304, square, 25 mm punch travel)

### 6.5.2 Variation of Punch Force with Punch Displacement on Square Cup Deep Drawing for SS304

In Figures 6.59-6.61, variations of punch forces with punch displacement are presented at room temperature, 300°C and 600°C respectively by using all mentioned models. Von Mises with isotropic hardening rule and YLD2003 yield criteria predicted the higher punch forces than other models at room temperature and 300°C. Moreover, the highest punch forces were predicted by only YLD2003 yield criterion at 600°C. The lowest punch force values were obtained from kinematic hardening rule with von Mises yield criterion at room temperature, 300°C and 600°C throughout the whole punch travel.

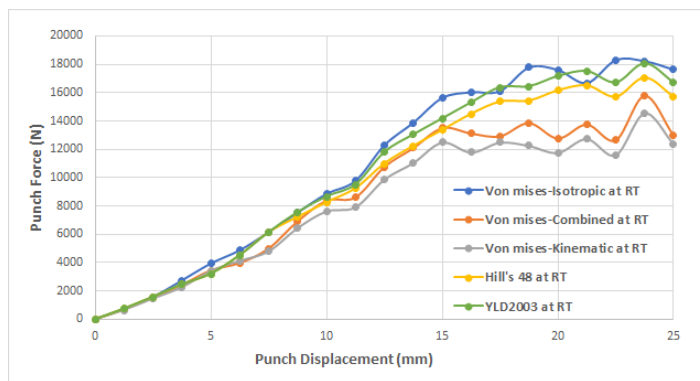


Figure 6.59: Punch force vs square punch displacement at room temperature for different models (SS304)

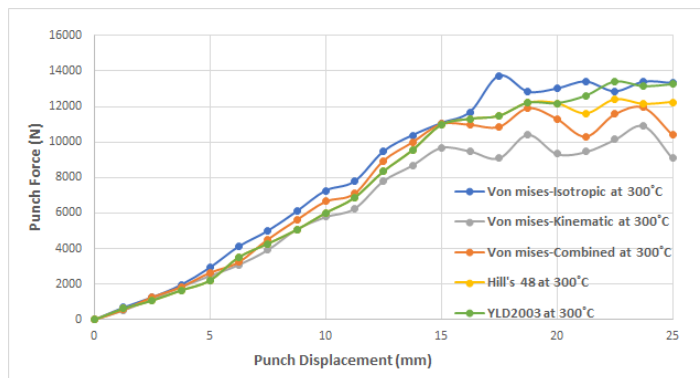


Figure 6.60: Punch force vs square punch displacement at 300°C for different models (SS304)

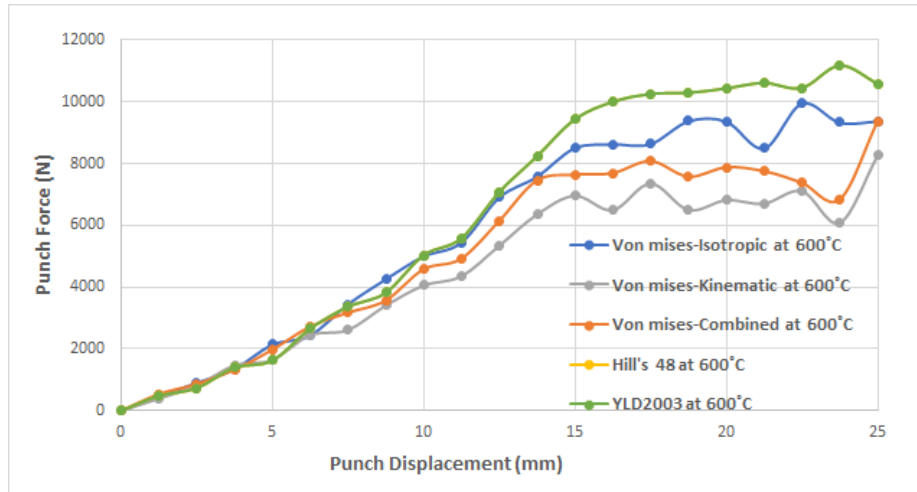


Figure 6.61: Punch force vs square punch displacement at 600°C for different models (SS304)

In Figures 6.62-6.66, effects of the temperature on variations of the punch force with punch displacements are shown for isotropic, kinematic and combined hardening rules with von Mises yield criterion, Hill48 and YLD2003 yield criteria respectively. The punch force values are lower at elevated temperatures than room temperature for all mentioned models, since strength of material decreases with increasing temperature.

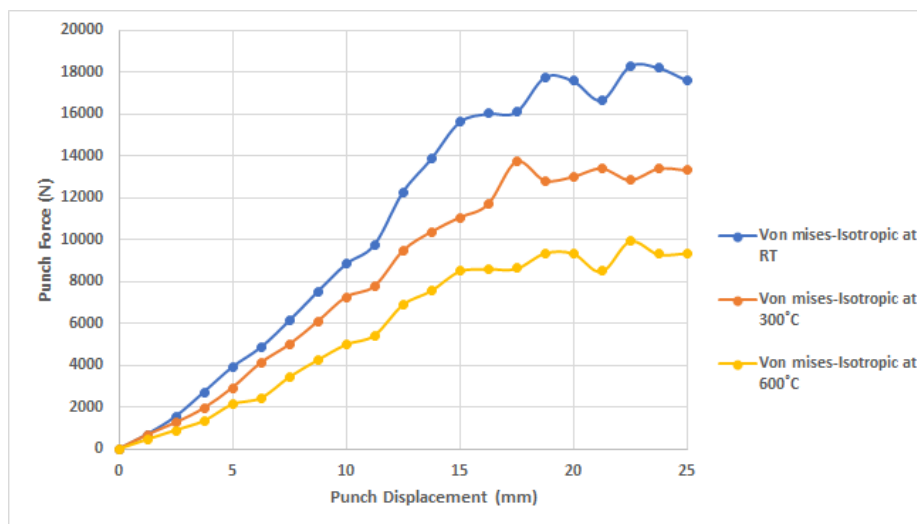


Figure 6.62: Punch force vs square punch displacement at different temperatures for von Mises-Isotropic (SS304)

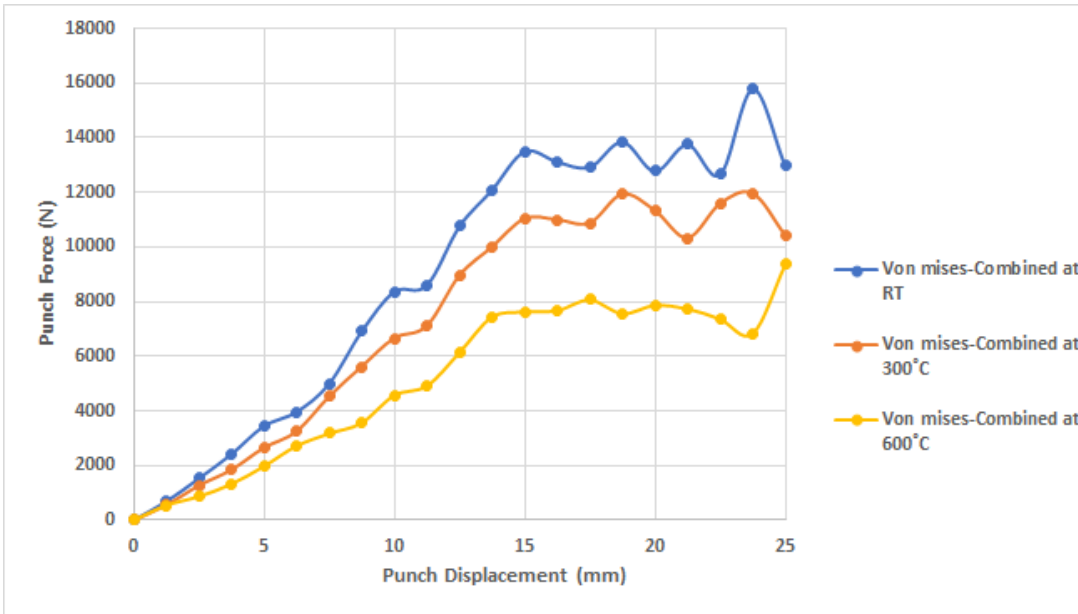


Figure 6.63: Punch force vs square punch displacement at different temperatures for von Mises-Combined (SS304)

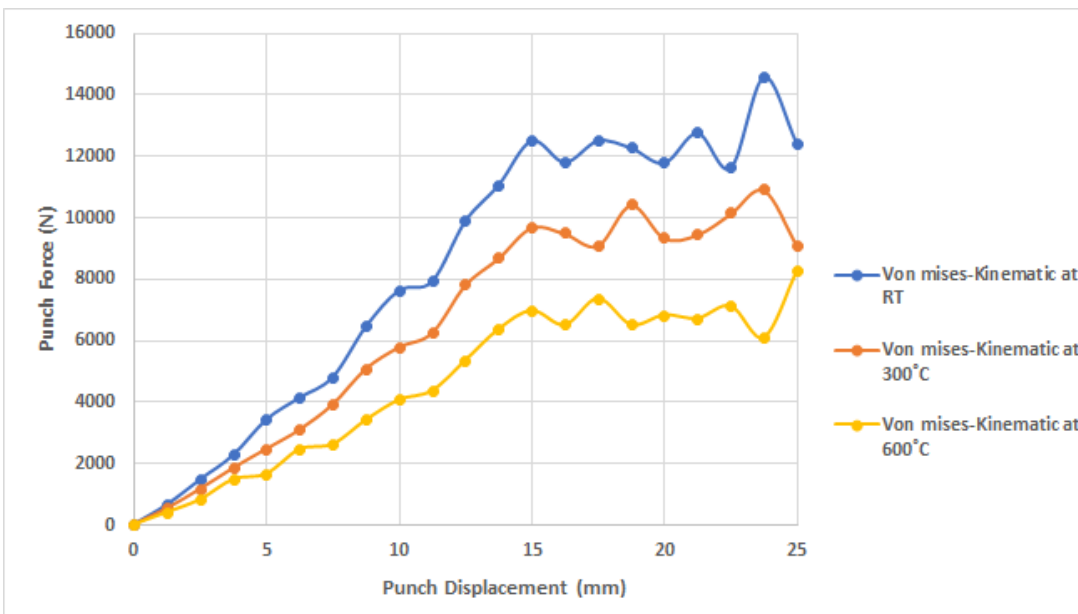


Figure 6.64: Punch force vs square punch displacement at different temperatures for von Mises-Kinematic (SS304)

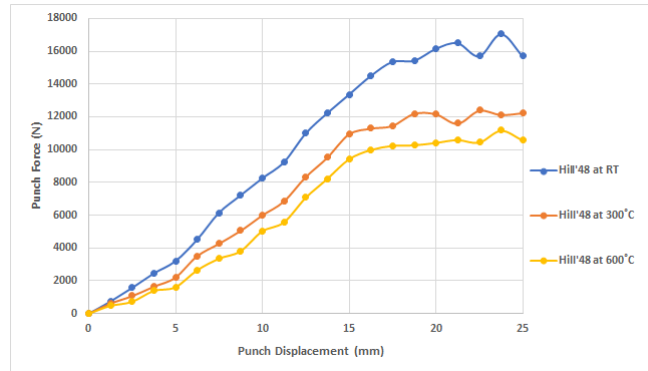


Figure 6.65: Punch force vs square punch displacement at different temperatures for Hill48 (SS304)

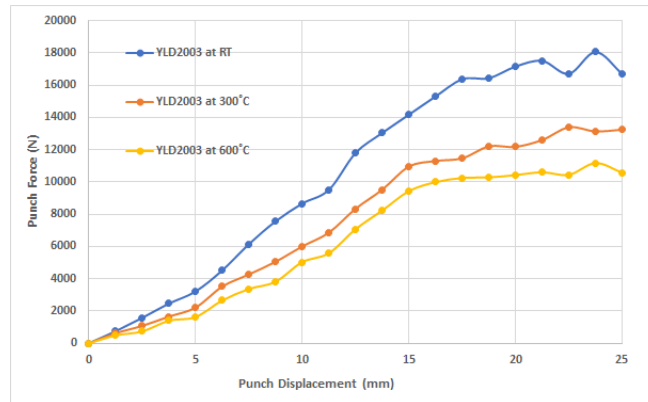


Figure 6.66: Punch force vs square punch displacement at different temperatures for YLD2003-8P (SS304)

### 6.5.3 Rim Shapes of Square Cup Deep Drawing for SS304

In Figures 6.67-6.71, effects of the temperature variation on rim shapes of deep drawn SS304 square cups are shown. By comparing these five figures, variations of the rim shapes are observed. The area of the rim shape of the deformed blank becomes smaller with decreasing temperature. Edges of the blank are more drawn to the center of the blank with decreasing temperature. At the corners of the blanks, the differences of flowing materials are lower for blanks at the different temperature values. The effects of the temperature on rim shapes were seen more easily for Hill48 and YLD2003 yield criteria, since these yield criteria are anisotropic.

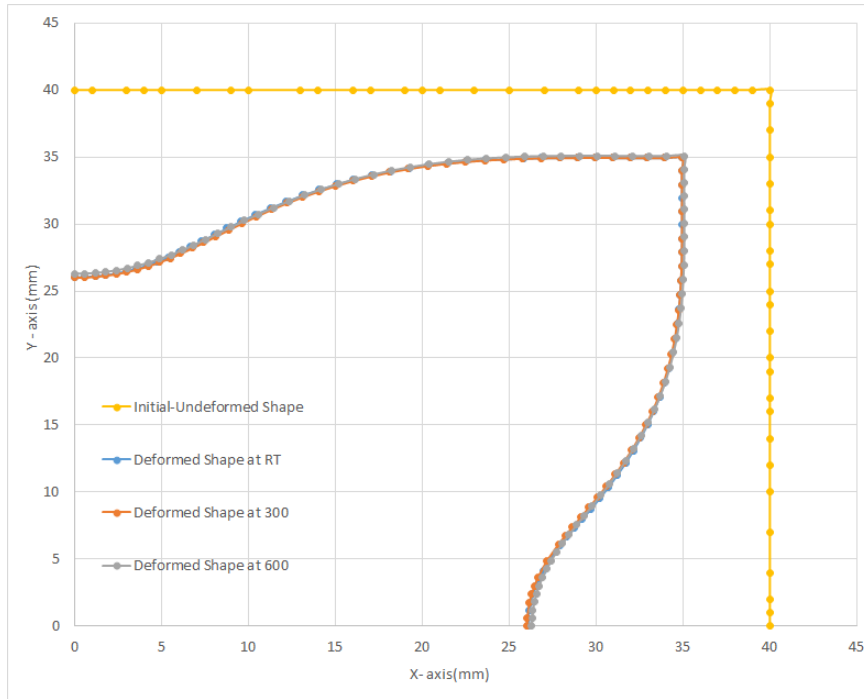


Figure 6.67: Rim shapes of the undeformed blank and deep drawn square cup at different temperatures. (SS304, VonMises-Isotropic)

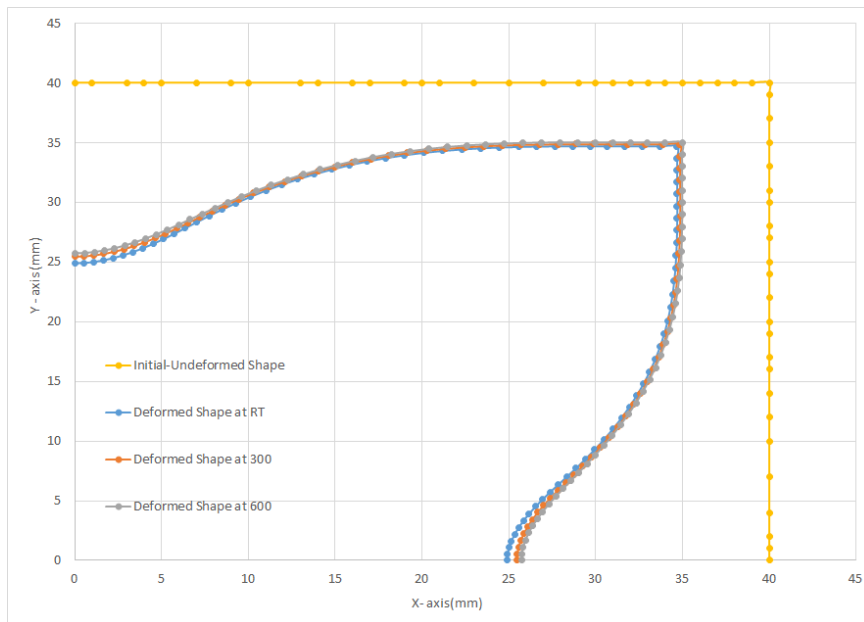


Figure 6.68: Rim shapes of the undeformed blank and deep drawn square cup at different temperatures. (SS304, VonMises-Kinematic)

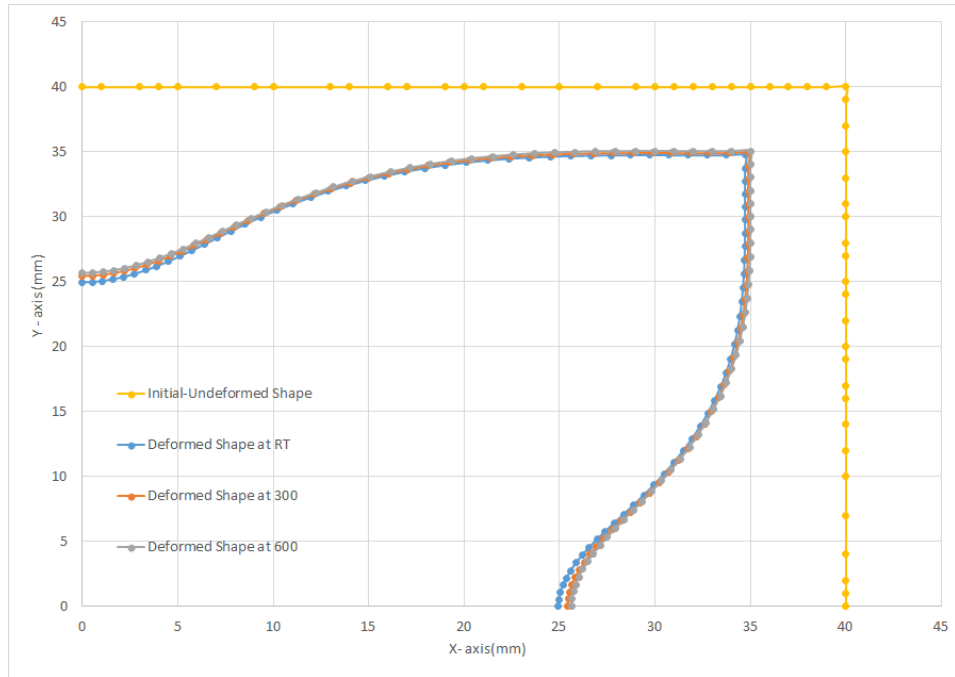


Figure 6.69: Rim shapes of the undeformed blank and deep drawn square cup at different temperatures. (SS304, VonMises-Combined)

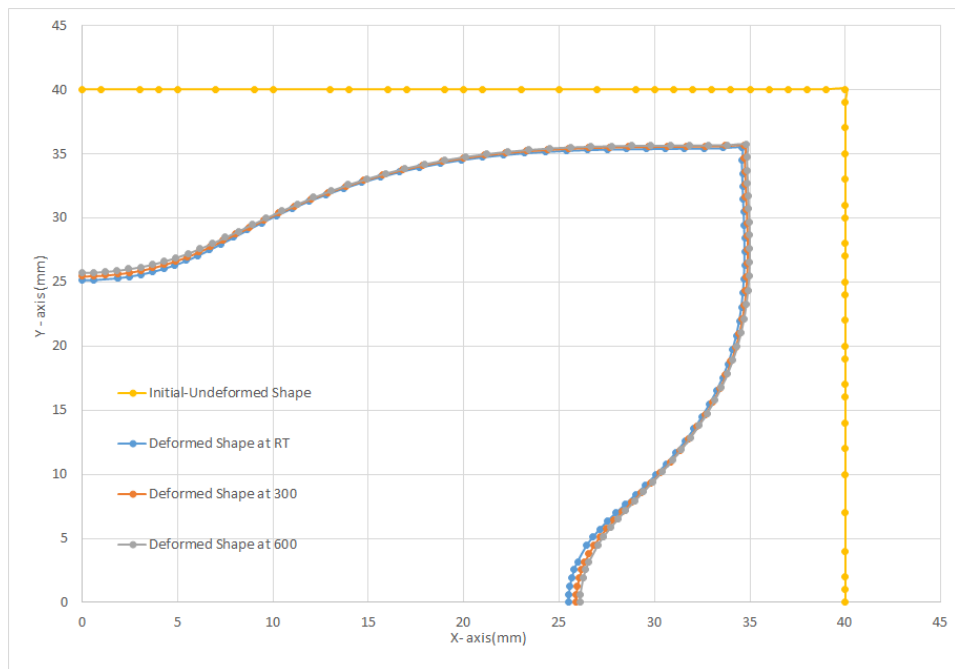


Figure 6.70: Rim shapes of the undeformed blank and deep drawn square cup at different temperatures. (SS304, Hill48)

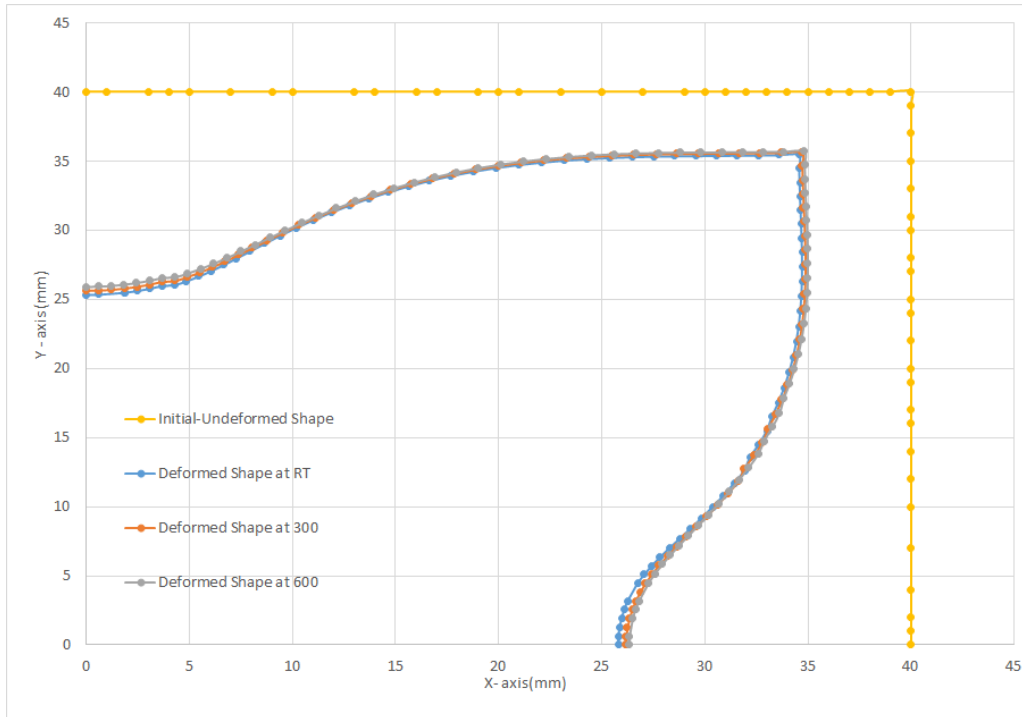


Figure 6.71: Rim shapes of the undeformed blank and deep drawn square cup at different temperatures. (SS304, YLD2003)

## 6.6 Results of Square Deep Drawing for AA5754

Since YLD2003-8p yield criterion has given the closest results to the experimental results in square deep drawing for SS304 sheet material, only YLD2003-8p yield criterion has been used with 25 mm punch travel at room temperature, 300°C and 520°C for AA5754 sheet material.

### 6.6.1 Thickness Strain Distribution on Square Cup Deep Drawing for AA5754

In Figure 6.72, effects of temperature variation on thickness strain distributions of deep drawn square cup made of AA5754 are shown. Thickness strains and thinning of the sheet decreased with increasing temperature at the region under the punch, however; thickness strain and thickening increased at the flange region. At the cup wall region, both thinning and thickening of the sheet were observed.

When the thickness strain values of AA5754 sheet material are compared with thickness strain values of SS304 sheet material, more uniform results are obtained from AA5754 sheet material at the region under the punch, however; at the flange region, SS304 sheet material gives more uniform results at the same temperature values.

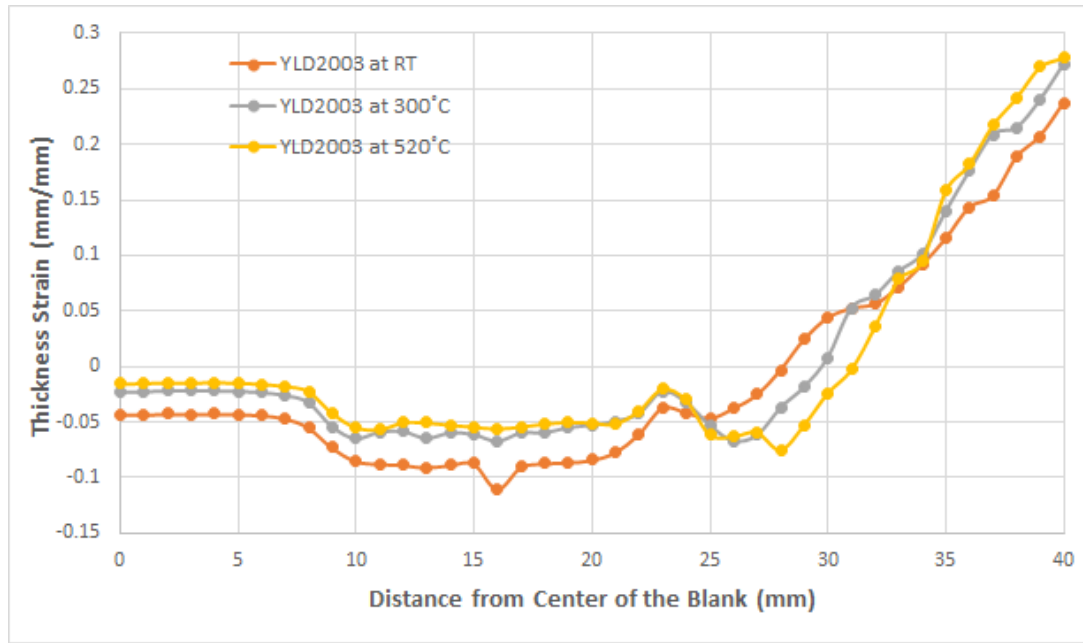


Figure 6.72: Effect of temperature on thickness strain distributions for YLD2003 (AA5754, square, 25 mm punch travel)

### 6.6.2 Variation of Punch Force with Punch Displacement on Square Cup Deep Drawing for AA5754

In Figure 6.73, variations of punch forces with punch displacement are shown at room temperature, 300°C and 520°C. Punch force values were higher at room temperature than elevated temperature, since strength of material decreases with increasing temperature. Punch force increased till 15 mm punch travel. After 15 mm punch travel, variations of punch forces became irregular due to instabilities.

When punch forces of AA5754 and SS304 sheet material, necessary punch force is lower for AA5754 sheet material than SS304 sheet material.

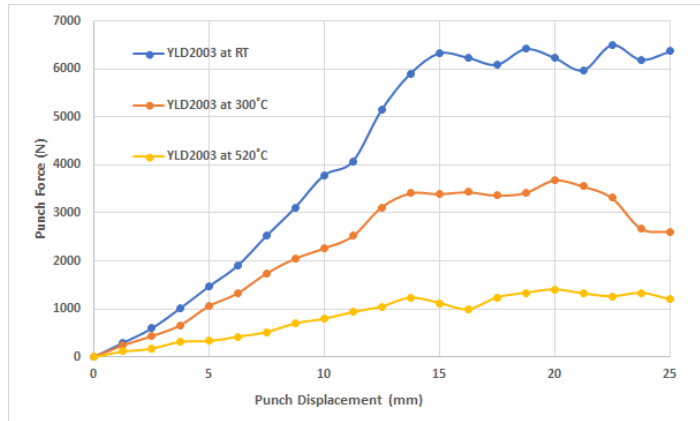


Figure 6.73: Punch force vs square punch displacement at different temperatures for YLD2003-8P (AA5754)

### 6.6.3 Rim Shapes of Square Cup Deep Drawing for AA5754

In Figure 6.74, rim shapes of deep drawn square cup are shown for AA5754. Area of the rim shape of the deformed shape became larger with increasing temperature. There are not any deviations between rim shapes for room temperature, 300°C and 520°C at the corners of the rim shapes. Variations of the predicted flow of the blank into the die cavity were easily observed at other parts of the edges of the blanks.

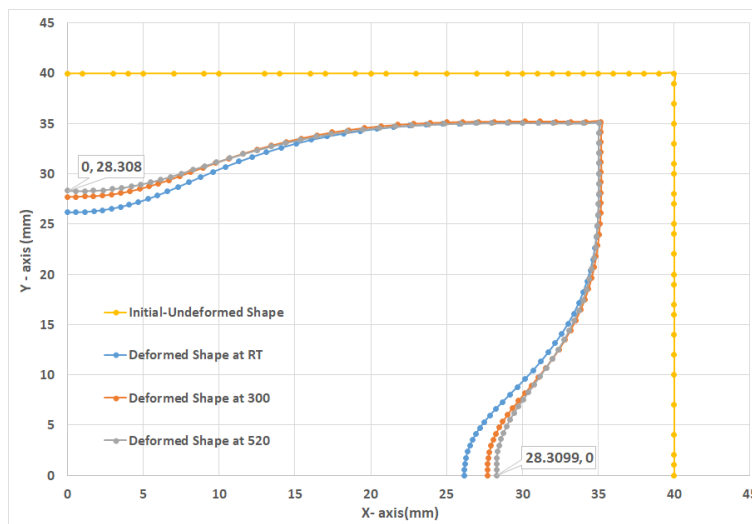


Figure 6.74: Rim shapes of the undefomed blank and deep drawn square cup at different temperatures. (AA5754, YLD2003)

## 6.7 Results of Local Heating of Cylindrical Deep Drawing

To observe the local heating effects on thickness strain distributions, 4 different cases were considered. The temperatures used in these cases are given in Table 6.1 for the blank, die and punch. The blank was divided into two parts to give the different temperature values as shown in 6.75.

Table 6.1: Temperature of the tools and regions of the blank in local heating processes

	Case-1	Case-2	Case-3	Case-4
Initial Temp. of Center of Blank (°C)	25	25	175	175
Initial Temp. of Flange (°C)	25	175	25	175
Temperature of Die (°C)	25	175	25	175
Temperature of Blank Holder (°C)	25	175	25	175
Temperature of Punch (°C)	25	25	175	175

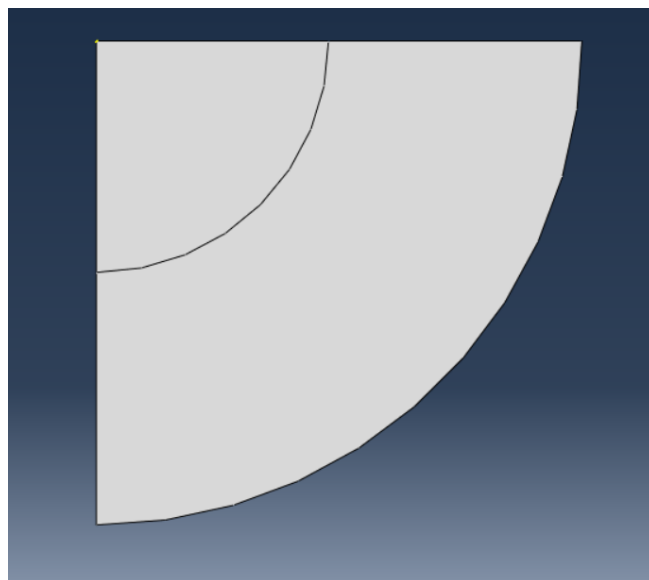


Figure 6.75: Partition of the blank for local heating process.

### 6.7.1 Thickness Strain Distribution, Temperature Distribution and Rim Shapes of Local Heating Circular Blank for AA5754

The thickness strain and temperature distribution obtained by local heating of the circular blank made of AA5754 sheet material are presented in Figures 6.76-6.81 at 80 mm punch travel except for Case 3. Since for Case 3 Johnson Cook failure criterion predicted the failure at 62.2 mm cup height.

Figures 6.76, 6.78 and 6.80 show that thickenings is observed at the regions under the punches. Thickness strain values increases from center of the blank to the punch shoulder. Moreover, thickening can be seen easily at the cup wall and flange regions.

Figures 6.77, 6.79 and 6.81 show that temperature increase is greater at the cup wall regions and at the outer flange regions for Cases 1,2 and 4. Since deep drawing process takes a very short time, heat flow from the part at room temperature to the part at 175°C is insignificant for Case 2.

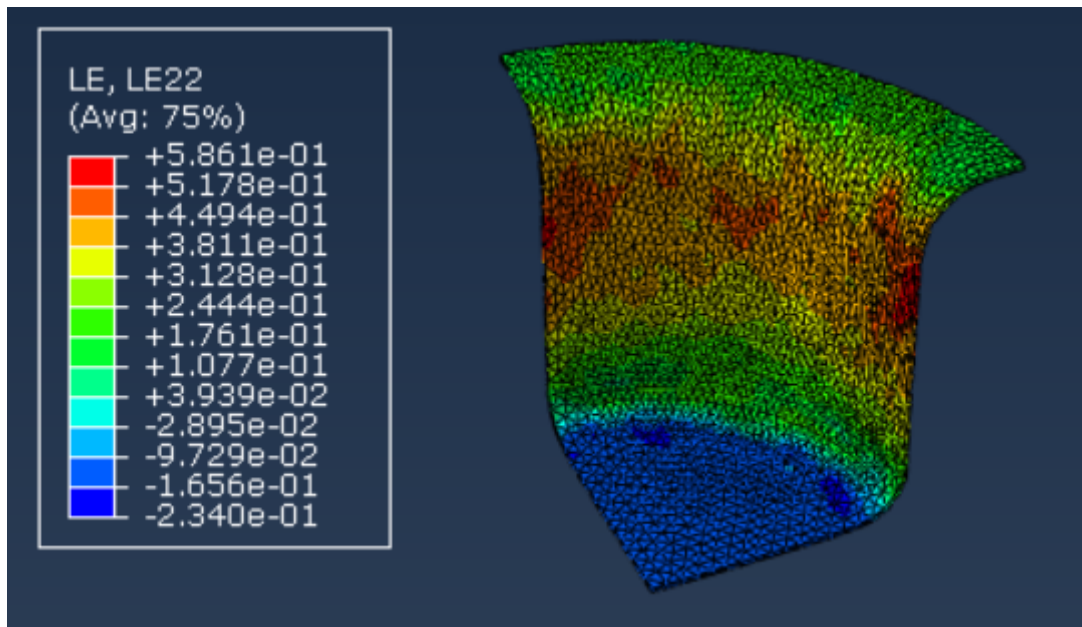


Figure 6.76: Thickness strain on deformed shape in Case-1 (AA5754-O)

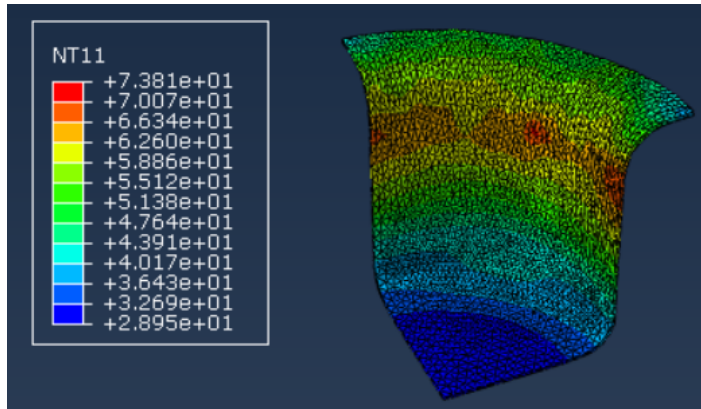


Figure 6.77: Temperature distribution on deformed shape in Case-1 (AA5754-O)

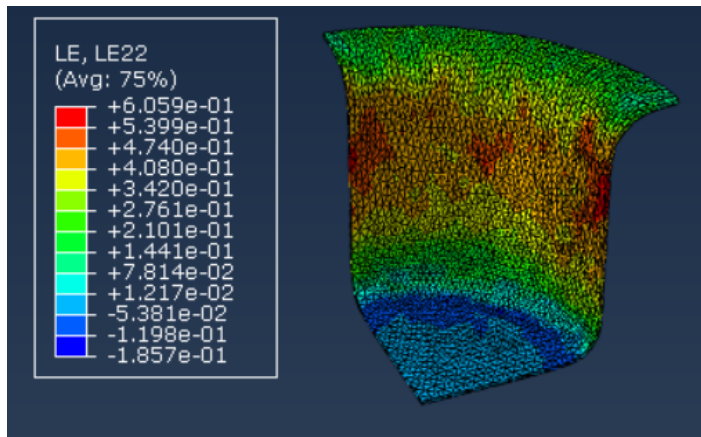


Figure 6.78: Thickness strain on deformed shape in Case-2 (AA5754-O)

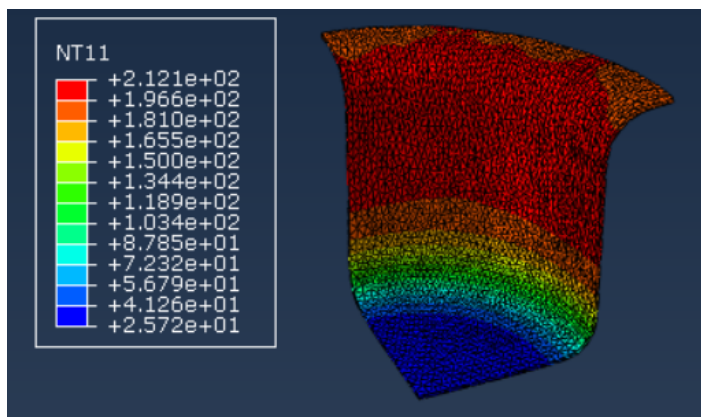


Figure 6.79: Temperature distribution on deformed shape in Case-2 (AA5754-O)

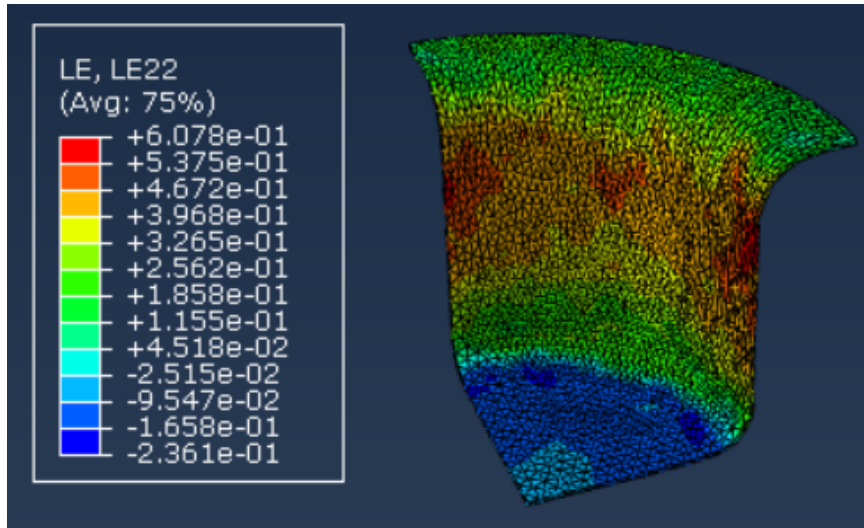


Figure 6.80: Thickness strain on deformed shape in Case-4 (AA5754-O)

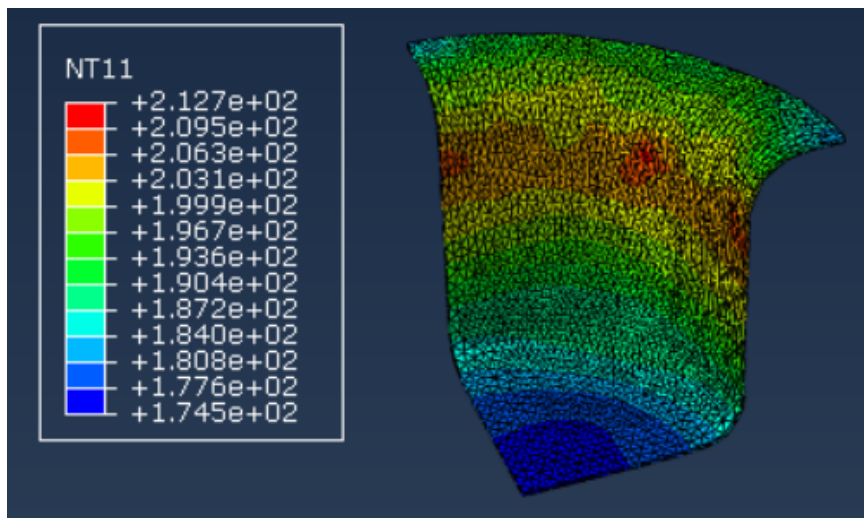


Figure 6.81: Temperature distribution on deformed shape in Case-4 (AA5754-O)

Figure 6.82 shows that although initial temperature of the blank and all tools are 25°C, temperature increased with deformation especially at the highly deformed regions due to the plastic work converted to heat. Similar trend can be also seen in other cases. Temperature values increase about 40°C at these regions due to plastic deformation.

It was observed that at end of the analysis of Case 3, fracture occurs near the punch corner. Therefore, any data related to Case 3 is not added in Figure 6.83.

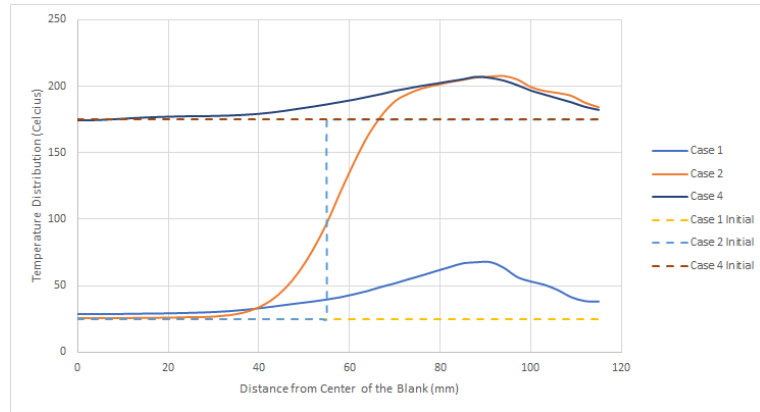


Figure 6.82: Temperature distribution vs distance from center of the blank for Cases 1, 2 and 4 (AA5754-O)

According to Figure 6.83, if blank is heated homogeneously, thickness strain decreases with increasing temperature, as seen for Case 1 and Case 4. When the flange region of the circular blank is heated and the inner region of the circular blank is at room temperature as in Case 2, thickness strain of the inner region of the blank becomes more uniform and change in the thickness decreases. Case 2 gave the closest results to the experimental results.

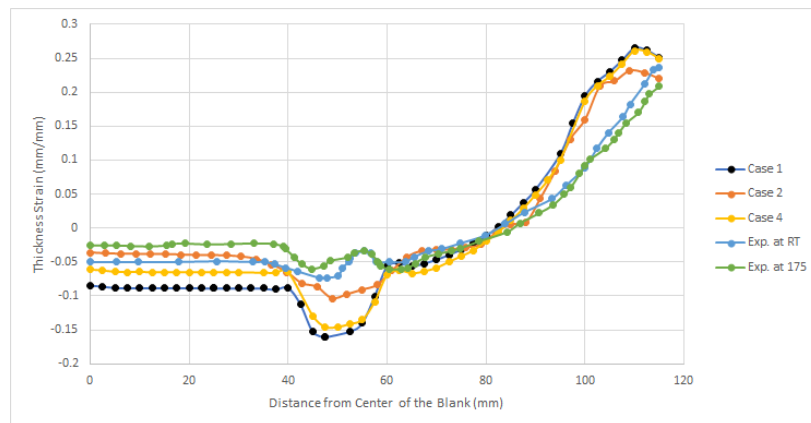


Figure 6.83: Thickness strain distribution vs distance from center of the blank for Cases 1, 2 and 4 (AA5754-O)

In Figure 6.84, rim shapes of deformed circular blanks, which are heated locally, are shown. The least deformation is observed for Case 4, but the results are close to each

other.

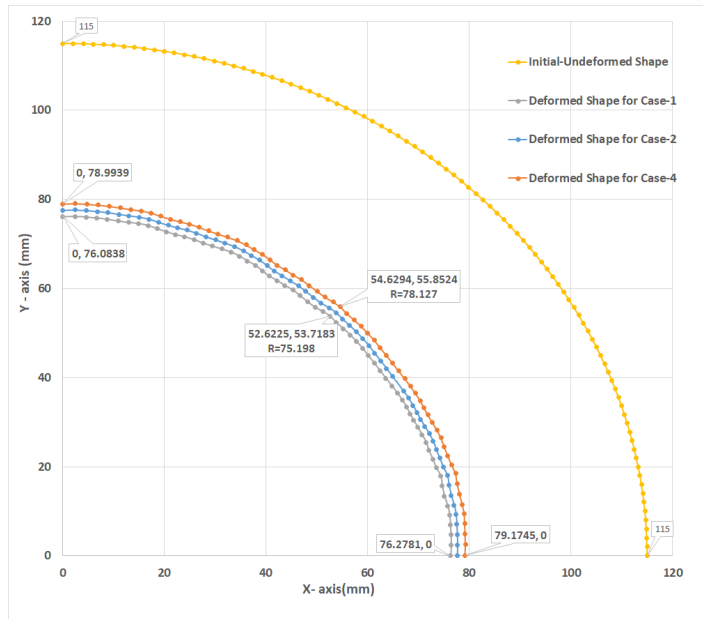


Figure 6.84: Rim shapes of undeformed blank and heated locally deep drawn cylindrical cup for Cases 1, 2 and 4 (AA5754-O)

### 6.7.2 Failure of the Deep Drawing of the Local Heating Circular Blank for AA5754

In this section, blank holder force was increased from 10000 N to 25000 N to observe the failure of the circular blank under same conditions for four cases. Beginning of the failure of the sheet is shown in Figure 6.85.

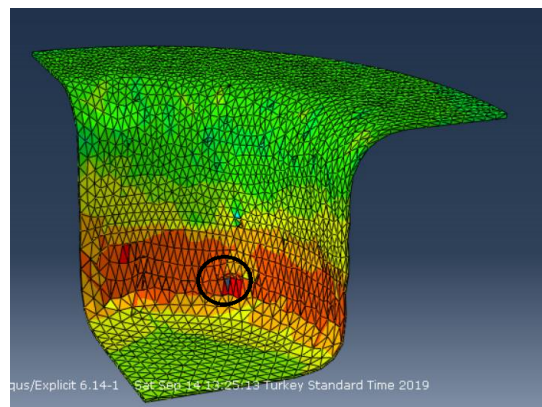


Figure 6.85: Beginning of failure for cylindrical deep drawing (AA5754-O)

In Table 6.2, height of cup values (punch) are shown when the fracture of the blank initiates. The highest cup height was reached for Case 4. Increasing the temperature of the flange region also help to reach higher cup height. However, heating the blank at region under the punch results earlier fracture even compared to the room temperature.

Table 6.2: Depth of cup at different local heating cases

	Case 1	Case 2	Case 3	Case 4
Temperature of Center of Blank (°C)	25	25	175	175
Temperature of Flange (°C)	25	175	25	175
Temperature of Die (°C)	25	175	25	175
Temperature of Blank Holder (°C)	25	175	25	175
Temperature of Punch (°C)	25	25	175	175
<b>Depth of Cup at Beginning of Failure (mm)</b>	<b>54.06</b>	<b>63.87</b>	<b>51.46</b>	<b>69.78</b>

## 6.8 HFQ Process and Local Heating of Complex Formed Blank

Developing FE model of the HFQ process was analyzed at 200°C, 350°C and 480°C with a speed of 250mm/s to get complex shape by using different yield criteria. Effects of temperature variation on thickness strain distribution and rim shape of the deformed complex shape. After that, analyses of the deep drawing process of the locally heated complex shaped blanks were carried out.

Formed whole sheet metal shape is demonstrated in Figure 6.86-a. However, to get rid of difficulties of collecting proper data, rectangular sheet metal shape with dimension of 200x65x1.5 mm<sup>3</sup>. Rectangle section of the part is shown in Figure 6.86-b. Hence

all analyses were carried out based on rectangular sheet metal.

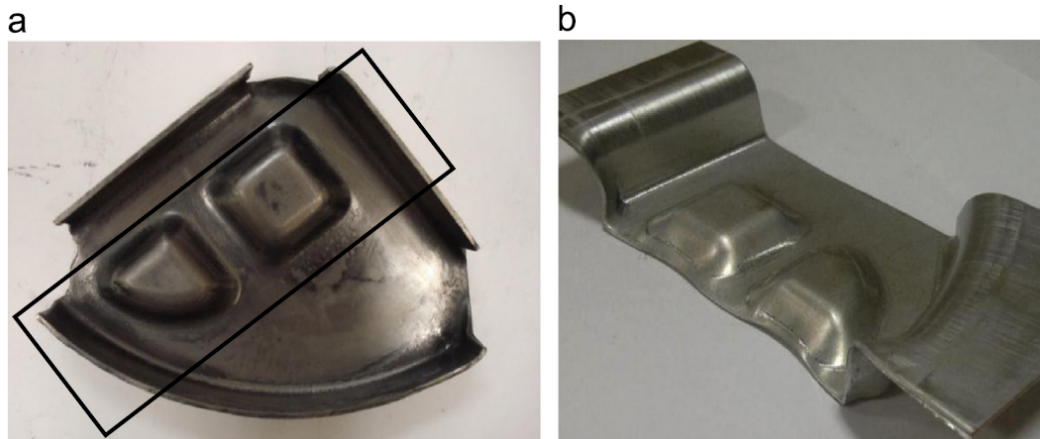


Figure 6.86: (a) Formed whole sheet metal shape and trimmed part of the sheet metal and (b) section formed, highlighted by rectangle in (a). [6]

### 6.8.1 Results of Complex Formed Blank for HFQ Process

In Figure 6.87, thickness strain distributions of the complex shaped blank obtained by FEM at 200°C are shown. The highest thickness strains are observed at the corner regions of the deformed part. Maximum thinning of the sheet is located at 92 mm along the section. Whereas YLD2003 yield criterion gives the closest results to the experimental results at most of the regions, the results of kinematic hardening rule with von Mises yield criterion deviate significantly from experimental results. At the regions which formed at second step of the deep drawing process, von Mises with combined hardening rule and Hill48 yield criteria also gave good results.

Stress and thickness strain distributions are shown in Figures 6.88 and 6.89 respectively for 200°C. Both stress and thickness strain values are the highest at the corner regions of the deformed complex shape. Stress values decrease at the edge sides of the the flange regions.

In Figure 6.90, thickness strain distributions of the complex shaped blank obtained by FEM at 350°C are shown. The highest thickness strains are observed again at the corner regions of the deformed part. YLD2003 and Hill48 yield criteria gave the best results that are closer to the experimental results at most of the regions. Kinematic

hardening rule with von Mises yield criterion could not predict the thickness strain variation good enough. Other models give closer results to experimental results at 350°C than 200°C.

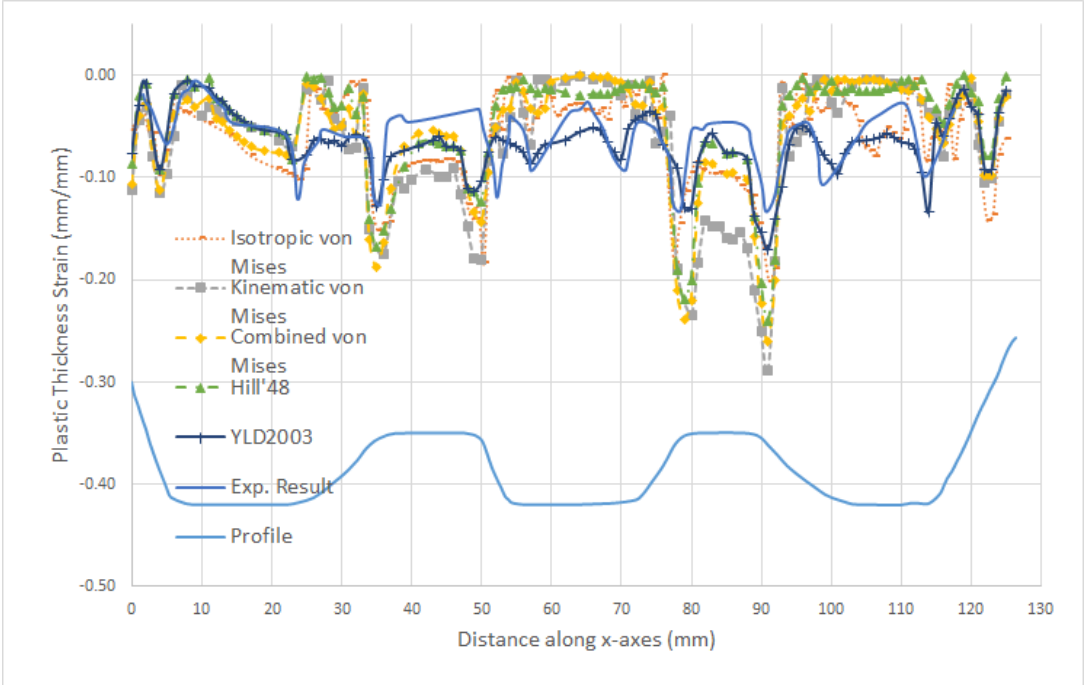


Figure 6.87: Plastic thickness strain distributions for different yield criteria at 200°C (HFQ process for complex shape)

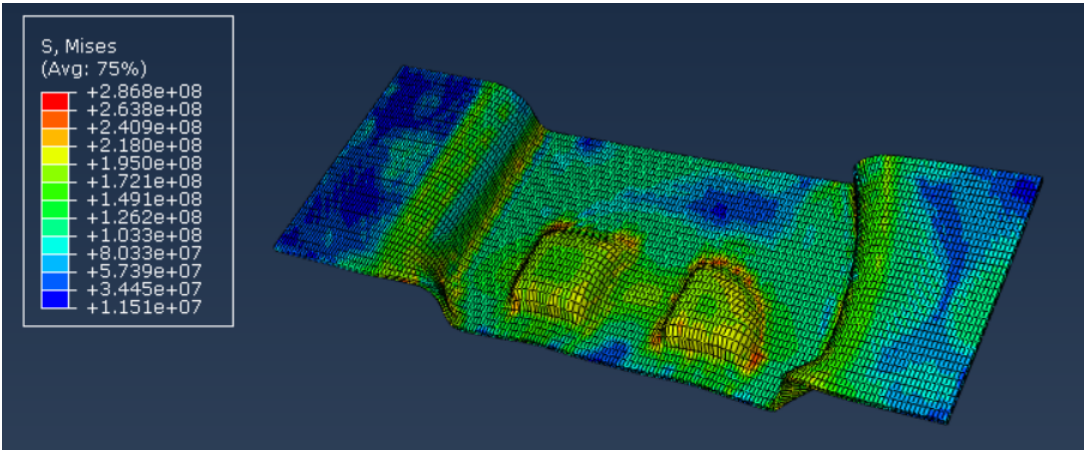


Figure 6.88: Stress distribution on deformed shape at 200°C

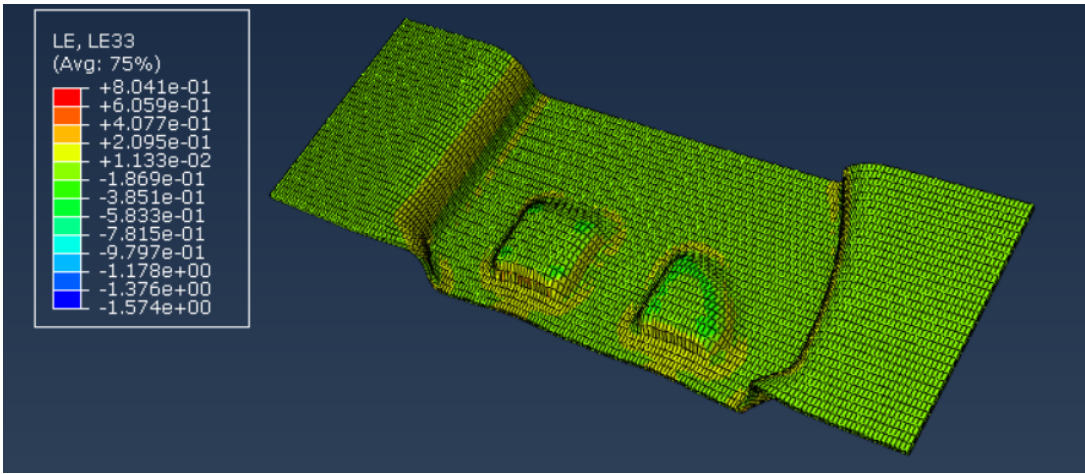


Figure 6.89: Plastic thickness strain distribution on deformed shape at 200°C

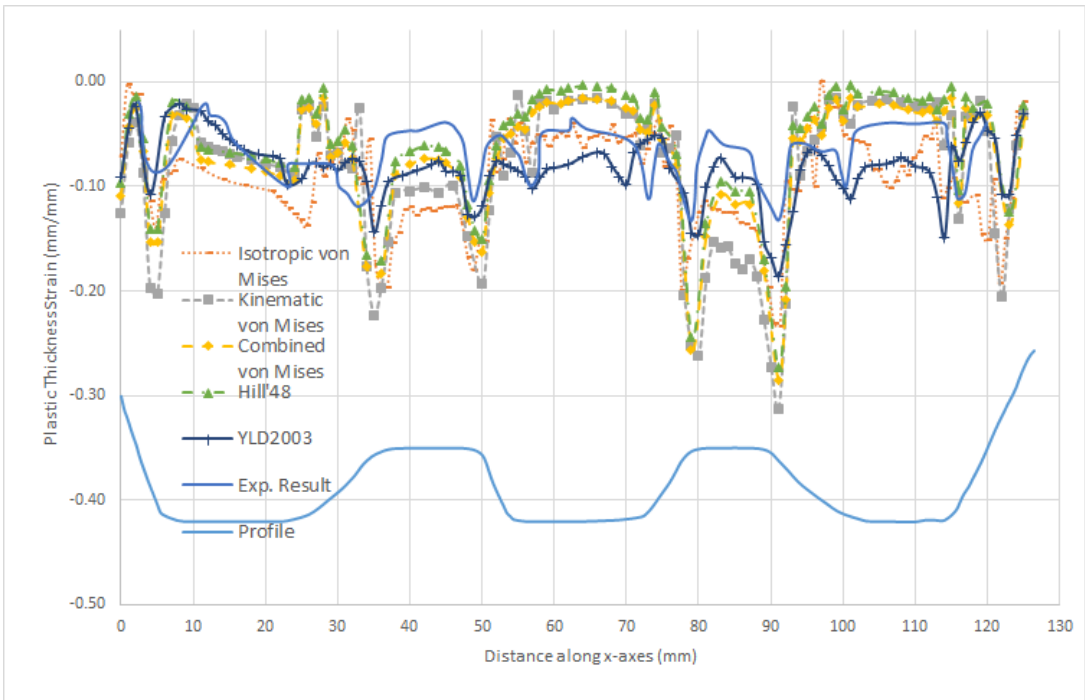


Figure 6.90: Plastic thickness strain distributions for different yield criteria at 350°C (HFQ process for complex shape)

Stress and thickness strain distributions are shown in Figures 6.91 and 6.92 respectively for 350°C. Both stress and thickness strains have the highest values at the corner regions of the deformed complex shape. Stress values increase as the sharpness of the corner increases.

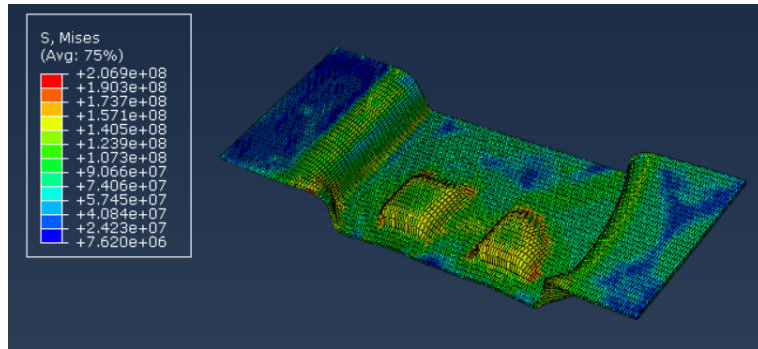


Figure 6.91: Stress distribution on deformed shape at 350°C

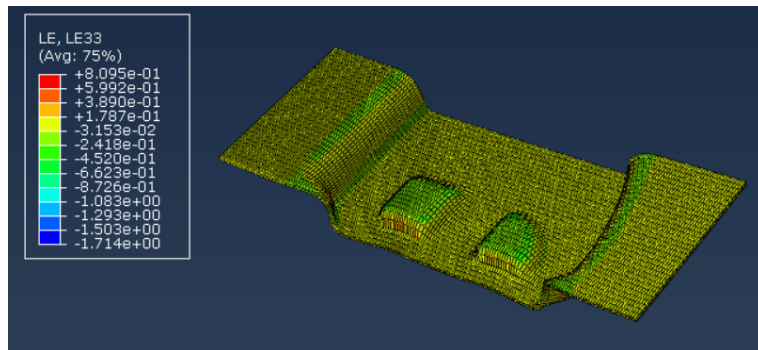


Figure 6.92: Plastic thickness strain distribution on deformed shape at 350°C

In Figure 6.93, simulated thickness strain distributions of the complex shaped blank at 480°C are shown. 480°C is the SHT temperature of AA5754. The highest thickness strains are observed at the corner regions of the deformed part for all models and experiment. YLD2003 yield criterion gave the closest result to the experimental result at most of the regions. Isotropic hardening rule with von Mises yield criterion predicted the results with a significant difference. Von Mises with combined hardening rule and Hill48 yield criteria gave close results to experimental results at the regions which occur in second step of the deep drawing process.

Stress and thickness strain distributions are shown in Figures 6.94 and 6.95 respectively for 480°C. Both stress and thickness strain have the highest values at the corner regions of the deformed complex shape. Stress values increase where the sharpness of the corner increases.

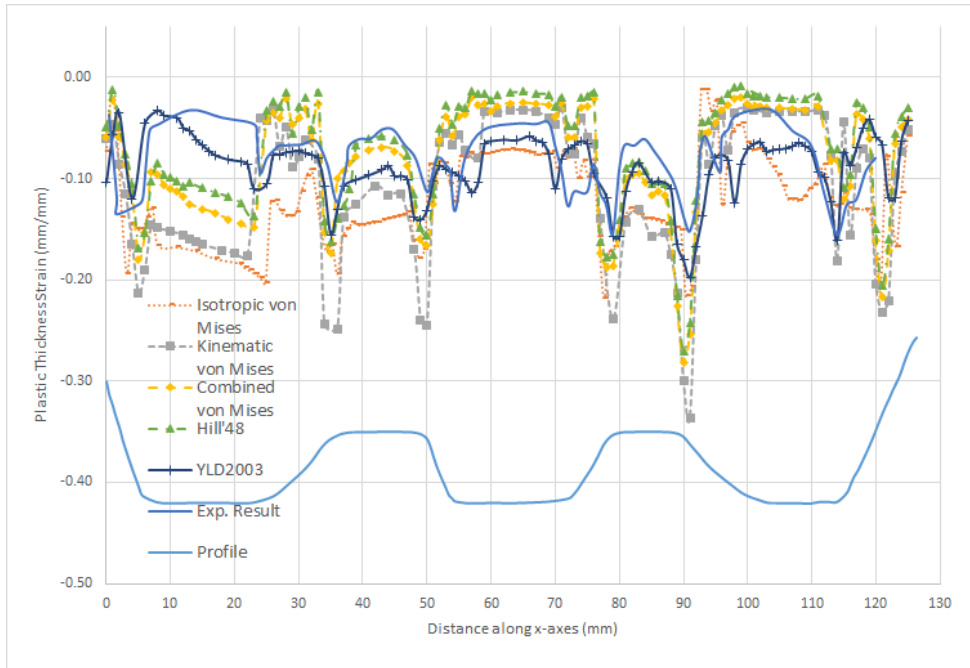


Figure 6.93: Plastic thickness strain distributions for different yield criteria at 480°C (HFQ process for complex shape)

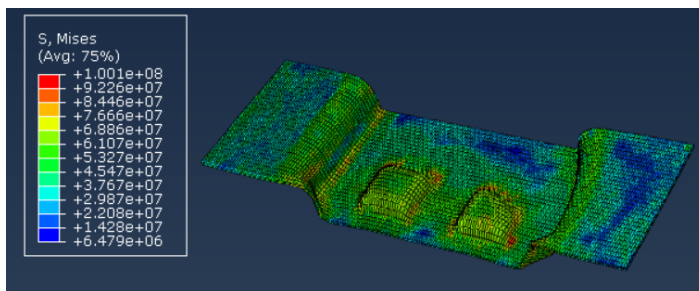


Figure 6.94: Stress distribution on deformed shape at 480°C

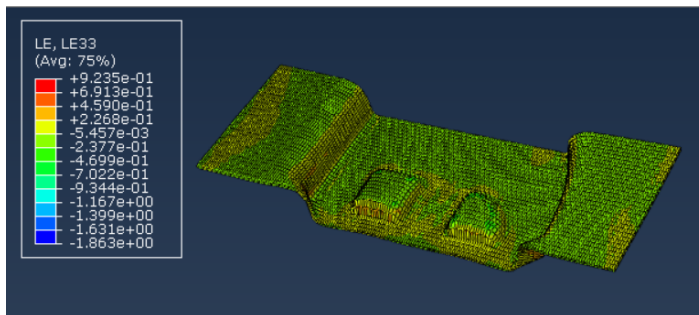


Figure 6.95: Plastic thickness strain distribution on deformed shape at 480°C

Figures 6.87-6.95 show that YLD2003 yield criterion gives reliable and closer results to experimental results with respect to thickness strain distribution. Minimum stress values are obtained from simulation of complex shaped blank at 480°C in all used temperature values. The most thinning regions are the corner regions of the complex shaped blanks and maximum thinning is located at the same region at different temperatures.

Effects of temperature variation on thickness strain distributions of complex shaped blanks are presented in Figures 6.96-6.100 for von Mises with isotropic, kinematic and combined hardening rules, Hill48 and YLD2003 yield criteria respectively.

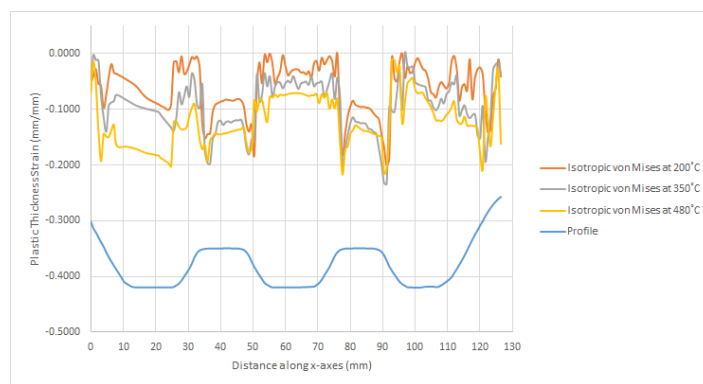


Figure 6.96: Effect of temperature on thickness strain distributions for vonMises-Isotropic (HFQ process for complex shape)

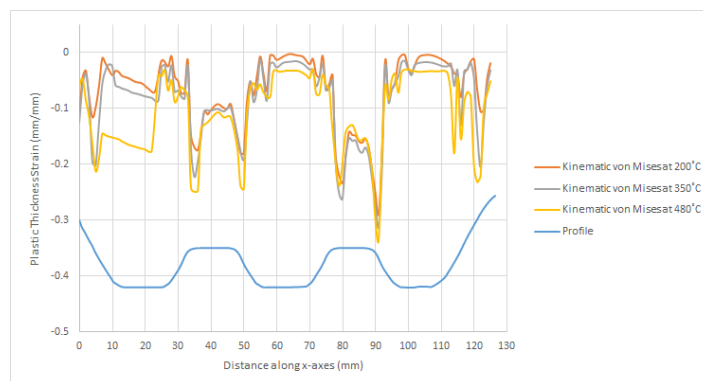


Figure 6.97: Effect of temperature on thickness strain distributions for vonMises - Kinematic (HFQ process for complex shape)

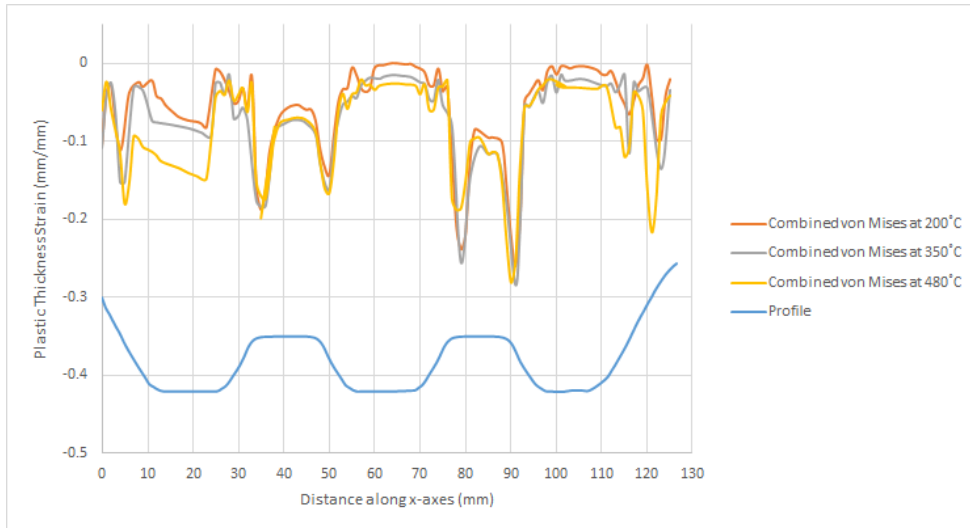


Figure 6.98: Effect of temperature on thickness strain distributions for vonMises - Combined (HFQ process for complex shape)

The thickness strain and thinning of the sheet increase with increasing temperatures for all used models. Maximum thinning of the blank is located at 92 mm along the section for all models and its maximum value is about -0.33 mm/mm at 480°C for kinematic hardening rule with von Mises yield criterion.

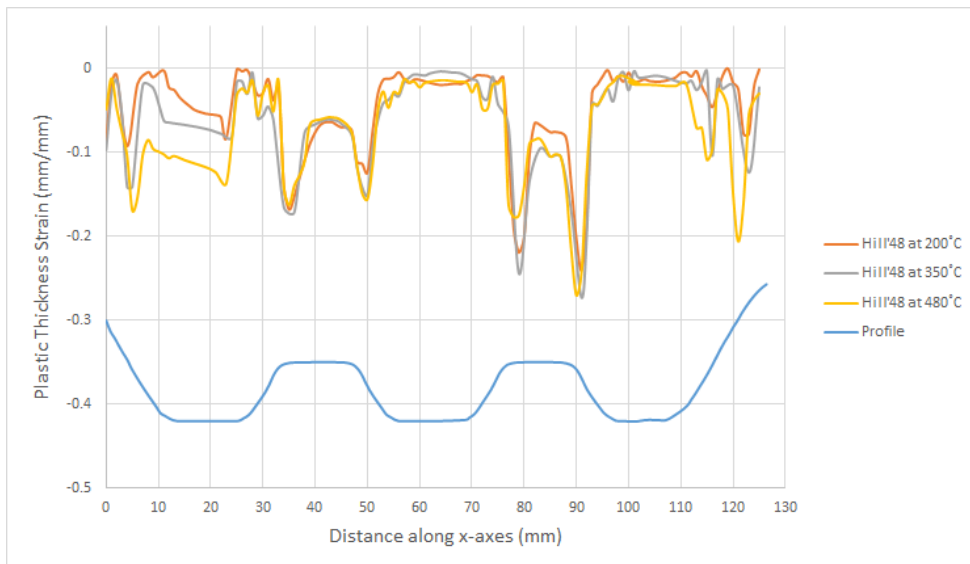


Figure 6.99: Effect of temperature on thickness strain distributions for Hill48 (HFQ process for complex shape)

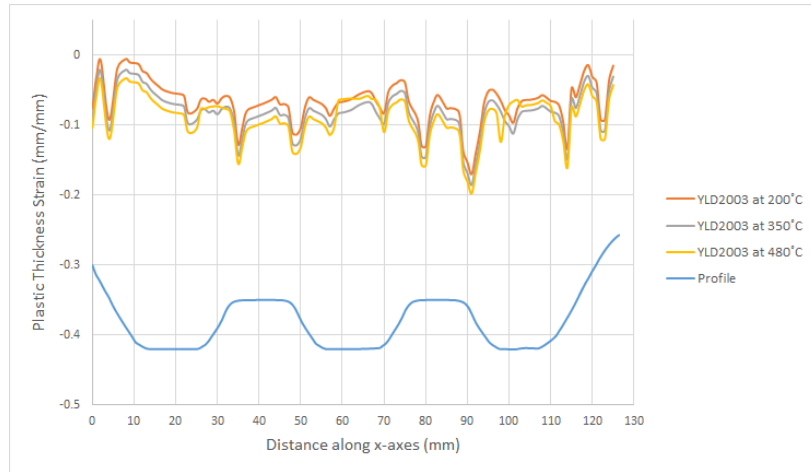


Figure 6.100: Effect of temperature on thickness strain distributions for YLD2003 (HFQ process for complex shape)

In Figure 6.101, the rim shapes of the undeformed rectangular blank and complex formed blank are shown at different temperatures for HFQ process. The flow of the material decreased with increasing temperature. Whereas effect of temperature on rim shape is clearly seen at short edges of the deformed shape, there are slight differences between rim shapes at long edges of the blank at different temperatures.

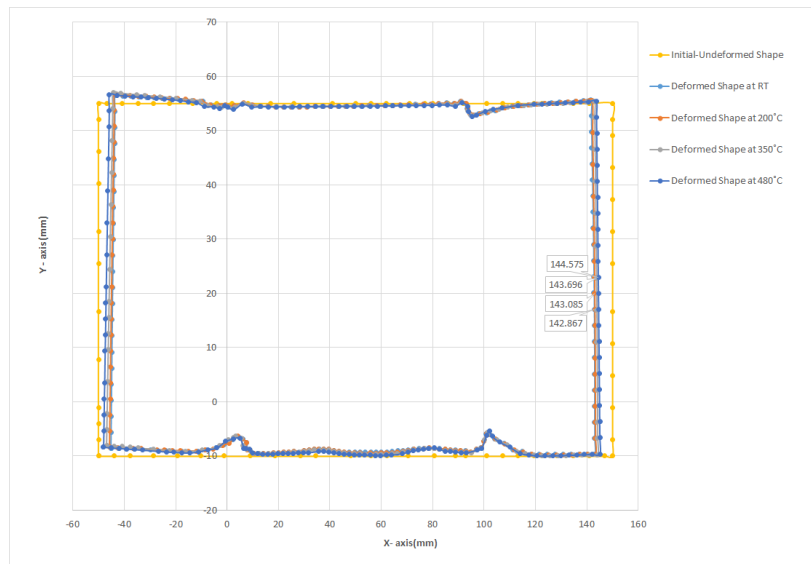


Figure 6.101: Rim shapes of undeformed blank and complex formed blank with HFQ process (AA5754-O)

### 6.8.2 Results of Local Heating of Complex Formed Shape

To investigate the effects of the local heating of the complex shaped blank, blank is divided four different parts as shown in Figure 6.102. FE analyses were carried out by giving different initial temperature values to the divided four region and tools. These given temperature values are presented in Table 6.3.

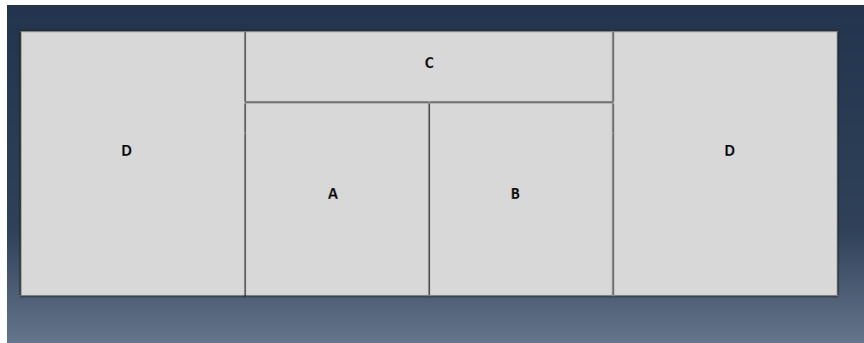


Figure 6.102: Partition of rectangular blank.

Table 6.3: Temperature of the tools and regions of the blank in local heating processes for complex shape

	Case-1	Case-2	Case-3	Case-4	Case-5
Initial Temp. of Region A (°C)	25	200	350	25	350
Initial Temp. of Region B (°C)	25	200	350	25	350
Temperature of Region C (°C)	25	25	25	25	350
Temperature of Region D (°C)	25	25	25	200	350
Temperature of Tools (°C)	20	20	20	20	20

In Figure 6.103, temperature distributions of complex shaped blanks are presented for local heating process. Although temperature values of tools and die are 20°C which is lower than temperatures of the blanks for all cases, temperature values of the blanks

increased about 25°C during deep drawing process, since a high percentage of plastic work is converted to heat significantly. Increases in temperature values of complex shaped blank occur at the corner regions of the blank where maximum thickness strain values are also observed.

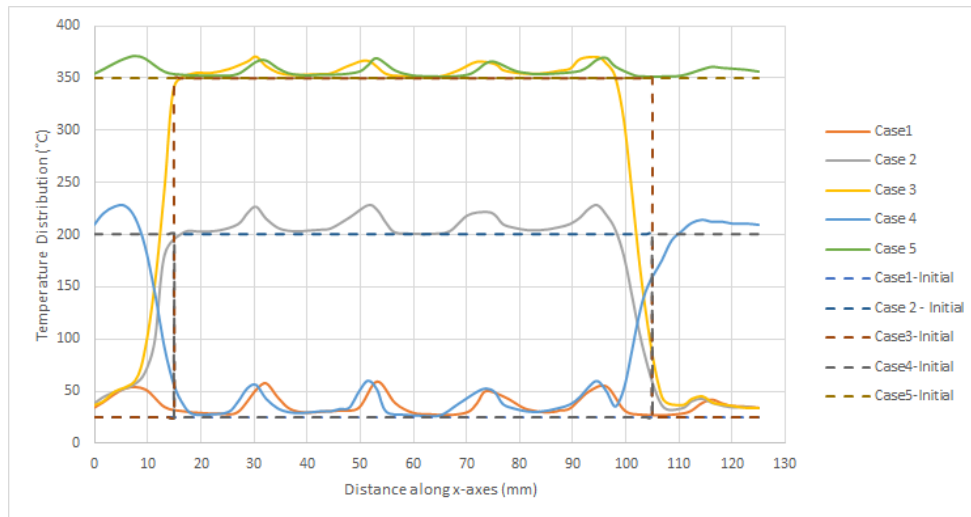


Figure 6.103: Temperature distribution with blank distance along x-axis for Cases 1, 2, 3, 4 and 5 ( for complex shape-AA5754-O)

According to Figure 6.104, if the flange region of the blank is heated and temperature of the inner region of the blank is kept at room temperature as in Case 4, more uniform thickness strain was obtained than homogeneous heating of blank as in Case 5. In the deep drawing process of complex shape of AA5754 sheet material, the most uniform shape was obtained with respect to thickness strain at room temperature. If the inner region of the blank is heated and the flange region is kept at room temperature, the complex shaped blank has the highest thickness strain and become thinner as shown in Case 2.

In Figures 6.106, 6.108, 6.110, 6.112 and 6.114, temperature distributions on deformed shapes are shown for Cases 1, 2, 3, 4 and 5 respectively. By the figures, increases of temperature values were seen at the corner regions of the blanks. All temperature values along-x axis were presented in Figure 6.103.

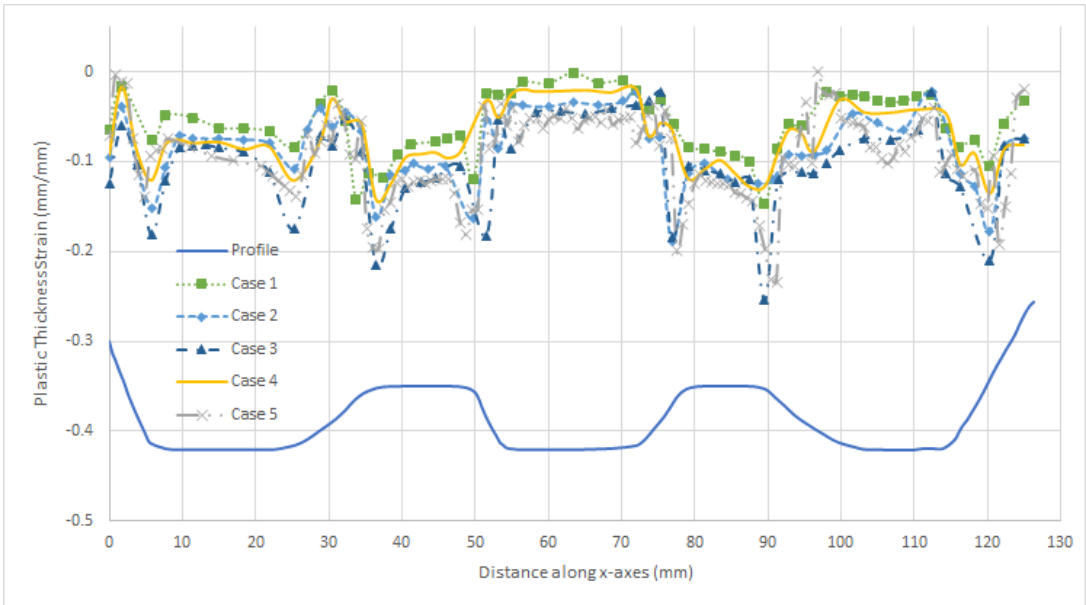


Figure 6.104: Thickness strain with distance along x-axis of local heating of complex shape for Cases 1, 2, 3, 4 and 5 (AA5754-O)

In Figure 6.105, stress distribution on complex deformed shaped is shown for Case 1. Stress values on deformed shaped is higher at the corner regions than other parts of the deformed shape. Minimum stress values are observed at the flange region.

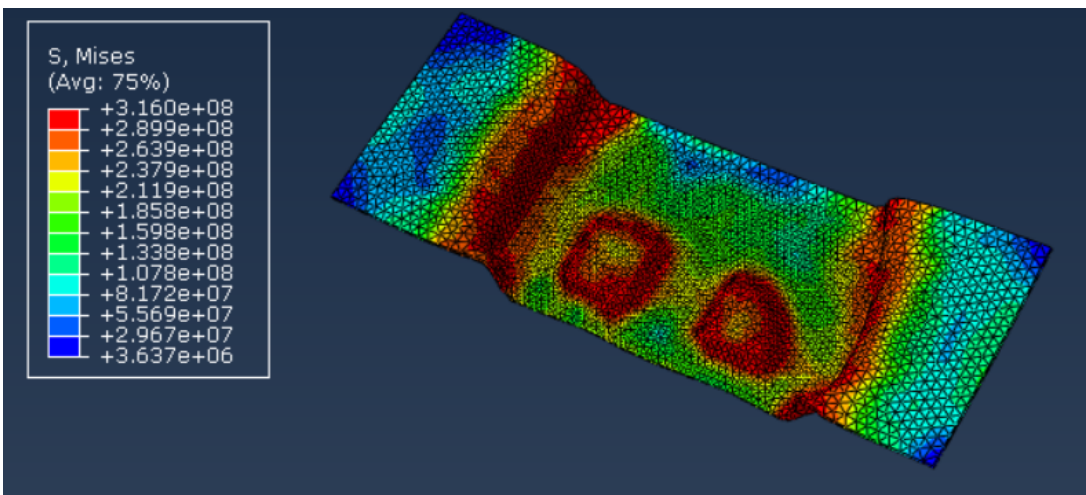


Figure 6.105: Stress distribution on deformed shape for Case-1

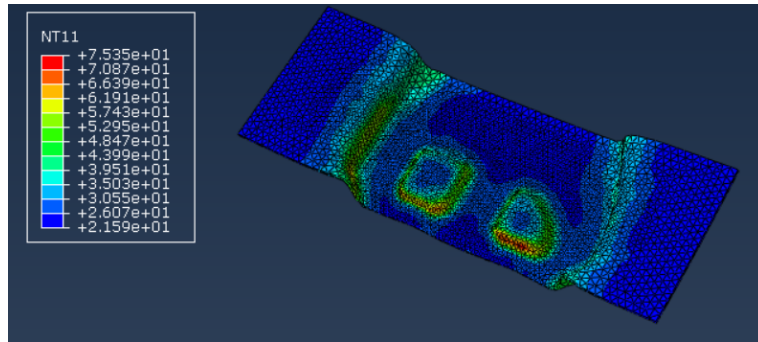


Figure 6.106: Temperature distribution on deformed shape for Case-1

In Figure 6.107, stress distribution on complex deformed shaped is shown for Case 2. Stress values on deformed shaped is higher at the corner regions than other parts of the deformed shape. Minimum stress values are observed at the flange region. Stress values is lower at the inner regions for Case 2 than Case 1, since temperatures of the inner regions are higher for Case 2 than Case 1.

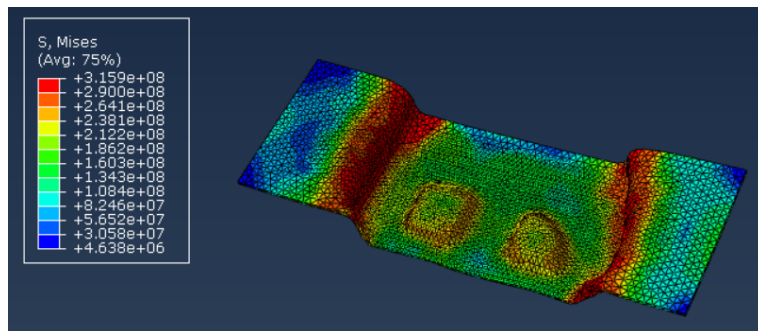


Figure 6.107: Stress distribution on deformed shape for Case-2

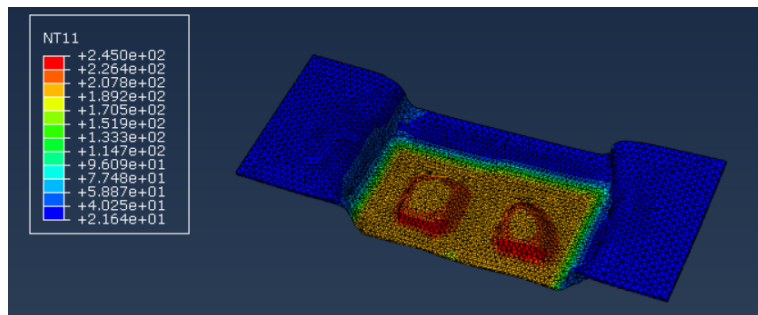


Figure 6.108: Temperature distribution on deformed shape for Case-2

In Figure 6.109, stress distribution on complex deformed shaped is shown for Case 3. Stress values on deformed shaped is higher at the corner regions than other parts of the deformed shape. Minimum stress values are observed at the flange region. Stress values is lower at the inner regions for Case 3 than Case 2, since temperatures of the inner regions are higher for Case 3 than Case 2.

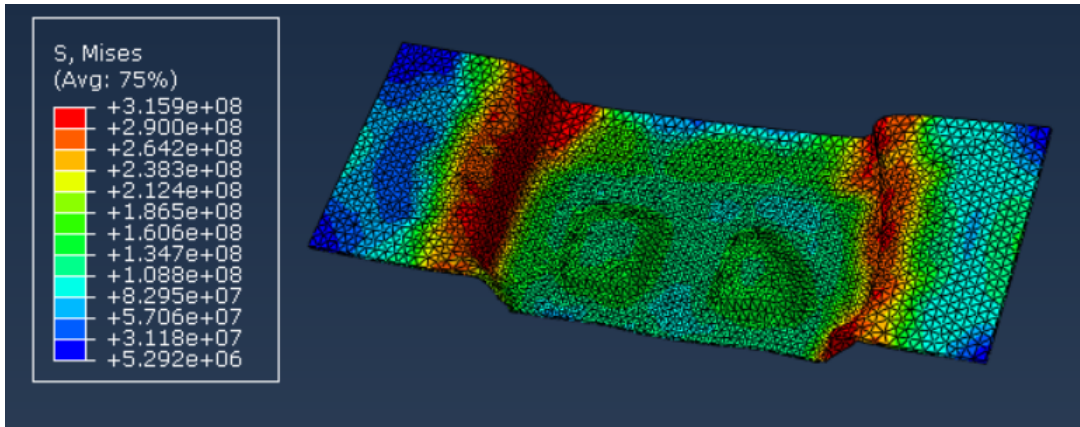


Figure 6.109: Stress distribution on deformed shape for Case-3

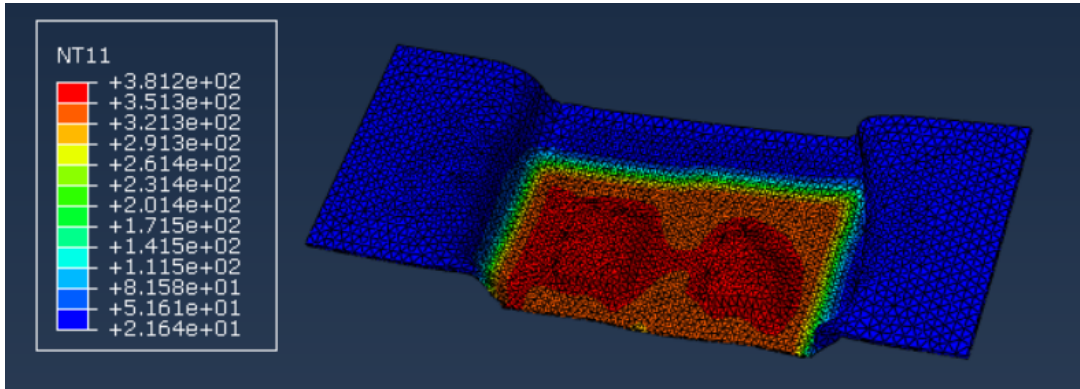


Figure 6.110: Temperature distribution on deformed shape for Case-3

In Figure 6.111, stress distribution on complex deformed shaped is shown for Case 4. Stress values on deformed shaped is higher at the corner regions than other parts of the deformed shape. Minimum stress values are observed at the flange region. Stress values is lower at corner of the top punch regions for Case 4 than Case 1, since temperatures of the flange regions are higher for Case 4 than Case 1.

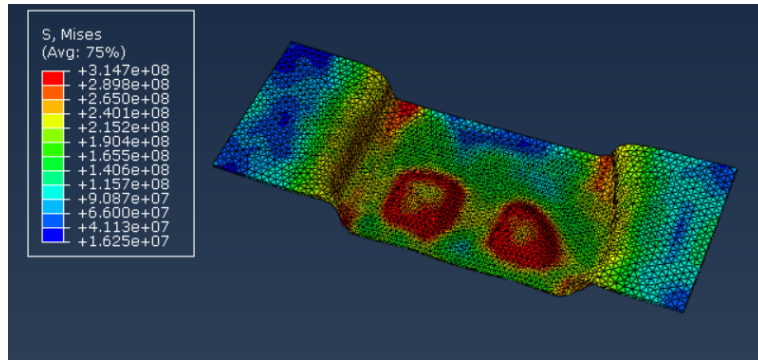


Figure 6.111: Stress distribution on deformed shape for Case-4

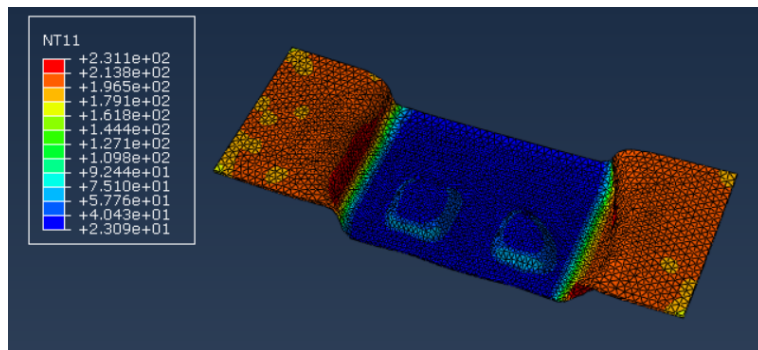


Figure 6.112: Temperature distribution on deformed shape for Case-4

In Figure 6.113, stress distribution on complex deformed shaped is shown for Case 5. Stress values on deformed shaped is higher at the corner regions than other parts of the deformed shape. Minimum stress values are observed at the flange region. Case 5 has the lowest stress values compared to all cases.

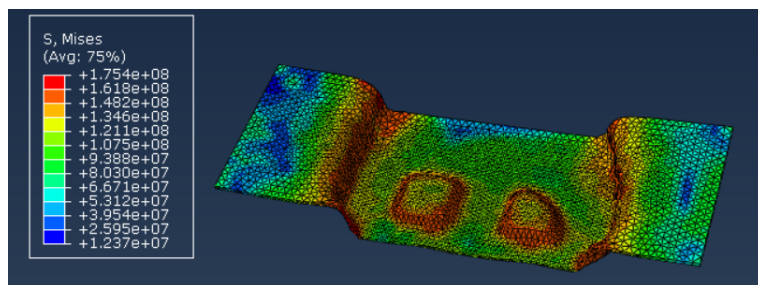


Figure 6.113: Stress distribution on deformed shape for Case-5

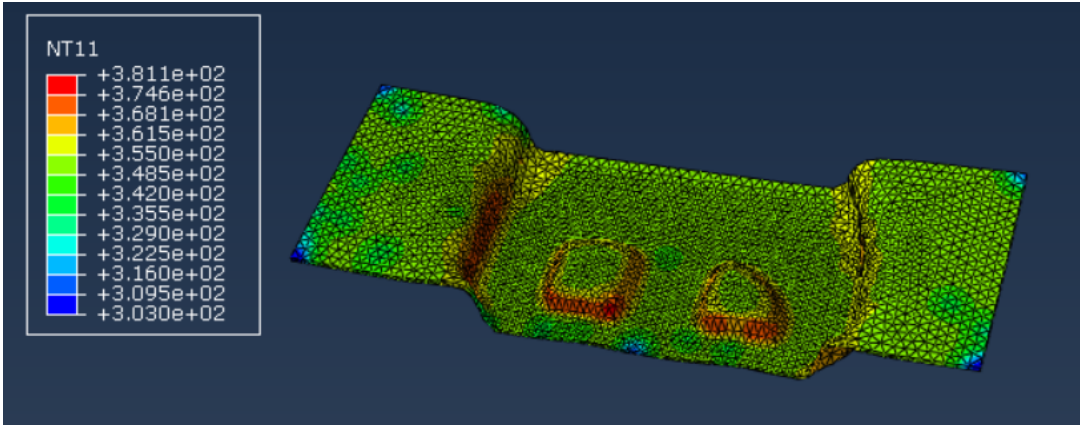


Figure 6.114: Temperature distribution on deformed shape for Case-5

## CHAPTER 7

### CONCLUSIONS

In this thesis, von Mises yield criterion with isotropic, kinematic and combined hardening rules, Hill48 and YLD2003-8P yield criteria and Johnson Cook model were considered. Cylindrical, hemispherical and square deep drawing processes were simulated for different temperature values. For cylindrical deep drawing processes, blank was also locally heated and drawn, and by Johnson Cook failure criterion the maximum cup height values were determined. Moreover, irregular complex shaped blanks were analyzed with different temperatures including SHT temperature for uniform and local heating.

The followings were concluded from the study:

- Necessary punch force value decrease with increasing temperature in all of the deep drawing processes.
- Since strength of SS304 material is higher than AA5754, needed punch force values is higher also.
- Failure occurs at higher cup height values at elevated temperatures than room temperature. Hence drawability increases with increasing temperature.
- Since a high percentage of plastic work is converted to heat, temperature of the sheet material increases during drawing process. The temperature increase is greater at the highly deformed regions. Change of temperature depends on depth of cup.
- Thickness strains of AA5754 and SS304 sheet materials decrease with increasing temperature for cylindrical deep drawing process at most of the

regions of the blank.

- Thickness strain of SS304 sheet material decrease with increasing temperature for hemispherical deep drawing process however, thickness strain increases with increasing temperature at region under the punch for AA5754.
- While thickness strains of both sheet materials increase with increasing temperature at region under the punch for square deep drawing, they decrease with increasing temperature at cup wall and flange regions.
- In cylindrical, hemispherical and square deep drawing processes, the thickness strain of the material under the punch changes highly compared to other regions by the temperature variation.
- For deep drawing of the used complex shaped part, thickness strain increased with increasing temperature.
- It is observed that as temperature increases for relatively simple forming processes such as cylindrical forming thickness change decreases under both punch (compressive thickness strain decrease) and flange region (tensile thickness strains decrease) whereas at room temperature thickness change is greater for both regions. On the other side as the part shape becomes complicated tensile thickness strains decrease whereas compressive thickness strains increase.
- YLD2003 yield criterion gives more reliable results with respect to the thickness strain, if compared with other yield criteria.
- For local heating process of circular blank, heating the flange region of the blank and keeping the inner temperature at room temperature gave more uniform results and thickness strain decreases compared to homogeneous heating of the blank.
- For relative simple deep drawing processes such as cylindrical process as temperature is increased, it is observed that the variation of flow of flange region into the die cavity is insignificant as observed by the rim shapes of the deformed parts.

## REFERENCES

- [1] J. Winklhofer, G. Trattnig, C. Lind, C. Sommitsch, and H. Feuerhuber, “Simulation of aluminium sheet metal deep drawing at elevated temperatures using LS-Dyna,” *AIP Conference Proceedings*, vol. 1252, pp. 927–934, 2010.
- [2] F. Cogun and H. Darendeliler, “Comparison of different yield criteria in various deep drawn cups,” *International Journal of Material Forming*, vol. 10, no. 1, pp. 85–98, 2017.
- [3] M. Rodriguez-Millan, D. Garcia-Gonzalez, A. Rusinek, and A. Arias, “Influence of Stress State on the Mechanical Impact and Deformation Behaviors of Aluminum Alloys,” *Metals*, vol. 8, no. 7, p. 520, 2018.
- [4] A. H. Van Den Boogaard and P. J. Bolt, “A material model for warm forming of aluminium sheet,” *VII international Conference on Computational Plasticity*, 2003.
- [5] H. Laurent, J. Coër, P. Y. Manach, M. C. Oliveira, and L. F. Menezes, “Experimental and numerical studies on the warm deep drawing of an Al-Mg alloy,” *International Journal of Mechanical Sciences*, vol. 93, pp. 59–72, 2015.
- [6] O. El Fakir, L. Wang, D. Balint, J. P. Dear, J. Lin, and T. A. Dean, “Numerical study of the solution heat treatment, forming, and in-die quenching (hfq) process on aa5754,” *International Journal of Machine Tools and Manufacture*, vol. 87, pp. 39–48, 2014.
- [7] N. Abedrabbo, F. Pourboghrat, and J. Carsley, “Forming of AA5182-O and AA5754-O at elevated temperatures using coupled thermo-mechanical finite element models,” *International Journal of Plasticity*, vol. 23, no. 5, pp. 841–875, 2007.
- [8] F. Barlat, J. Brem, J. Yoon, K. Chung, R. Dick, D. Lege, F. Pourboghrat, S.-H.

- Choi, and E. Chu, "Plane stress yield function for aluminum alloy sheets part 1 : theory," *International Journal of Plasticity*, vol. 19, pp. 1297–1319, 2003.
- [9] M. A. Basril, H. M. Teng, M. Azuddin, and I. A. Choudhury, "The effect of heating temperature and methods towards the formability of deep drawn square metal cup," *IOP Conference Series: Materials Science and Engineering*, vol. 210, no. 1, 2017.
- [10] Q. F. Chang, D. Y. Li, Y. H. Peng, and X. Q. Zeng, "Experimental and numerical study of warm deep drawing of AZ31 magnesium alloy sheet," *International Journal of Machine Tools and Manufacture*, vol. 47, no. 3-4, pp. 436–443, 2007.
- [11] F. K. Chen, T. B. Huang, and C. K. Chang, "Deep drawing of square cups with magnesium alloy AZ31 sheets," *International Journal of Machine Tools and Manufacture*, vol. 43, no. 15, pp. 1553–1559, 2003.
- [12] S. H. Zhang, K. Zhang, Y. C. Xu, Z. T. Wang, Y. Xu, and Z. G. Wang, "Deep-drawing of magnesium alloy sheets at warm temperatures," *Journal of Materials Processing Technology*, vol. 185, no. 1-3, pp. 147–151, 2007.
- [13] N. Ethiraj, P. Ganesh, and V. Senthil Kumar, "Theoretical Prediction of Thickness Distribution on Warm Deep Drawn AISI 304 Steel Cup," *Applied Mechanics and Materials*, vol. 766-767, no. June, pp. 974–981, 2015.
- [14] N. Kotkunde, A. D. Deole, A. K. Gupta, and S. K. Singh, "Experimental and numerical investigation of anisotropic yield criteria for warm deep drawing of Ti-6Al-4V alloy," *Materials and Design*, vol. 63, pp. 336–344, 2014.
- [15] N. Kotkunde, A. D. Deole, A. K. Gupta, S. K. Singh, and B. Aditya, "Failure and formability studies in warm deep drawing of Ti-6Al-4V alloy," *Materials and Design*, vol. 60, pp. 540–547, 2014.
- [16] L. Jayahari, B. B. Naik, and S. K. Singh, "Effect of Process Parameters and Metallographic Studies of ASS-304 Stainless Steel at Various Temperatures under Warm Deep Drawing," *Procedia Materials Science*, vol. 6, no. Icmcp, pp. 115–122, 2014.
- [17] P. Venkateshwar Reddy, J. Ramesha, P. S. Rao, and P. Janaki Ramulu, "Experimental and numerical analysis on deep drawing rectangular cups made

- of different anisotropic materials,” *Materials Today: Proceedings*, vol. 5, no. 13, pp. 27171–27177, 2018.
- [18] K. Zheng, Y. Dong, J.-H. Zheng, A. Foster, J. Lin, H. Dong, and T. A. Dean, “The effect of hot form quench (hfq®) conditions on precipitation and mechanical properties of aluminium alloys,” *Materials Science and Engineering: A*, 2019.
- [19] X. Fan, Z. He, S. Yuan, and P. Lin, “Investigation on strengthening of 6a02 aluminum alloy sheet in hot forming-quenching integrated process with warm forming-dies,” *Materials Science and Engineering: A*, vol. 587, pp. 221–227, 2013.
- [20] H. K. Farahani, “Determination of Johnson Cook Plasticity Model Parameters for Inconel718,” no. October, 2017.
- [21] D. V. Hutton and J. Wu, *Fundamentals of finite element analysis*, vol. 1. McGraw-hill New York, 2004.
- [22] *Abaqus 6.14 Theory Manual*. Dassault Systemes Simulia Corporation, 2014.
- [23] G. Chagas and I. Machado, “Numerical model of machining considering the effect of mns inclusions in an austenitic stainless steel,” *Procedia CIRP*, vol. 31, pp. 533–538, 2015.



## APPENDIX A

### THICKNESS STRAIN DISTRIBUTION AT DIFFERENT DIRECTIONS OF THE BLANK

In Figures A.1 and A.2, thickness strains distributions of deep drawn cylindrical cup for Hill48 yield criterion are shown at different directions. Since Hill48 yield criterion is an anisotropic yield criterion, properties of the materials change in different directions. At the flange and cup wall regions thickness strain variations deviated in direction of  $0^\circ$ ,  $45^\circ$  and  $90^\circ$ .

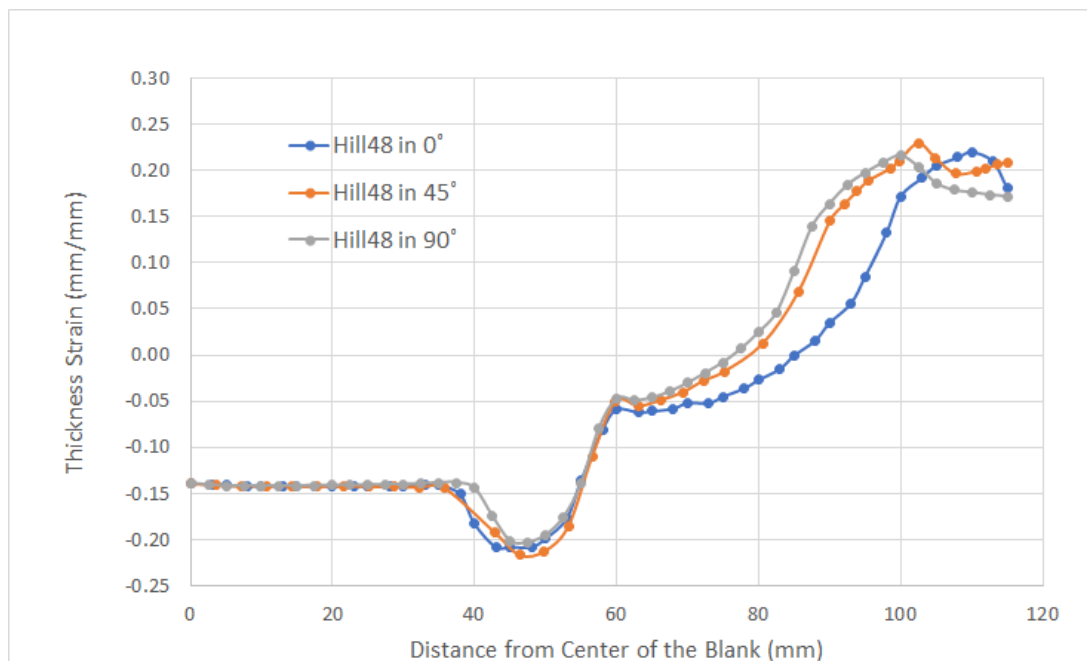


Figure A.1: Thickness strain distributions of circular blank on different directions at room temperature for Hill48 (80 mm punch travel, cylindrical)

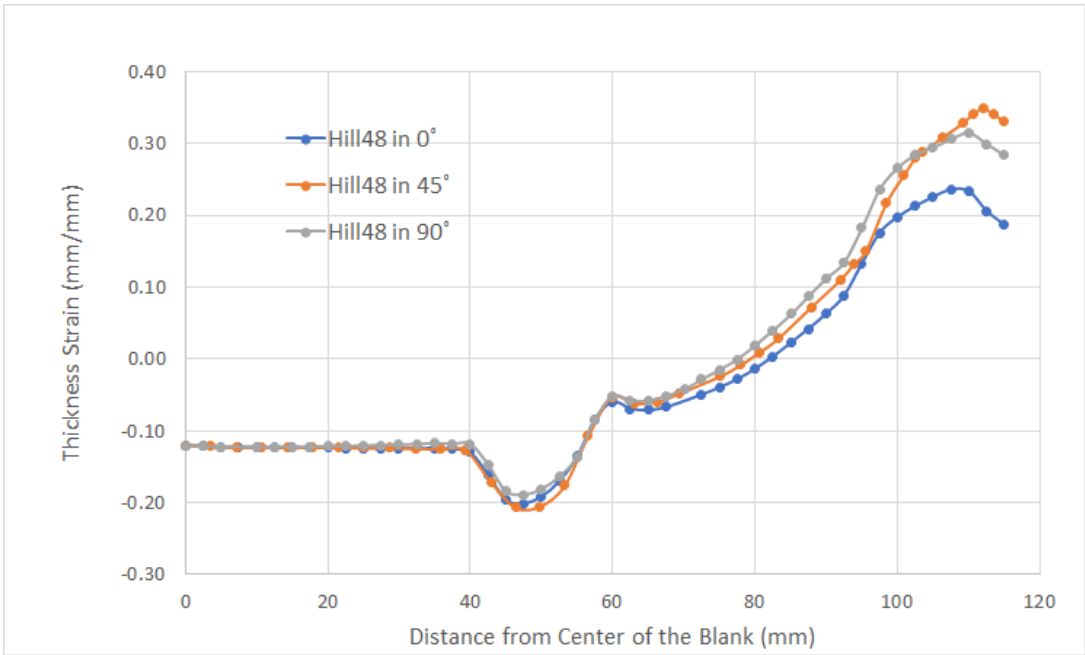


Figure A.2: Thickness strain distributions of circular blank on different directions at 175°C for Hill48 (80 mm punch travel, cylindrical)